Stockholm University

Licenciate thesis

Marine Geology

Characterization of iron particles in the Lena River, NE Russia

Catherine Hirst


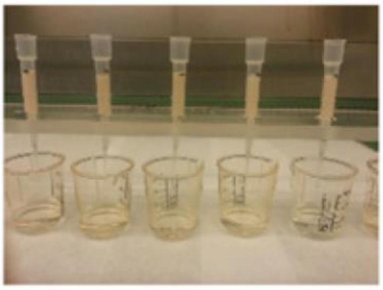

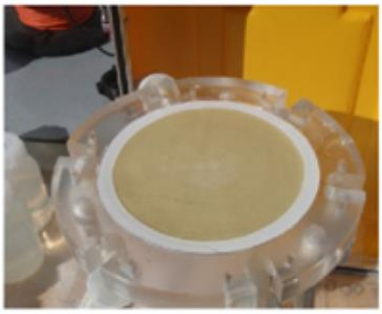

Stockholm 2016

Department of Geological Sciences
Stockholm University
SE-106 91 Stockholm

Abstract

Iron (Fe) is an important micronutrient for primary production in the ocean. The Arctic Ocean is strongly affected by inflows from the surrounding boreal rivers and this governs the supply of major nutrients and important micronutrients. Riverine Fe is mainly transported in particulate from and the size and mineralogy of Fe particles governs their bioavailability on the continental shelf. The characteristics of Fe-bearing particles are a function of their origin and processing in the boreal catchment area. Climate change in the Arctic is predicted to alter the landscape of boreal river catchment areas which will alter the flow path and composition of constituents entering the Arctic Ocean. It is therefore important to characterize the present day Fe-bearing particles and understand their origin, in order to predict future changes to the flux of bioavailable iron entering the Arctic Ocean.

The aim of this study is to characterise Fe-bearing particles in a major boreal river catchment area, the Lena River in NE Russia. Samples were collected in the main channel and major tributaries between 2012 and 2015 and span broad range in topography and permafrost extent. The aim of study i) was to characterise the Fe-bearing particle size and mineralogy. Firstly, size separation techniques were used to quantify the abundance of Fe in the operationally defined particulate (>0.22 µm), colloidal (<0.22 µm – 1 kDa) and dialysis (< 1 kDa) fractions. Thereafter, Transmission Electron Microscopy (TEM) and Scanning Transmission X-ray microscopy (STXM) were used to characterize the mineralogy of the Fe-bearing particles and a sequential extraction of the particulate fraction was applied to quantify the identified Fe particles. Future studies ii) and iii) will use Fe isotope ($\delta^{56}Fe$) analysis of the identified Fe-bearing particles alongside bulk geochemical analysis of the particulate and dissolved fraction, to determine how the origin of Fe-bearing particles varies with space and time in the Lena River catchment area. Overall, these findings will contribute towards an understanding of present day land to ocean Fe transport in this understudied region that is subject to significant future climate change.

En av de viktigaste mikronäringsämnen för primärproduktionen i havet är järn. Artiska oceanen påverkas kraftigt genom tillflödet från kringliggande boreala flodar som justerar tillförda mängden av både vanliga och mikrnäringsämnen. Järn transporteras huvudsakligen som små partiklar. Storleken och mineralogi av dessa partiklar bestämmer tillgängligheten på kontinentalsockeln. Järnpartiklarnas egenskaper beror på deras ursprung och processerna pågående i avrinningsområdet. Det förväntas att klimatförändringarna i Arktiset ska förändra avrinningsområdena som i sin tur ska förändras flödet och samansättningen av partiklar som tillföras Arktiska oceanen. Därför är det viktigt att beskriva nutida järnpartiklar och att bestämma deras urpsrung för att kunna sia framtidens förandringar i tillflödet av „bioavailable“ järn i Arktiska oceanen.

Syftet av den här studien är en beskrivning av järnpartiklar i ett stort boreal upptagningsområde, Lena floden i nordostliga Ryssland. Proverna samlades in under 2012 och 2015 på flodens huvudkanal och biflodar. Materialet täcker ett stort urval av både topografi och permafrost typer. Studiens första del fokuserar på partiklarnas storlek och mineralogi. Separationsteknologi användes för att kunna kvantifiera frekvenserna av partiklar och järn i lösning. Med hjälpen av STEM och STXM mineralogin av järnpartiklarna bestämdes. Kvantiteten av olika järnpartiklar i hela partikelformiga delen mättes med Sequential extraction. I blivande forskningsarbete ska göras en analys av järnisotoper ($\delta^{56}Fe$) i partiklar i partikelformiga (>0.22 µm) och kolloidala (<0.22 µm) andelen tillsammans med en geokemisk analys för att bestämma rumsliga och tidsmässiga variationer i partiklarnas ursprung inom Lena flodens upptagningsområde. På det hela taget ska denna studie förbättra vår nuvarande förståelse av particle transport i detta lite utforskade område som påverkas signifikant med kommande klimatförändringar.

Contents

Front cover photos (left top to right bottom): sunset reflections on the eastern shore of the Lena River; separation of iron from the particle matrix using column chromatography; ice break up on the Lena River; a 0.22 µm filter with river particles; giant blocks of fragile ice – sprawling the banks of the Lena River during spring flood; R/V Merelotoved moored at our northern most sample station, June 2013.

1. Introduction

1.1 Project overview

This aim of this work is to determine the composition, origin and transport of iron (Fe) - bearing particles in the Lena River, NE Russia (Fig 1.). Samples were taken between 2012 and 2015 in the main channel and in tributaries of different stream order from a wide latitudinal range that have varying topography, lithology and permafrost extent. While there have been some recent efforts at monitoring the flux of metals and DOC in Arctic rivers (e.g. Cooper et al., 2005; Escoube et al., 2015), these studies have been confined to a small number of closely spaced sample locations. Hence, there is still insufficient information to characterise the total Fe flux from the Lena River, or to quantify regional seasonal variations and differences between sub-basins with contrasting hydrology and permafrost cover. Increasing global temperature threatens to thaw the permafrost, changing the fluxes of river constituents, and so altering the biogeochemistry of the Arctic Ocean. It is therefore crucial to understand the present day system before assessing the response to changing climatic conditions. The studies outlined in this work are contributing to the Lena River project, which aims to broadly characterise the carbon and metal transport in the Lena River catchment area to gain a wide, integrated picture of the catchment sources.

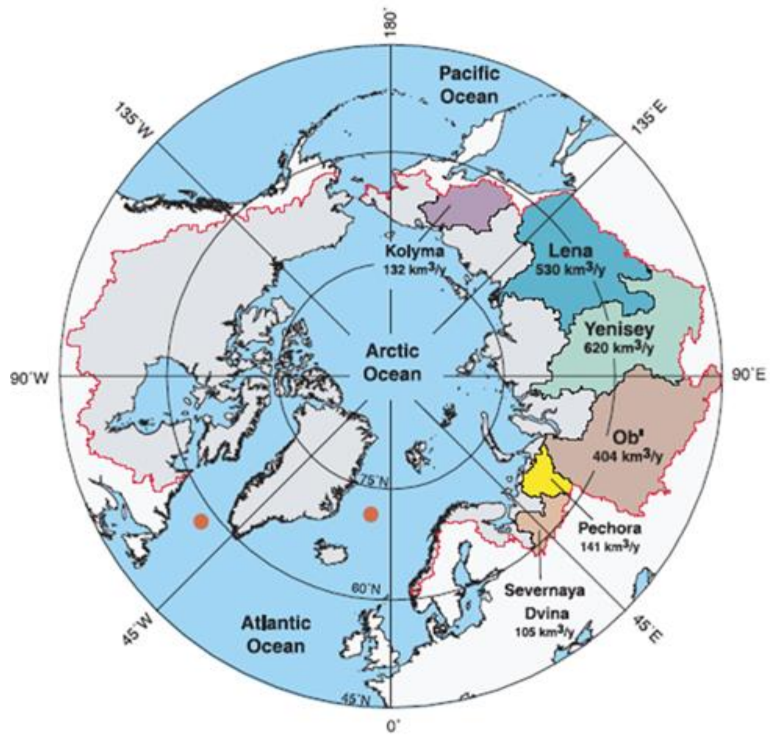

Fig 1. The Arctic Ocean and the surrounding landmass. The major boreal rivers catchments on the Eurasian landmass and their discharge into the Arctic Ocean are outlined.

1.2 The Boreal Zone

Vast areas of the Northern Hemisphere in Europe, Asia and North America are covered by Taiga and Tundra biomes and hold a huge stock of carbon in soil and litter (Tarnocai et al., 2009). Permafrost constitutes 24% of this northern hemisphere land (Zhang et al., 1999) and preserves vast reserves of organic carbon (OC). Siberia contains extensive permafrost and also contributes 50% of the entire river runoff to the Arctic Ocean (McLelland et al., 2012) via the Ob, Yenisei, Kolyma, and Lena Rivers (Fig. 1).

Permafrost is defined as any subsurface material that remains below 0 °C for at least two consecutive years (Zhang *et al*., 1999). Permafrost controls the distribution and routing of water across boreal river catchment areas (see summary by Woo et al., 2012), as outlined in the simplified cross section of permafrost across Alaska (Fig. 2). Permafrost can be subdivided according to aerial extent, as continuous (90–100 %), discontinuous (50–90 %), sporadic (10–50 %), or isolated patches (0–10 %). However, the thickness of permafrost is highly variable and can range from 800 m in continuous permafrost to < 10 m in sporadic permafrost (Anisimov and Reneva, 2006). The surface flow is confined to the active layer as this is the upper section of the frozen soil and bedrock that thaws in the summer months and refreezes in the autumn. Groundwater influx will contribute to the discharge in boreal rivers in regions of open talik (Fig. 2) and where supra and sub permafrost groundwater flow meets the surface (see summary in Woo., 2012). Enhanced surface temperatures across the Arctic (Fedorov and Konstantinov, 2003) have resulted in (i) increased seasonal active layer thickness in regions of permafrost that store substantial OC (Zhang et al., 2005; Romanovsky et al., 2007), (ii) increased river water temperature (Liu et al., 2005) (iii) increased river discharge (Peterson et al., 2002; Yang et al., 2002) and (iv) enhanced thermal erosion from the river banks (Costard et al., 2007). Therefore, future predicted temperature and precipitation increases are predicted to alter the origin and flow path of constituents in boreal rivers (Stein et al., 2000). In this study, we characterize Fe-bearing particles in order to determine their origin and transport in a boreal river catchment area.

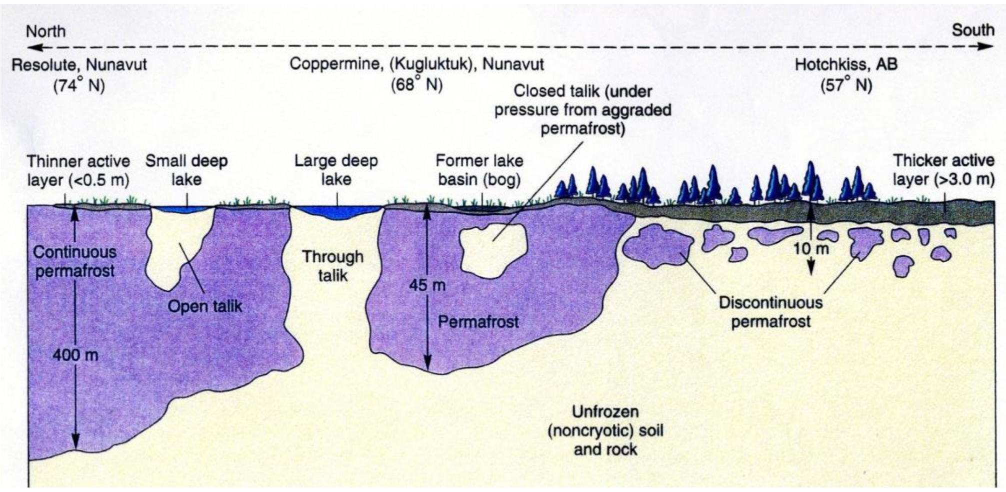

Fig. 2 A simplified cross section of permafrost characteristics across a north – south profile in Alaska. The continuous permafrost in the north, becomes discontinuous to the south. Christopherson, 2003.

1.3.1 Overview

Iron (Fe) is the 4th most abundant element in earth's crust (4.3 wt% as Fe) and has four naturally occurring stable isotopes: ^{54}Fe (5.84%), ^{56}Fe (91.76%), ^{57}Fe (2.12%), ^{58}Fe (0.29%). Iron is a key requirement for metabolic processes and is therefore a limiting nutrient for primary production in the oceans (Wells., 1999). Iron enters the ocean via rivers, aeolian dust, ice-rafted sediments and by hydrothermal vents at the sea floor (see review in Raiswell and Canfield 2012). Iron commonly occurs as soluble Fe^{2+} in oxygen poor environments and Fe^{3+} in oxygen rich environments. Nonetheless, Fe^{3+} rapidly forms Fe oxides and is therefore poorly soluble in aqueous systems and Fe is only present in trace levels in the ocean (Boyle et al., 2005). Further, estimates of the residence time of Fe in the oceans range from 70 – 270 years (Bruland et al., 1994; Bergquist and Boyle, 2006a), shorter than the mixing time of the ocean. Hence the concentration of Fe in the ocean varies because the influx of Fe to the world's oceans is not uniformly distributed (Boyle 1997). Subsequently, an enhanced or reduced flux of bioavailable Fe to the ocean can alter the extent of primary production and atmospheric carbon dioxide sequestration (Field et al., 1998). For example, a study of glacial and interglacial climate conditions (Marz et al., 2012) observed a higher Fe input from Arctic rivers during an interglacial, which resulted in greater Arctic Ocean primary productivity and carbon burial. Rivers transport a large amount of Fe, but the river to ocean flux is limited by the removal of Fe in estuaries (see review in Sholkovitz et al., 1976). The supply of Fe-bearing particles (larger particles and smaller colloids) from river to ocean is three orders of magnitude greater (Martin and Maybeck, 1979; Poulton and Raiswell, 2002) compared to Fe supplied in dissolved form. Fe-bearing particles will sediment on the continental shelf and can contribute to the flux of bioavailable Fe released from shelf sediments (Moffett., 2001).

1.3.2 Size and mineralogy of iron particles

The solubility of Fe-bearing particles in the ocean is a function of their mineralogy (Schroth et al., 2009). For example, ferrihydrite is a highly reactive nanoparticulate iron oxide that is metastable and formed by the rapid oxidation of Fe^{2+}. In contrast, haematite is a highly crystalline Fe oxide, which forms from recrystallization of ferrihydrite (Cornell and Schwertmann, 2003), to form closely spaced octahedral layers of atoms (Cornell and Schwertmann, 2003). Haematite and ferrihydrite have highly contrasting solubility's; however both can be evident as particles in a river (Raiswell et al., 2008). The shuttle of Fe-bearing particles from continental shelf sediments to ocean includes both i) young reactive nanoparticles formed from oxidation of microbially reduced Fe^{2+} and ii) resuspended micron sized lithogenic particles, of lower reactivity and derived from the weathering processes on land (Lam et al., 2012). Therefore, both primary and secondary mineral Fe-bearing particles can contribute to ocean "fertilization", though with varying efficiency. Further competitive ligand exchange studies (see review in Raiswell and Canfield, 2012) suggest that the surface properties of Fe-bearing particles are controlled by organic carbon (OC). Raiswell and Canfield (2012) highlight two end members (Fig. 3): i) Fe absorbed to OC and ii) Fe coprecipitated with OC. They propose that Fe coprecipitated with OC will have very different surface properties to Fe that is absorbed to the surface of OC. However, these phases are often nano particulate (e.g. ferrihydrite nanoparticles of 2-10nm) and their intimate association with organic carbon makes them difficult to characterise using conventional filtrations and microanalysis techniques. This study aims to characterise the mineralogy of Fe-bearing particles and their association with OC in the Lena River, in order to understand their trajectory across the salinity gradient of the Laptev Sea estuary and subsequent speciation and bioavailability of Fe in the Laptev Sea.

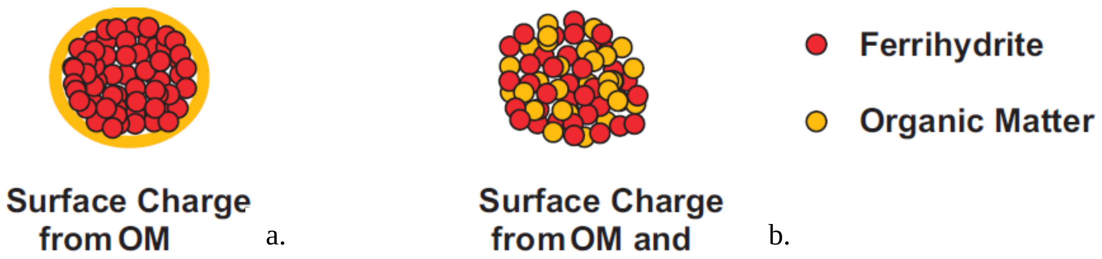

Fig.3 a and b End member characteristics of nanoparticulate iron – organic carbon association. In 3 a. the OC is surrounding the ferrihydrite (absorbed to the surface). Whereas is 3b. the OC is coprecipitating with the ferrihydrite. Adapted from Raisewell and Canfield, 2012. Geochemical Perspectives.

Previous studies of Fe in boreal rivers have used a variety of size separation techniques including membrane filtration, ultrafiltration and dialysis (Ingri et al., 2000; Pokrovsky and Schott 2002; Pokrovsky et al., 2005; Ingri et al., 2006; Bagaard et al., 2010; Vasyukova et al., 2011; Illina et al., 2013) to analyse the composition of Fe-rich particles and their association with trace elements (TE) and organic carbon (OC). These studies focused on the dissolved (< 0.22 μm or < 0.45 μm) fraction in boreal rivers and suggest that Fe is either in the form of Fe (oxyhydr) oxides or Fe-OC coprecipitated complexes (Ingri et al., 2000). Recent work using iron isotopes (Ilina et al., 2013) suggests that Fe also complexes with OC at smaller (<1 kilo Dalton (kDa)) size fractions. Nonetheless, observations of Fe-OC association have been mainly made in low to medium order Boreal Rivers with high OC concentration and low pH (see review by Stolpe et al., 2013).

However, in larger rivers, for example the Amazon River, the role of siliclastic weathering in the source mountains and supply of primary and secondary Fe particles (Benedetti et al., 2003; Allard et al 2004) outweighs the supply of Fe-OC complexes from the organic rich Negro River (dos Santos Pinhiero et al., 2014). On a catchment scale, the iron isotope (δ^{56}Fe) signature is dominated by Fe-bearing particles derived from siliclastic weathering in the mountainous source region (Poitrasson et al., 2014). However, the mineralogy of Fe-bearing particles and their association with OC is less understood in major Arctic River catchments but is crucial when seeking to understand the origin and fate of Fe in the Arctic Ocean. In this study we employ the size separation scheme outlined in Fig.4. Transmission Electron Microscopy (TEM) is used to identify the mineralogy of primary and secondary Fe minerals. Further, Scanning Transmission X-Ray Spectroscopy (STXM) is used to identify the oxidation state of Fe in the particles and identify their association with OC. The secondary mineral Fe is quantified by a one-stage sequential extraction, using weak HCl. Finally, the mineralogy and quantity of Fe particles is compared with pH and organic carbon concentrations in the Lena River and major tributaries.

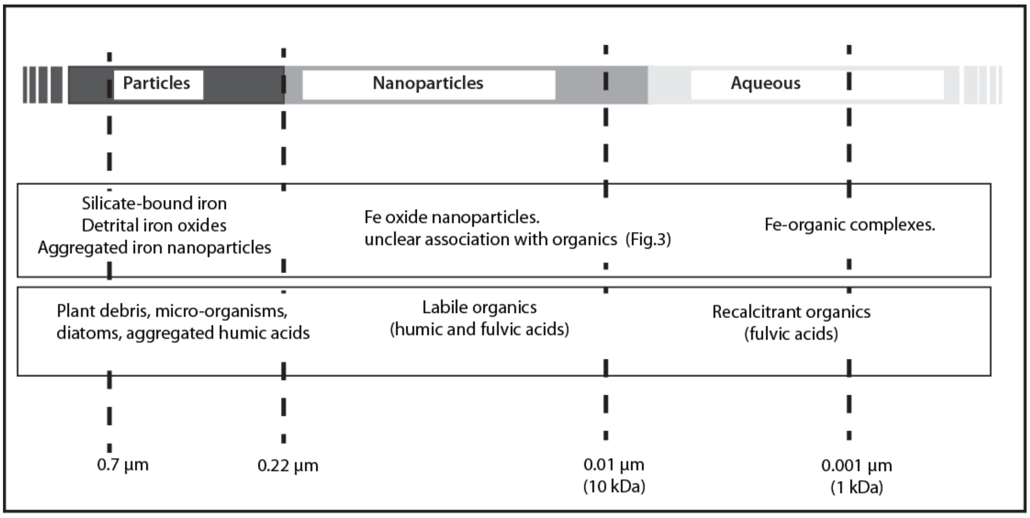

Fig. 4 Iron and organic carbon size separation scheme used in this study. Iron was separated at 0.22 µm, 10 kiloDalton (kDa) and 1 kiloDalton (KDa). Organic carbon was separated at 0.7 µm, 10 kiloDalton (kDa) and 1 kiloDalton (kDa). The hypothesized Fe and OC particles for different size fractions are outlined.

Outline of studies

The following manuscript is included in this work:

i) **The composition, mineralogy and size distribution of iron particles in the Lena River and major tributaries.** Samples were collected in the post-spring flood period (July 2012, June 2013).

The following future studies are described, in brief:

ii) **Spatial variation in the iron isotope composition of particles in the Lena River and major tributaries.** Samples were collected in the post-spring flood period (July 2012, June 2013).

iii) **Temporal variation in iron isotope composition of Lena River particles: from winter baseflow to spring flood.** Samples were taken during summer base flow (2012), winter base flow (2012-2013), ice break-up (2015) and spring flood (2015)

2. Sample Area

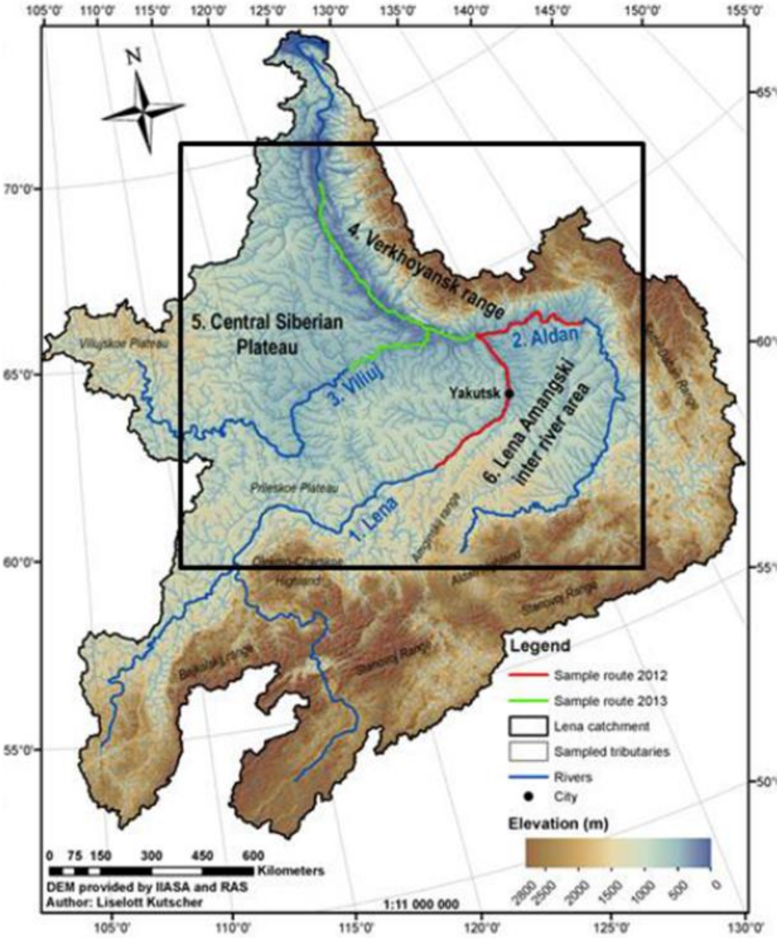

Fig. 5 The Lena River catchment area. Sampling routes from July 2012 and June 2013 are outlined. The catchment area spans a wide range in elevation: mountains in the south and east and lowlying plateau in the north and west of the catchment area. The Lena River and two major tributaries (the Aldan River and Viliuj River) are outlined. Figure also included in manuscript 1 (11.1) Author: Liselott Kutscher

2.1 Climate and hydrology

The Lena River is 4260 km long (Fig. 5) and has a catchment area of 2.5 million km^2 (Rachold et al., 1996) The river enters the Arctic Ocean via the Laptev Sea NE Russia (Fig 1) and has an annual freshwater discharge of 581 km^3 (Amon et al., 2012), second only to the Yenisei in its contribution to the Arctic Ocean. The Lena River catchment is subject to long cold winters (with an average winter temperature of -45 to -50°C from November to March) and short hot summers (with an average temperature of +30°C to +35°C from June to August) (Rachold et al., 1996). The average annual precipitation in the Lena River catchment is 330 mm, with 70 – 80% occurring during the summer (Gordeev and Siderov, 1993). The hydrological year can be divided into four major periods: (i) winter base flow, (ii) spring snowmelt, (iii) spring flood (iv)summer - autumn base flow. The discharge is lowest during the winter months and highest in spring, though exact timing depends on the latitude and altitude of the sub-basin (Rachold et al., 1996).

2.2 Permafrost

The whole Lena River basin is underlain by permafrost, this is discontinuous in the south (thickness 25-100m) and continuous in the north (thickness 100-200m) (Gordeev and Siderov, 1993). The permafrost thickness reaches 400-600m in the Vilyui lowlands. The active layer varies between is 1.4 – 2.5m deep for sandy/clayey soils and 0.6 – 0.8m deeps for peat bog soils (Huh and Edmond, 1998). Thermokarst lakes and bogs are prevalent in the northern lowlands (Gordeev and Siderov, 1993). The permafrost is mainly composed of cryogenic mineral soils (Tarnocai et al., 2009). However, there is extensive Yedoma in the Lena River catchment area, as much as 35.7 percent of the land area based on the Quaternary geological maps of central Yakutia (Grosse et al., 2013). The Yedoma is mainly found in low-lying regions adjacent to the main channel (Romanovskii, 1993). Yedoma are periglacial deposits from the late Pleistocene glacial period that consists of very large syngenetic ice wedges and intrasedimentary ice. Yedoma contain deep and frozen soil carbon pools, which remain understudied (Vonk et al., 2015).

2.3 Geology

This study subdivides the data according to the regional geology (Fig.6). These subdivisions are outlined in Table 1 (Manuscript 1, Supplementary Information). The geology of the Lena River catchment area is outlined in detail by Resources of surface waters of the USSR (1972).

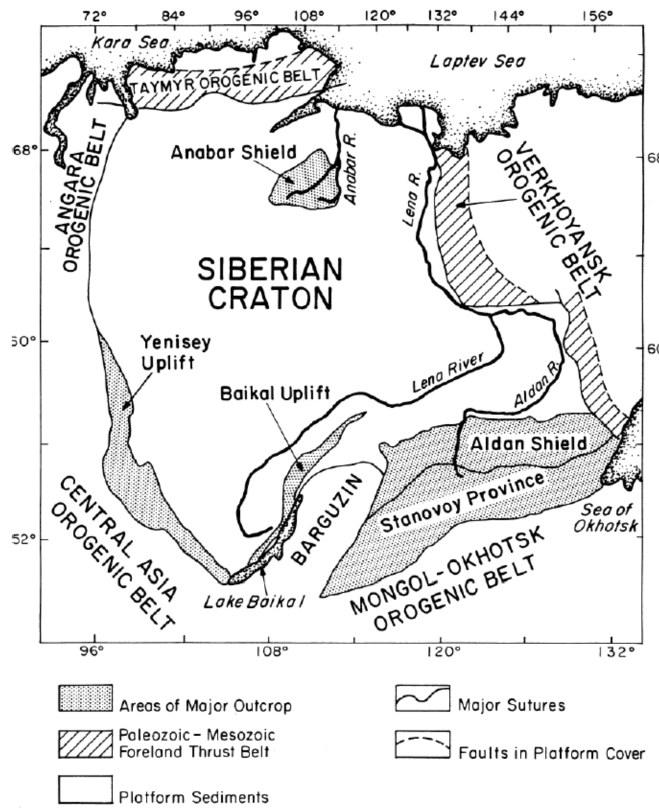

Fig. 6 Geotectonic map of the Siberian Craton which shows the outcropping Precambrian basement rock. The Baikal Uplift and Barguzin terrain are together referred to as the Trans Baikal Highlands (Table 1) and the Stanovoy Province and Aldan Shield are referred to as the Southern Mountains (Table 1). The Verkhoyansk Mountain Range is referred to as the Eastern Mountains (Table 1). Rosen et al., 1994, adapted by Huh and Edmond, 1998.

In summary, the central part of the Lena River catchment area is made up of a low lying plateau (*central plateau*) that is composed of Mesozoic terrigenous sediments of Jurassic to Cretaceous age; these are predominantly carbonate and evaporite karst. Quaternary alluvial deposits, preserved to form Yedoma permafrost (Gordeev and Siderov, 1993) overlay the Mesozoic sediments in the south and east of the plateau and can be observed along the banks of the Vilyuy River, the largest tributary draining the central plateau. The source of the Lena River is in the Trans Baikal Highlands, which lie to the south west of the central plateau. These highlands are composed of Proterozoic schist, gneiss, quartzite and marble. The central plateau is bordered in the south the Stanovoy Mountains and South Aldan Shield, (*southern mountains*). These mountains are composed of Archean and Proterozoic metamorphosed rocks. To the north-east, the central plateau is bordered by the Verkhoyansk Mountain Range, (*eastern mountains*) composed of Carboniferous and Permian terrigenous sediments and Mesozoic volcanic plutons. The Aldan River enters the Lena River from the southeast and drains the Stanovoy Mountain Range, South Aldan Shield and Verkhoyansk Mountain Range (*southern mountains* and *eastern mountains*). A vast delta, 500 km wide, separates the Lena River from the Laptev Sea.

3. Field sampling

The periods of field sampling and 2012 to 2015 river hydrograph (measured at Kursur) are outlined in Fig.7.

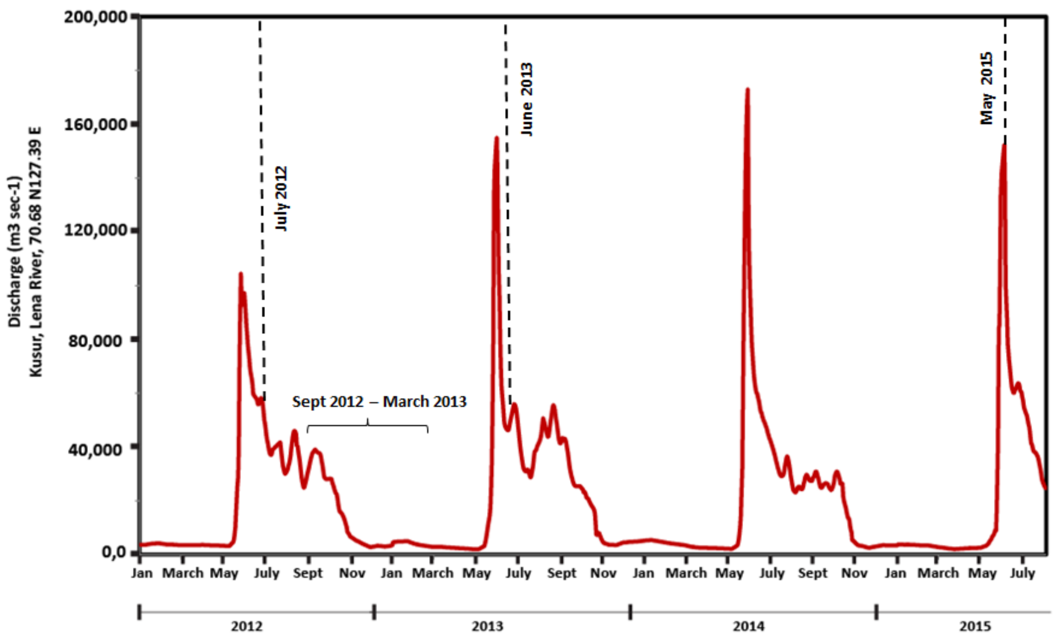

Fig. 7 Hydrograph showing the Lena River discharge from January 2012 to July 2015. The discharge was measured daily at Kursur, near the mouth of the Lena River (70.68 N, 127. 39 E). The sampling periods are outlined on the graph. Data is from the Arctic Great Rivers Observatory (NSF-1107774).

All sampling and analytical equipment were acid washed using 0.5M HNO_3 and deionised water. All acid washing and sample analysis was conducted in Class 100 laminar flow hoods. Mineral acids from Seastar® and 18MΩ grade deionised water from a MilliQ® system was used throughout preparations and analysis. The pH of the water was measured in *situ* using an YSI 556 multi probe system (MPS) calibrated against NIST buffer solutions (pH 4, 6.5 and 9 at 25°C) with an accuracy of ± 0.03 pH units. Water temperature (accuracy: 0.1°C) and conductivity (accuracy: 1 uS/cmC) were also measured with the same probe. Sample positions were taken using a hand-held global positioning system (GPS) receiver.

3.1 Spatial sampling

River water samples were collected at 77 locations in July 2012 and June 2013. Fig. 8 shows the sampling locations for samples in study 1 and 2. The samples were collected from the surface water using a plastic bucket from either the upstream side of the main river vessel or by using a small motorised boat. The water was transferred to 10 L HDPE containers.

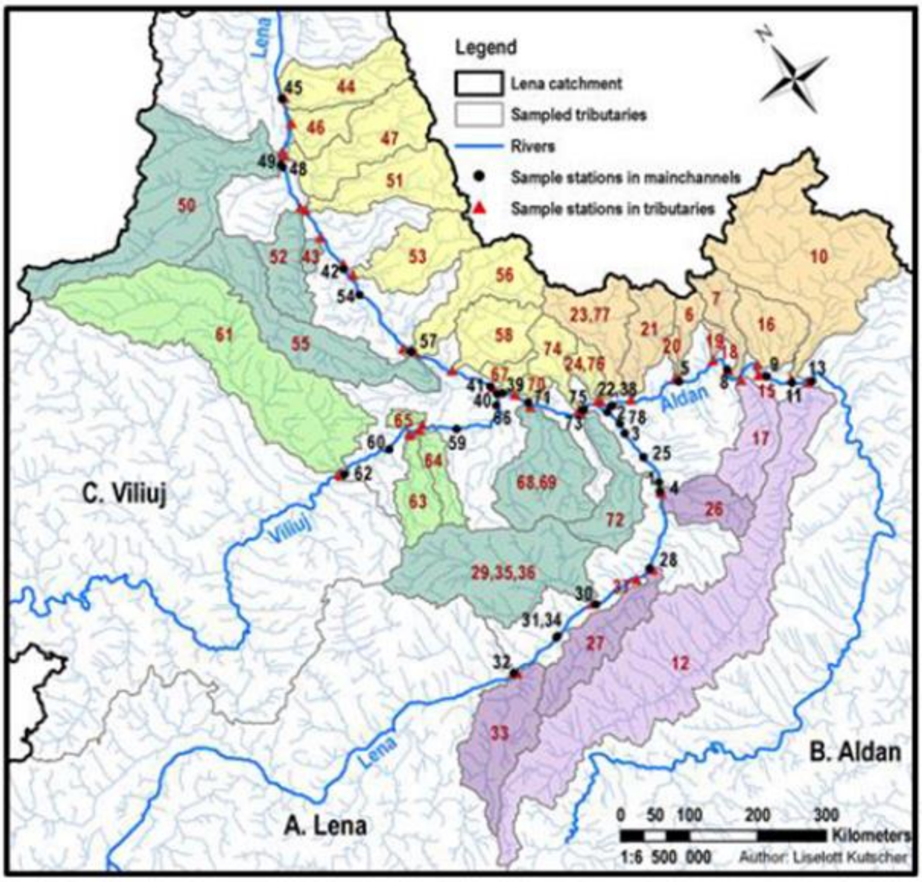

Fig. 8 Main channel and tributary sample stations from July 2012 and June 2013. The sample numbers correspond to those in Table 3, Supplementary Information. Figure also included in manuscript 1, (11.1). Author: Liselott Kutscher

3.2 Temporal Sampling

River water samples were collected every month (apart from January) from September 2012 to March 2013, in Yakutsk. Further, river water samples were collected at Tabaga gauging Station (Fig. 9b), 30km south of Yakutsk (Fig. 9a) between May 6th 2015 and May 28th 2015. This location is draining a catchment of 897,000 km^2, which contributes about 42% of the basin flow at the mouth of the Lena River (Ye et al., 2003; Tananaev., 2016) Samples were collected every three days, from the river bank.

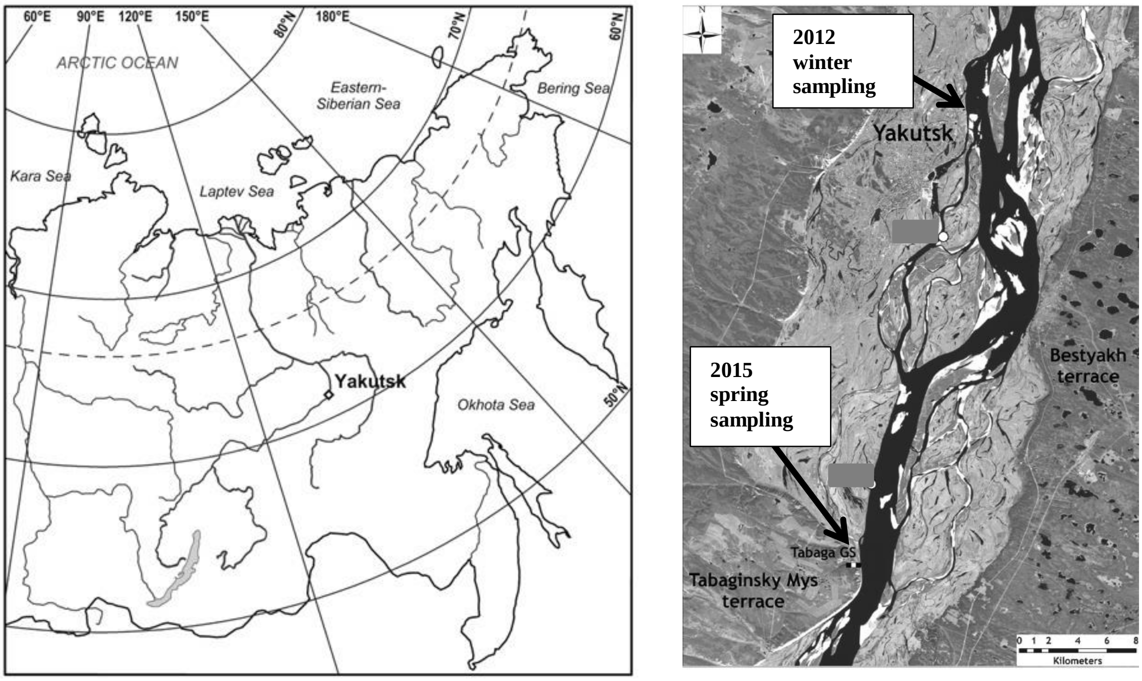

Fig. 9 a Outlined is a map of north-west Russia. Yakutsk, on the Lena River, is highlighted. Winter samples were taken at Yakutsk in 2012. Spring samples were taken at Tabaga gauging station which is highlighted on the Landsat Image (September 2015) in Fig.9b 30km south of Yakutsk. These maps are adapted from Tananaev et al., 2015.

4. Sample processing and analysis

4.1 Size separation techniques

The collected waters were filtered within 3 h through 0.22 µm nitrocellulose filters (Millipore®) with diameter of 142mm. The filters were prewashed in 5% acetic acid for 72 hours (Odman et.,al 2006) and subsequently rinsed in ultrapure (MilliQ®) water for a week. Filtrations were carried out using silicon tubing and a Masterflex® portable peristaltic pump connected to a Geotech® polycarbonate filter holder. The first 200ml was systematically discarded and the filtration unit was rinsed with

MilliQ® water between each sample. The filters were frozen (-18 °C) immediately after filtration. Water samples were refrigerated (+8 °C) on board the vessel and acidified to pH 2, with 8M HNO_3 seastar®, three weeks after sampling.

Dialysis was used to separate the colloidal fraction from the aqueous dissolved fraction. The dialysis technique has been previously used in preference to ultrafiltration (Gasser et al., 1994, Apte and Rogers, 1993) and is now a common size separation technique used in boreal river studies (Pokrovsky et al., 2011; Vasyukova et al., 2012; Illina et al., 2013; Pokrovsky et al., 2015) allowing our work to be directly comparable. This study followed the procedure outlined in Pokrovsky et al., (2011), which is summarized in Study 1 Manuscript (Appendix 1). Dialysis membranes with a molecular weight cut-off (MWCO, the lowest molecular weight solute in which 90% of the solute is retained by the membrane) of 1 kilo Dalton (kDa, 1000 MWCO)) and 10 kilo Dalton (kDa, 10000 MWCO) from Spectrapore® were used, as outlined in Fig).

4.2 Chemical separation and particle digestion

Iron fractions	Size fraction	Separation Technique	Symbol
Particulate	Fe >0.22µm	Microwave dissolution of 0.22µm filter	$\mathbf{[Fe]_{particulate}}$
Leach	Fe >0.22µm	Addition of 0.5M HCl to a 0.22µm filter, 24 hours, room temperature	$\mathbf{[Fe]_{leach}}$
Residual	Fe >0.22µm	Microwave dissolution of 0.22µm filter after leach	$\mathbf{[Fe]_{residual}}$
Dissolved	Fe <0.22 µm	Membrane filtration, 0.22µm filter	$\mathbf{[Fe]_{dissolved}}$
Colloidal	<0.22µm < Fe > 1 kDa	Fraction of Fe that does not pass through < 1 kDa dialysis membrane	$\mathbf{[Fe]_{colloidal}}$
Dialysis	Fe < 1 kDa	Dialysis filtration, 1 kDa dialysis membrane, 72 hours, room temperature	$\mathbf{[Fe]_{dialysis}}$

Table 2. Outline of the iron size and chemical fractions in this study. Each fraction is allocated an abbreviated name in this study.

Particulate material from 36 sample stations was analyzed. Details of this analysis are outlined in Fig 3 of the manuscript (11.1) and Table 2 outlines the chemical and size separation subdivisions referred to in this study. Two filters were analyzed from each station, unless otherwise outlined. One filter underwent total dissolution to determine the $[Fe]_{particulate}$. The second filter was leached using 0.5M HCl at room temperature for 24 hours (Leventhal and Taylor 1990; Lam et al., 2006; Lam and Bishop 2008) to separate the secondary mineral Fe – amorphous and crystalline Fe oxides. This is equivalent to a 24 hour extraction using Na-dithionite (Leventhal and Taylor 1990) and has been used in more recent iron isotope studies (Rouxel et al., 2005; Severmann et al., 2006; Fehr et al., 2008). The amorphous and crystalline Fe oxides are termed $[Fe]_{leach}$ and the remaining siliclastic Fe is termed $[Fe]_{residual.}$ The chemical separates are analyzed with the caveat that sampling protocols may alter the ratio of $[Fe]_{leach}$ / $[Fe]_{residual}$ (i.e. 0.5 M HCl leaching may dissolve some clay mineral bound Fe and overestimate the size of the $[Fe]_{leach}$ pool; also the process of filtration (0.22 µm) may trap some colloid size Fe particles, resulting in an underestimation of the $[Fe]_{dissolved}$ pool. Therefore, the method of quantifying Fe in different size fractions must be used as a general indicator and not a precise measurement.

4.3 Major and Trace Element analysis

Major and trace element (TE) concentrations were measured on the water and dissolved filters within 6 months of sample collection. The major element analysis was done on an ICP-OES (Thermo ICAP 6500 Duo). The detection limit for all major elements was approximately 1 ppb or better and precision of measurements were ±5%, estimated from measurements of NIST 1640a. Trace element analysis was done using a single collector Element ICP-MS (Nu Instruments). The detection limit was 0.1 ppb for Fe. The international geostandard SLRS-5 (Riverine Water Reference Material for Trace Metals) was used as an external standard. A good agreement was obtained between replicated measurements of SLRS-5 and certified values for ICP-OES and ICP-MS analysis (relative difference < 5%, n = 3). DOC were determined by high-temperature catalytic oxidation (Shimadzu TOC-VCPH) at the Department of Applied Environmental Science, Stockholm University (0.7 µm) and Abisko Research Station (10 kDa and 1 kDa), with a detection limit of 0.1 mg/L and uncertainty in measurement varying from 0.1 to 2.0 mg/L.

4.4 Scanning Transmission Electron Microscopy

Scanning Transmission Electron Microscopy (STEM) is a technique where electrons of certain energy are directed at a particle of interest, using an electromagnet. The electrons hit the particle and are then focused onto a fluorescent screen, which in turn generates an image of the particle in different amounts of darkness, depending on the difference in density (http://www.britannica.com/technology/transmission-electron-microscope). Electron diffraction patterns can be taken of a desired region in the particle of interest. Electrons of certain energy are directed at the area and the electrons are diffracted according to the spacing of atoms. The resulting diffraction pattern corresponds with a certain atomic structure and therefore particle composition. These techniques have been used previously to characterize particulate material in river systems (Benedetti et al 2003; Allard et al 2004), especially in the identification of Fe oxides, such as ferrihydrite (e.g. Banfield et al., 2000) and clay mineral (Raiswell et al., 2006). In this study, STEM was used to analyze

(i) Particles collected on the 0.22 µm nitrocellulose filters;
(ii) Particles in the < 0.22 µm water.

In total, 10 samples were analysed using TEM (7 in the >0.22 µm fraction and 3 in the < 0.22 µm fraction). Little aging of Fe oxides was expected since collection as the half-life of transformation to crystalline forms is > 500 days when refrigerated or frozen (see Hawkings et al., 2014). The full method of analysis is outlined in Manuscript 1 (Supplementary Information, 11.1). In short, all samples were imaged and analyzed using a FEI Tecnai F20 200 kV FEGTEM fitted with a Gatan Orius SC600 CCD camera and an Oxford Instruments X-Max 80 mm2 EDX SDD running INCA software. Scanning Electron Diffraction patterns (SAED) were acquired for the particulate material but no usable patterns were collected for the <0.22 µm filtered water due to the very small particle size and interferences with the silicon nitride film.

4.5 X-Ray Spectroscopy

In this study we apply Fe L-edge Scanning Transmission X-Ray Microscopy (STXM) on particulate material from the (i) main channel, (ii) central plateau tributaries and (iii) eastern mountain tributaries on the soft X-ray beamline 108 at Diamond Light Source (Harwell Science Park, UK). The sample preparation and analysis is outlined in Manuscript 1 (Appendix 1).

The principle aim of this work was:

(i) Characterise the iron particles using X-Ray Absorption Near Edge Structure (XANES) spectroscopy to confirm the identification of iron particle, made using STEM.

(ii) Characterise the Fe –OC association, using X-Ray diffraction (XRD) and STXM elemental mapping techniques.

X-Ray Absorption Near Edge Structure (XANES) spectroscopy is an element specific spectroscopy method (see summary by Brown & Calas, 2013). X-Rays of sufficient energy are absorbed by a core-level (1s electron) in the “target” atom of a region of interest. The excited electron becomes a photoelectron and is ejected. The resulting spectra (as seen in Fig. 9, Supplementary Information, 11.1) is caused by the interference of the photoelectron as it travels from the absorbing atom: the photoelectron scatters off the surrounding first shell ligands which results in a backscattering of photoelectron waves that interfere constructively and destructively with the outgoing photoelectron waves from the absorber. The interference is dependent on the number, type and position of atoms. The resulting XANES spectra are a measure of the intensity of interference and energy of the initial X-Rays. Synchrotron X-ray sources are needed to produce sufficient signal to noise spectra in reasonable time periods. In this study, XANES spectra are supported by X-Ray diffraction (XRD) mapping of a broader, micron size region of the Fe particles and associating organics.

4.6 Iron isotope analysis

The iron isotope composition was measured on 60 samples (particulate, residual, leach and colloidal fractions) for study (ii). Further, 48 samples from the winter base flow and spring flood for study (iii). Iron was purified from the matrix particulate material using anion exchange chromatography. One ml of Bio Rad AG-MP1 100 - 200 mesh anionic resins was loaded into columns and the resin was washed with 3ml MilliQ™ water and preconditioned with 4ml 10M HCl. The sample was loaded in 1ml 10M HCl. A further 4ml 10M HCl was added to the column. The matrix was eluted using 6.5 ml 5M HCl and iron was then eluted with 2ml 1M HCl. The purified iron samples were analyzed in 0.3M HNO_3 solutions.

The Fe isotope analyses were performed with a Nu Plasma II HR-MC-ICPMS (Nu Instruments) at the Swedish Museum of Natural History (Vegacenter) in wet plasma solution mode. The main challenge in analyzing iron isotopes is to separate the mass-peak of the Iron isotopes ($^{54}Fe^{+}$, $^{56}Fe^{+}$ and $^{57}Fe^{+}$) from polyatomic interferences such as $^{40}Ar^{14}N^{+}$, $^{40}Ar^{16}O^{+}$ and $^{40}Ar^{16}O^{1}H^{+}$. This was achieved in pseudo-high-resolution mode with a 50µm defining slit with a resolving power M/ΔM of approximately 6500-7500 (ΔM is defined as $M_{0.95} - M_{0.05}$ where $M_{0.95}$ and $M_{0.05}$ are measured at 5% and 95% of the peak height). Measurements were then carried out on the interference free shoulders of the Fe peaks (Fig.11).

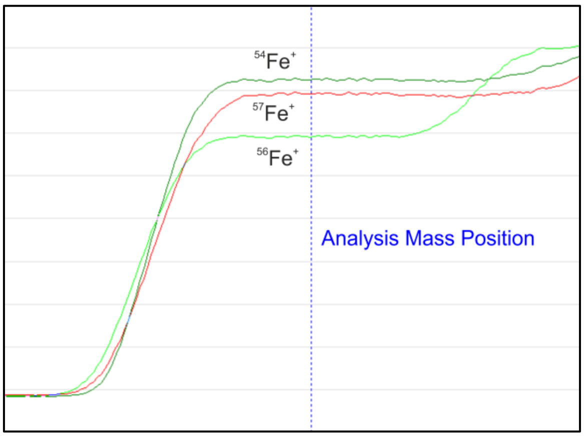

Fig.11 Interference free shoulders of the Fe peaks.

Instrumental mass fractionation was corrected by the standard-sample bracketing technique, where each sample is referenced to an IRMM-14 standard that is measured before ('std1') and after ('std2') each unknown. All analyses are reported in delta notation relative to the IRMM-14 standard, expressed as $\delta^{56}Fe$, which represents the deviation in per mil relative to a reference material:

$$\delta^{56}Fe\ (‰) = \left(\frac{(^{56}Fe\ /\ ^{56}Fe)_{sample}}{(^{56}Fe\ /\ ^{56}Fe)_{IRMM\text{-}14}} - 1 \right) * 1000$$

Both δ^{56}Fe and δ^{57}Fe were measured; however since the relationships between δ^{56}Fe and δ^{57}Fe of the samples plot on a single mass fractionation line (Fig. 12), only δ^{56}Fe are presented in this study. The concentration of standard and samples were matched, in most cases deviating between less than 20 % although no effect on results could be noticed having larger differences. This supports observations previously made by Schoenberg and von Blanckenburg (2005) and Dauphnas et al. (2009). The external reproducibility 2σ (2σ = 2SD) for standard solutions (BCR-2, IRMM-14, Alfa Aesar (inhouse), FeCl (inhouse)) measured with the standard-sample bracketing technique was on average 0.08‰ for δ^{56}Fe and 0.10‰ for δ^{57}Fe for both wet plasma mode and with the Apex Q. The accuracy of the measurements was monitored by measuring the standard Alfa Aesar at the beginning of each sequence. This standard has been repeatedly measured over the time of 6 months and gives consistent values for δ^{56}Fe and δ^{57}Fe (δ^{56}Fe = 0.15 ± 0.08 (2σ) and δ^{57}Fe = 0.24 ± 0.13 (2σ); N = 49 on wet plasma; δ^{56}Fe = 0.17 ± 0.08 (2σ) and δ^{57}Fe = 0.24 ± 0.11 (2σ); N = 29 on the Apex Q) that agree with previous measurements that have been performed on the same standard with the Micromass Isoprobe at the Swedish Museum of Natural History ((δ^{56}Fe = 0.15 ± 0.10 (2σ) and δ^{57}Fe = 0.22 ±0.16 (2σ); N = 61; Fehr et al., 2008)

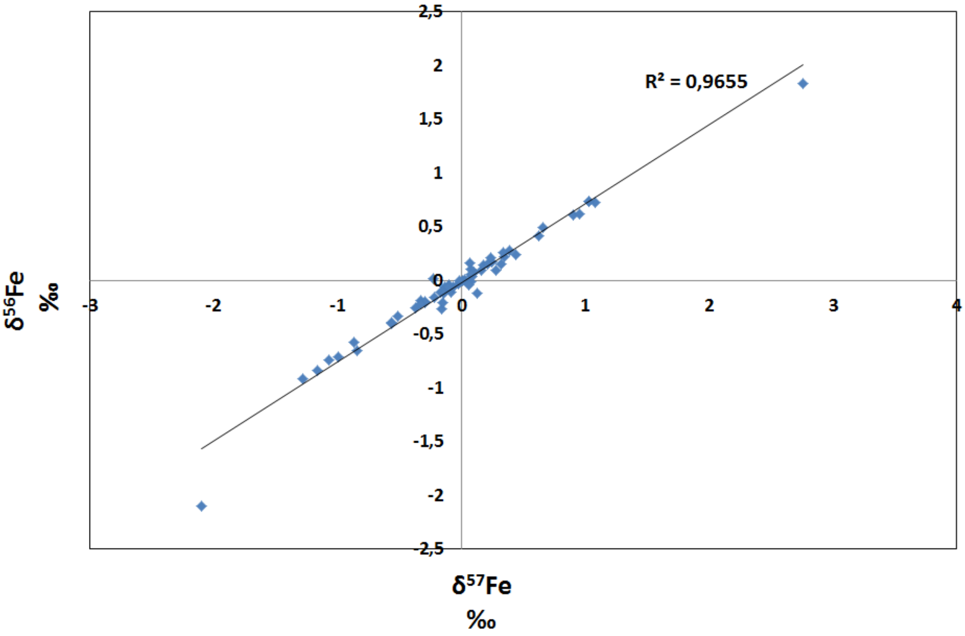

Fig. 12 The relationship between δ^{56}Fe and δ^{57}Fe in all 60 samples measured for Study (ii).

5. Results and Discussion

The results and discussion are presented in the manuscript (Appendix 11.1). A brief summary is given here:

5.1 Size and chemical distribution of Fe

On average 70% of Fe is $[Fe]_{particulate}$, this is consistent with other major global rivers (see summary by Viers et al., 2009) where Fe is mainly found in the suspended fraction. The sub catchments and main channel show little variation in average $[Fe]_{particulate}$. However, the proportion of $[Fe]_{residual}$ and $[Fe]_{leach}$ in the Fe particles is very variable across the catchment area. The $[Fe]_{leach}$ fraction contributes 44% (n =8, SD = 8%) of the $[Fe]_{particulate}$ in the Lena River and the $[Fe]_{leach}$ contributes 26% (n = 3, SD = 8%) of the $[Fe]_{particulate}$ in the Aldan River. In contrast, in the central plateau, $[Fe]_{leach}$ contributes 76% (n = 8, SD = 27%) of the $[Fe]_{particulate}$.

$[Fe]_{colloidal}$ contributes 92% of the $[Fe]_{dissolved}$ in the system as such $[Fe]_{dissolved}$ is referred to as $[Fe]_{colloidal}$. The Vilyuy River has the highest proportion of Fe in the < 1 kDa fraction, 11% of the total $[Fe]_{dissolved}$. In contrast, the remaining tributaries of the central plateau have 3% of the Fe in < 1 kDa fraction. The tributaries draining the central plateau contain the highest $[Fe]_{colloidal}$: 115 µg/L (n = 22, SD= 75 µg/L), whereas the eastern mountains contain the lowest $[Fe]_{colloidal}$ 44 µg/l (n=22 SD =28 µg/L). The $[Fe]_{dissolved}$ is also comparable with other Arctic rivers sampled at the same time of year, for example, a 0.22 µm filtered water sample from the Nizhniya Tunguska River (tributary of the Yenisey River) has $[Fe]_{dissolved}$ of 300 ug/L (Pokrovsky et al., 2006), whereas 0.22 µm filtered water samples from Severnaya Dvina river (draining into the White Sea basin), has $[Fe]_{dissolved}$ of 287 ug/L in May and 231 ug/L in June (Pokrovsky et al., 2010) and the Kalix River (Northern Sweden), where filtered water samples had $[Fe]_{dissolved}$ of 346 µg/l in early May and 119 µg/l in June (Ingri et al., 2000).

The contribution of $[Fe]_{colloidal}$ in the Lena River catchment area is greater than in the Amazon River (Allard et al., 2004), where 95% of the Fe is transported as $[Fe]_{particulate}$. However, in both the Amazon River and Lena River, >50% of the particulate material is transported as secondary formed Fe phases (Allard et al., 2004). In summary, the particle size distribution varies between major boreal and tropical rivers, but both boreal rivers and tropical rivers contribute a significant flux of secondary reactive Fe.

5.2 Iron particle mineralogy

The following Fe-bearing particles were identified using TEM: (i) Fe within the framework of clay minerals (ii) 10 nm wide nanocrystals of ferrihydrite (in the <0.22 μm fraction), (iii) 100 nm aggregates of nano crystalline Fe (in the >0.22 μm fraction) and (iv) detrital heamatite. Aggregates of nanoparticle ferrihydrite were observed in the $[Fe]_{colloidal}$ and $[Fe]_{particulate}$ fractions. The dominant Fe particles, in < 0.22 μm fraction, were 20-30 nm aggregates of 2-5 nm ferrihydrite particles. In the $[Fe]_{particulate}$ fraction, the dominant morphology of ferrihydrite aggregates is 100 – 200 nm wide spheroidal particles. These spheroids are also observed to aggregate to form micron sized ferrihydrite particles, which are mainly associating with the surface of clay minerals. Minor needle shaped, crystalline goethite was also observed. Haematite was only observed in $[Fe]_{particulate}$ from the eastern mountains. These observations are consistent with major tropical rivers, which show ferrihydrite to be the dominant secondary Fe mineral in the main channel (Benedetti et al., 2003; Allard et al., 2004) and studies of ice-rafted debris (Hawkings et al., 2014) and glacial-fed rivers (Raiswell et al., 2006) which have identified ferrihydrite as the reactive iron phase. This study also supports iron isotope (Ingri et al., 2006) and field flow fractionation (Stolpe et al., 2013) studies of iron-bearing particles in boreal rivers where it is suggested that Fe exists as nano-sized iron oxides in the colloidal fraction.

5.3 Iron – organic carbon association

Notably, >50% of DOC is found in the < 1 kDa fraction in all sampled water; whereas, the Particulate Organic Carbon (POC) constitutes the lowest proportion of the OC, <8% of the Total Organic Carbon (TOC) in all samples. For the eastern mountains, 63% of DOC is in the < 1 kDa fraction. However, for the Lena River and Aldan River, 37% and 34% of DOC is found in the < 1 kDa fraction, respectively. The central plateau and Vilyuy River contain an average of 56% of the DOC in the < 1 kDa fraction (n = 3). The central plateau contains the highest average DOC at 120 μg/L (n = 14, SD = 33 μg/L). In contrast, the eastern mountains contain the lowest average DOC at 36 μg/L (n = 22 SD =27 μg/L).

The size separation observations in this study can be compared with those made in smaller catchment areas underlain by permafrost. Fig. 13 provides an overview of the Fe and OC size distribution and composition in the Lena River and major tributaries. These observations are in contrast to studies of lakes and bogs in western Siberia show that up to 60 % of the $[Fe]_{dissolved}$ is found in the < 1 kDa fraction (Illina et al.,2013). In contrast, this study is consistent with major tributaries of the Yukon river (Stolpe et al., 2013) where only 5-16% of the colloidal Fe was in the 0.5 – 4nm size fraction, with the majority of the colloidal Fe in the >40nm size fraction.

The highest concentrations of OC are observed in tributaries draining the central plateau and the highest concentration of ferrihydrite are also observed in tributaries. Nonetheless, TEM has not identified any Fe-OC complexes in central plateau tributaries. Instead, the 20-30nm wide particles of ferrihydrite in the $[Fe]_{colloidal}$ fraction retained the amorphous ferrihydrite structure as seen in the $[Fe]_{particulate}$ particles. Further, TEM identified two main associations between POC and aggregated $[Fe]_{particulate}$ particles. In the central plateau, the spherical ferrihydrite aggregates were attached to the surface of primary produced OC, similar to the particles outlined in the Supplementary Information, 11.3. In contrast, in the eastern mountain tributaries, smaller aggregates of ferrihydrite, 30 – 50 nm wide (i.e. $[Fe]_{colloidal}$) were trapped within the network of OC. This association was investigated further using STXM. The sub rounded particles were observed to be Fe rich and dispersed amongst the POC. The XANES analysis identified these particles as ferrihydrite and therefore a separate entity from the POC. This association was observed multiple times in tributaries draining the eastern mountain range. Although the POC contributes a small percentage of the total OC, it may play a role as an absorption surface for $[Fe]_{colloidal}$ ferrihydrite in both the central plateau and mountain tributaries. Therefore, the POC is providing a surface on which ferrihydrite is attached or trapped. Hence, OC is only observed as a transporter of Fe particles in the sub-catchments of the Lena River, but the association between POC and ferrihydrite is no longer observed in the Lena River main channel, suggesting that processes of desorption or disaggregation are occurring when the tributaries meet the main channel, as has been previously observed at the Negro River – Amazon River confluence (dos Santos Pinhiero et al., 2014).

The pH of the river water plays a key role in the speciation of Fe particles and association with OC (Stumm and Morgan, 1996). The pH values in the Lena River catchment area span a range from 6.3 – 9.0 (Fig. 12). These values are within the low solubility range for ferrihydrite, which is at minimum between pH 7 and pH 8.5 (Stumm and Morgan, 1996). Neubauer et al., (2013) compiled data of Fe-OC complexation and pH from tropical, temperate and boreal rivers. The data showed that Fe-OC complexation decreases with increasing pH for all rivers. Further, results from modelling show a decrease in Fe-OC complexation from almost 100% at pH 4 to about 10% or less at pH 7 (Lofts and Tipping 2008). These observations are supported by data from Siberian Rivers (Vasyukova et al., 2012; Pokrovsky et al., 2011), which have used ultrafiltration and dialysis to separate the < 1 kDa fraction from the remaining OC. In summary, the pH range of the sampled main channel and tributaries in the Lena River catchment area is consistent with the formation of ferrihydrite, in preference to Fe-OC complexation.

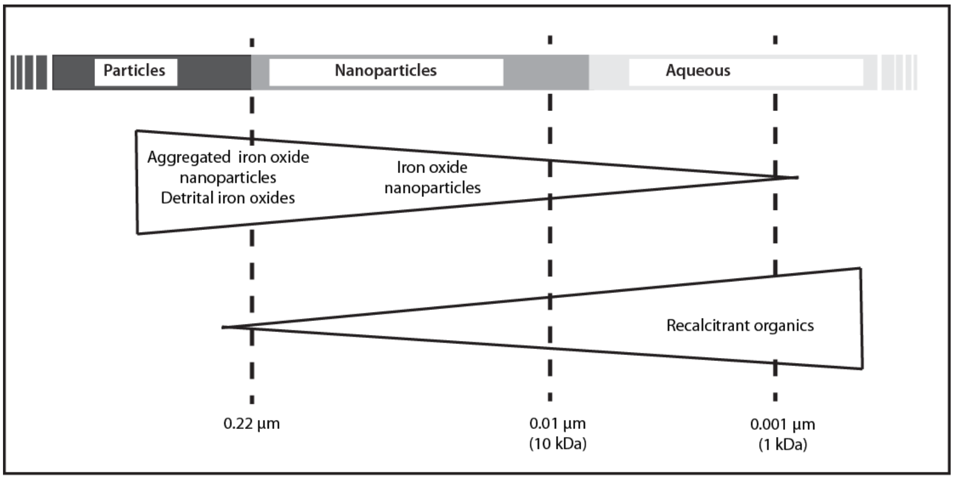

Fig. 13 Summarised conclusions about the distribution of Fe and OC in the Lena River main channel and major tributaries.

In summary, this study of a major boreal river shows that there is a notable difference in the association between OC and Fe between (i) low order streams within the sub catchments of major Boreal rivers and (ii) major tributaries and the main channel of major boreal rivers. We can suggest, based on the relationship between organic carbon size and reactivity (Amon et al., 1996), that larger particles of OC are more labile and degraded in the smaller sub catchments, which shifts the OC size range towards smaller fractions as observed in this study. This degradation may provide a mechanism for the increased formation of ferrihydrite (in Fe] $_{colloidal}$ and [Fe] $_{leach}$ fractions) in the central plateau, and requires further investigation (see Section 8). In summary observations suggest that the DOC in the smaller low to medium order tributaries may play a key role in determining the extent of ferrihydrite formation. However, the role of OC as a complexing agent and carrier of Fe is minimal in the Lena River and major tributaries. Previous work (Creed et al., 2015) has shown that OC reaches a point of "chemostasis" when transported from low to high order streams. In low order streams, the DOC sources are spatially connected to each other (Freeman et al., 2007). These smaller catchment areas are regions of extensive permafrost OC degradation (Vonk et al., 2013) for example in thermokarst lakes, which are extensive in the low-lying central plateau (Gordeev and Siderov., 1993). In contrast, in high order rivers such as the Lena River, the OC is disconnected from the processes occurring in regions of permafrost degradation. Unlike previous studies of iron particles in boreal catchments (Ingri et al., 2006; Pokrovsky et al., 2005; Dahlvqvist et al., 2007; Vasyukova et al., 2012; Illina et al., 2013), the Lena River main channel and tributaries are greater than 100 m to 1 km wide and so by definition they are high order streams (Strahler., 1957). Hence, we can argue that the "chemostasis" of OC results in an iron "chemostasis", whereby processes of degradation in the main channel are minimal and the origin of Fe particles are from sources distal from one another. This is consistent with the near to neutral pH and predominance of DOC in the <10 kDa fraction. However, predicted warming and resulting enhanced thermal and mechanical erosion of connected sources of OC (Yedoma and cryoturbated mineral soils) (Costard et al., 2007) may contribute a flux of reactive

OC, which would unbalance this chemostasis Nonetheless, the high concentration of reactive ferrihydrite released from tributaries in the central plateau, suggests that the degradation of OC in the thermokarst lakes and smaller tributaries, could significantly contribute to reactive Fe budget in the Lena River main channel. Future work will consider this idea in more detail by using iron isotopes to identify the sources of Fe.

6. Conclusions

This study has shown that >70% of iron in water from the Lena River occurs in the particulate fraction. In contrast the >50% of DOC occurs in the truly dissolved (<1 kDa) fraction. The main form of secondary mineral Fe is ferrihydrite and this is observed as aggregates of different sizes that span the operational size range between particulate and colloidal particles. Results from sequential extraction show that tributaries draining the central plateau contain the highest proportion of ferrihydrite. The ferrihydrite is observed to absorb to the surface of particulate organic carbon, but there is no evidence of Fe coprecipitating with OC.

We propose that the formation of ferrihydrite is mainly due to the close to neutral pH of the water column in all sampled tributaries and main channel. Secondly, the size discrepancy between the Fe and OC, suggests that there is less available OC for Fe to complex with. Further, we suggest that the predominance of ferrihydrite in these high order rivers is partly the result of chemostasis in the system and disconnection from the sources of Fe in lower order rivers.

This study shows that ferrihdyrite is the dominant form of iron particle phase forming in the Lena River catchment area, during this post-spring flood period. The ferrihydrite is sustained in the main channel and consequently, ferrihydrite is the dominant iron particle transported to the Lena River delta, estuary and to the Laptev Sea.

7. Future work

7.1 Spatial variation in the origin and processing of iron particles

The dominant form of Fe in boreal river particles depends on the source of Fe and the transport pathway (Ingri et al., 2000; Dahlqvist et al., 2007). Previous studies have used iron isotopes to determine the origin of Fe particles in river systems. The dissolved fraction, (in this study referred to as $[Fe]_{colloidal}$ due to the low concentration of Fe in the dialysis fraction), shows a wider variation in iron isotope composition in arctic rivers (Escoube et al., 2015) compared to the particulate fraction. Heavy isotope enrichment in the dissolved fraction has been previously ascribed to: (i) weathering of specific lithologies (e.g. shales), (Yesavage et al., 2012), (ii) weathering of isotopically heavy rocks (e.g. granites) (Poitrasson and Freydier., 2005), (iii) binding of the heavy isotope to organic carbon in the dissolved fraction (Dideriksen et al., 2008; Illina et al., 2013). Conversely, light isotope enrichment in the dissolved fraction has been ascribed to (i) the oxidation of Fe(II) to Fe(III) from groundwaters (Rouxel et al., 2008), (ii) kinetic mineral dissolution in the presence of chelating ligands that release the lighter isotope into solution (Brantley et al., 2001), (iii) release of Fe from plants, which are enriched in the lighter isotope (Guike et al., 2007). Previous studies of boreal rivers have observed tthe dissolved Fe fraction to have both light and heavy iron isotope compositions, whereas the particulate fraction is consistently enriched in the lighter isotope (Ingri et al., 2006; Ingri et al., in press; Escoube et al., 2015). In this study, we compare the iron isotope composition of $[Fe]_{particulate}$ and $[Fe]_{colloidal}$ in the main Lena River channel and sub catchments of contrasting geochemistry (Fig. 8). Further, unlike previous studies of boreal rivers, the $[Fe]_{residual}$ and $[Fe]_{leach}$ fractions of particulate iron are investigated in order to understand the origin of the Fe-bearing particles identified in Study 1. The data for this study is outlined in Supplementary Information, 11.2.

7.2 Temporal variation in the origin and processing of iron particles

Boreal rivers show dramatic seasonal variations. During winter baseflow, the active layer and river are frozen and groundwater influx via taliks and regions of discontinuous permafrost, contribute large portion of the river water (Land and Öhlander, 1997). The spring flood occurs after river ice break up. Surface flow is now reactivated, however the active layer remains frozen so overland flow contributes the largest portion of water in this period. During summer base flow, the active layer is at its greatest depth and surface flow occurs through the active layer soil horizon. In the autumn, the river and active layer freeze and the winter base flow commences again. These seasonal variations result is large variations in dissolved organic carbon (DOC) (Guo et al., 2003), dissolved inorganic carbon (Striegel et al., 2005), major cations (Ingri et al., 2005) and trace elements (Bagard et al., 2011). The aim of this study is to characterize the origin and transport of iron particle from the summer base flow, winter base flow, ice break up and spring flood in the Lena River. Iron isotope composition of the particles in the particulate and colloidal fraction will be analyzed alongside geochemical data. The data used in this study is outlined in Supplementary Information, 11.3.

8. Acknowledgements

There is still a long way to go, but many thanks are overdue! Firstly, to my supervisors Magnus Mörth and Per Andersson. Thank you for your patience, wisdom and undoubting support. Thanks also to Don Porcelli for your longstanding support and to Don, Per and Magnus for their hard work in setting up MetTrans and for teaching me invaluable field and communication skills. Thank you also to Ian Burke and Sam Shaw for the great collaborations and detailed paper discussions. I am grateful to all members of the MetTrans family for the fun meetings and scientific discussion.

I am lucky to be surrounded by a group of inspiring scientists. Liselott - many thanks for all you taught me in the field and all your support since then. I have happy memories of filtering and singing on the Lena River. Thank you to Xiaole, Ernest and Chris for the exciting iron and silica discussions. Mel and Becca – thank you for being great long distance work companions and a constant source of confidence. Karin Wallner and Hans Schöberg have been an enormous support over the last three years. Karin, thank you for your help with field work preparation, lab work and data processing. Hans, thank you for joining me on this "particle dissolution microwave adventure". Our method discussion is always coupled with laughter and debate (from standards to skiing). I cannot thank you both enough. A huge thank you goes to the second "dream team", Ellen Kooijman, Melanie Schmidtt and Hans Schöberg, for their hard work in the Vegacenter and developing the iron isotope method. Thank you to Magnus Mörth, Phil Holdship, Mike Ward, Heike Siegmund, Marcus Sundbom, Carina Johansson, Pår Hjelmquist, Reiner Giesler and Burkhard Kaulich for your help with analysis. Thank you to our colleagues at the Institute of Biological Problems of the Cryolithozone and the Permafrost Institute, in Yakutsk. Thanks, especially, to Trofim Maximov for his logistical support and Roman Petrov who performed the winter 2012-2013 sampling. Thank you also to Stas Ksesta and Maria Petrunova for their invaluable help with logistics.

The geo-world of NRM and IGV is full of wonderful people. A special thanks to the PhD students at IGV and NRM for the fika, GeoPub and Green Villa parties. Special thanks to my office mate Franz, for the regular tea breaks and translating the abstract in this thesis. Thank you to my wonderful Stockholm friends for the laughter, adventures and support. The biggest thanks must go to my family and friends in the UK, for encouraging me to seize every opportunity. I look forward to a longer catch-up with you all soon.

9. References

Allard, T., Menguy, N., Salomon, J., Calligaro, T., Weber, T., Calas, G., & Benedetti, M. F. (2004). Revealing forms of iron in river-borne material from major tropical rivers of the Amazon Basin (Brazil). *Geochimica et Cosmochimica Acta*, *68*(14), 3079-3094.

Amon, R. M., & Benner, R. (1996). Bacterial utilization of different size classes of dissolved organic matter. *Limnology and Oceanography*, *41*(1), 41-51.

Amon, R. M. W., Rinehart, A. J., Duan, S., Louchouarn, P., Prokushkin, A., Guggenberger, G., ... & McClelland, J. W. (2012). Dissolved organic matter sources in large Arctic rivers. *Geochimica et Cosmochimica Acta*, *94*, 217-237.

Anisimov, O., & Reneva, S. (2006). Permafrost and changing climate: the Russian perspective. *AMBIO: A Journal of the Human Environment*, *35*(4), 169-175.

Apte, S. C., & Rogers, H. R. (1993). Speciation and partitioning of atrazine and gamma-hexachlorocyclohexane in estuarine waters. *Science of the total environment*, *132*(2), 313-325.

Bagard, M. L., Chabaux, F., Pokrovsky, O. S., Viers, J., Prokushkin, A. S., Stille, P., ... & Dupré, B. (2011). Seasonal variability of element fluxes in two Central Siberian rivers draining high latitude permafrost dominated areas.*Geochimica et Cosmochimica Acta*, *75*(12), 3335-3357.

Banfield, J. F., Welch, S. A., Zhang, H., Ebert, T. T., & Penn, R. L. (2000). Aggregation-based crystal growth and microstructure development in natural iron oxyhydroxide biomineralization products. *Science*, *289*(5480), 751-754.

Benedetti, M. F., Ranville, J. F., Allard, T., Bednar, A. J., & Menguy, N. (2003). The iron status in colloidal matter from the Rio Negro, Brasil. *Colloids and Surfaces A: Physicochemical and Engineering Aspects*, *217*(1), 1-9.

Bergquist, B. A., & Boyle, E. A. (2006). Iron isotopes in the Amazon River system: Weathering and transport signatures. *Earth and Planetary Science Letters*, *248*(1), 54-68.

Boyle, E. A., Bergquist, B. A., Kayser, R. A., & Mahowald, N. (2005). Iron, manganese, and lead at Hawaii Ocean Time-series station ALOHA: Temporal variability and an intermediate water hydrothermal plume.*Geochimica et Cosmochimica Acta*, *69*(4), 933-952.

Bruland, K. W., Orians, K. J., & Cowen, J. P. (1994). Reactive trace metals in the stratified central North Pacific. *Geochimica et Cosmochimica Acta*,*58*(15), 3171-3182.

Brown, G. E., & Calas, G. (2012). Mineral-aqueous solution interfaces and their impact on the environment. *Geochemical Perspectives*, *1*(4-5), 483-484.

Cooper, L. W., Benner, R., McClelland, J. W., Peterson, B. J., Holmes, R. M., Raymond, P. A., ... & Codispoti, L. A. (2005). Linkages among runoff, dissolved organic carbon, and the stable oxygen isotope composition of seawater and other water mass indicators in the Arctic Ocean. *Journal of Geophysical Research: Biogeosciences*, *110*(G2).

Ingri et al., in press. Iron isotope signatures in brown rivers.

Cornell, R. M., & Schwertmann, U. (2003). *The iron oxides: structure, properties, reactions, occurrences and uses*. John Wiley & Sons.

Costard, F., Gautier, E., Brunstein, D., Hammadi, J., Fedorov, A., Yang, D., & Dupeyrat, L. (2007). Impact of the global warming on the fluvial thermal erosion over the Lena River in Central Siberia. *Geophysical Research Letters*, *34*(14).

Creed, I. F., McKnight, D. M., Pellerin, B. A., Green, M. B., Bergamaschi, B. A., Aiken, G. R., ... & Aulenbach, B. T. (2015). The river as a chemostat: fresh perspectives on dissolved organic matter flowing down the river continuum. *Canadian Journal of Fisheries and Aquatic Sciences*, *72*(8), 1272-1285.

Dahlqvist, R., Andersson, K., Ingri, J., Larsson, T., Stolpe, B., & Turner, D. (2007). Temporal variations of colloidal carrier phases and associated trace elements in a boreal river. *Geochimica et Cosmochimica Acta*, *71*(22), 5339-5354.

Dauphas, N., Pourmand, A., & Teng, F. Z. (2009). Routine isotopic analysis of iron by HR-MC-ICPMS: How precise and how accurate?. *Chemical Geology*, *267*(3), 175-184.

Dideriksen, K., Baker, J. A., & Stipp, S. L. S. (2008). Equilibrium Fe isotope fractionation between inorganic aqueous Fe (III) and the siderophore complex, Fe (III)-desferrioxamine B. *Earth and Planetary Science Letters*,*269*(1), 280-290.

dos Santos Pinheiro, G. M., Poitrasson, F., Sondag, F., Cochonneau, G., & Vieira, L. C. (2014). Contrasting iron isotopic compositions in river suspended particulate matter: the Negro and the Amazon annual river cycles. *Earth and Planetary Science Letters*, *394*, 168-178.

Escoube, R., Rouxel, O. J., Pokrovsky, O. S., Schroth, A., Holmes, R. M., & Donard, O. F. (2015). Iron isotope systematics in Arctic rivers. *Comptes Rendus Geoscience*, *347*(7), 377-385.

Fehr, M. A., Andersson, P. S., Hålenius, U., & Mörth, C. M. (2008). Iron isotope variations in Holocene sediments of the Gotland Deep, Baltic Sea.*Geochimica et Cosmochimica Acta*, *72*(3), 807-826.

Fedorov, A., & Konstantinov, P. (2003, July). Observations of surface dynamics with thermokarst initiation, Yukechi site, Central Yakutia. In*Proceedings of the VII International Permafrost Conference* (pp. 239-243).

Field, C. B., Behrenfeld, M. J., Randerson, J. T., & Falkowski, P. (1998). Primary production of the biosphere: integrating terrestrial and oceanic components. *Science*, *281*(5374), 237-24

Freeman, M. C., Pringle, C. M., & Jackson, C. R. (2007). Hydrologic connectivity and the contribution of stream headwaters to ecological integrity at regional scales1.

Gasser, U. G., Juchler, S. J., & Sticher, H. (1994). CHEMISTRY AND SPECIATION OF SOIL WATER FROM SERPENTINITIC SOILS: IMPORTANCE OF COLLOIDS IN THE TRANSPORT OF Cr, Fe, Mg, AND Ni. *Soil Science*, *158*(5), 314-322.

Gordeev, V. V., & Sidorov, I. (1993). Concentrations of major elements and their outflow into the Laptev Sea by the Lena River. *Marine Chemistry*, *43*(1-4), 33-45.

Grosse, G., Robinson, J. E., Bryant, R., Taylor, M. D., Harper, W., DeMasi, A.& Harden, J. (2013). Distribution of late Pleistocene ice-rich syngenetic permafrost of the Yedoma Suite in east and central Siberia, Russia. *US Geological Survey Open File Report*, *2013*(1078), 1-37.

Guelke, Monika, and Friedhelm Von Blanckenburg. "Fractionation of stable iron isotopes in higher plants." *Environmental science & technology* 41.6 (2007): 1896-1901.

Guo, L., Ping, C. L., & Macdonald, R. W. (2007). Mobilization pathways of organic carbon from permafrost to arctic rivers in a changing climate.*Geophysical Research Letters*, *34*(13).

Hawkings, J. R., Wadham, J. L., Tranter, M., Raiswell, R., Benning, L. G., Statham, P. J.& Telling, J. (2014). Ice sheets as a significant source of highly reactive nanoparticulate iron to the oceans. *Nature communications*,*5*.

Huh, Y., Tsoi, M. Y., Zaitsev, A., & Edmond, J. M. (1998). The fluvial geochemistry of the rivers of Eastern Siberia: I. Tributaries of the Lena River draining the sedimentary platform of the Siberian Craton. *Geochimica et cosmochimica acta*, *62*(10), 1657-1676.

Ilina, S. M., Poitrasson, F., Lapitskiy, S. A., Alekhin, Y. V., Viers, J., & Pokrovsky, O. S. (2013). Extreme iron isotope fractionation between colloids and particles of boreal and temperate organic-rich waters. *Geochimica et Cosmochimica Acta*, *101*, 96-111.

Ingri, J., Widerlund, A., Land, M., Gustafsson, Ö., Andersson, P., & Öhlander, B. (2000). Temporal variations in the fractionation of the rare earth elements in a boreal river; the role of colloidal particles. *Chemical Geology*,*166*(1), 23-45.

Ingri, J., Malinovsky, D., Rodushkin, I., Baxter, D. C., Widerlund, A., Andersson, P., ... & Öhlander, B. (2006). Iron isotope fractionation in river colloidal matter. *Earth and Planetary Science Letters*, *245*(3), 792-798.

Lam, P. J., Ohnemus, D. C., & Marcus, M. A. (2012). The speciation of marine particulate iron adjacent to active and passive continental margins.*Geochimica et Cosmochimica Acta*, *80*, 108-124.

Lam, P. J., & Bishop, J. K. (2008). The continental margin is a key source of iron to the HNLC North Pacific Ocean. *Geophysical Research Letters*, *35*(7).

Land, M., & Öhlander, B. (1997). Seasonal variations in the geochemistry of shallow groundwater hosted in granitic till. *Chemical geology*, *143*(3), 205-216.

Leventhal, J., & Taylor, C. (1990). Comparison of methods to determine degree of pyritization. *Geochimica et Cosmochimica Acta*, *54*(9), 2621-2625.

Lofts, S., Tipping, E., & Hamilton-Taylor, J. (2008). The chemical speciation of Fe (III) in freshwaters. *Aquatic Geochemistry*, *14*(4), 337-358.

Martin, J. M., & Meybeck, M. (1979). Elemental mass-balance of material carried by major world rivers. *Marine chemistry*, *7*(3), 173-206.

McClelland, J. W., Holmes, R. M., Dunton, K. H., & Macdonald, R. W. (2012). The Arctic ocean estuary. *Estuaries and Coasts*, *35*(2), 353-368.

März, C., Poulton, S. W., Brumsack, H. J., & Wagner, T. (2012). Climate-controlled variability of iron deposition in the Central Arctic Ocean (southern Mendeleev Ridge) over the last 130,000 years. *Chemical Geology*, *330*, 116-126.

Moffett, J. W. (2001). Transformations among different forms of iron in the ocean. *IUPAC Series on Analytical and Physical Chemistry of Environmental Systems*, *7*, 343-372.

Neubauer, E., Schenkeveld, W. D., Plathe, K. L., Rentenberger, C., Von Der Kammer, F., Kraemer, S. M., & Hofmann, T. (2013). The influence of pH on iron speciation in podzol extracts: Iron complexes with natural organic matter, and iron mineral nanoparticles. *Science of the Total Environment*,*461*, 108-116.

Perret, Didier, et al. "The diversity of natural hydrous iron oxides."*Environmental science & technology* 34.17 (2000): 3540-3546.

Peterson, B. J., Holmes, R. M., McClelland, J. W., Vörösmarty, C. J., Lammers, R. B., Shiklomanov, A. I & Rahmstorf, S. (2002). Increasing river discharge to the Arctic Ocean. *science*, *298*(5601), 2171-2173.

Poitrasson, F., & Freydier, R. (2005). Heavy iron isotope composition of granites determined by high resolution MC-ICP-MS. *Chemical Geology*,*222*(1), 132-147.

Pokrovsky, O. S., & Schott, J. (2002). Iron colloids/organic matter associated transport of major and trace elements in small boreal rivers and their estuaries (NW Russia). *Chemical Geology, 190*(1), 141-179.

Pokrovsky, Oleg S., B. Dupré, and J. Schott. "Fe–Al–organic colloids control of trace elements in peat soil solutions: results of ultrafiltration and dialysis."*Aquatic Geochemistry* 11.3 (2005): 241-278.

Pokrovsky, O. S., Schott, J., & Dupré, B. (2006). Trace element fractionation and transport in boreal rivers and soil porewaters of permafrost-dominated basaltic terrain in Central Siberia. *Geochimica et Cosmochimica Acta*, *70*(13), 3239-3260.

Pokrovsky, O. S., Viers, J., Shirokova, L. S., Shevchenko, V. P., Filipov, A. S., & Dupré, B. (2010). Dissolved, suspended, and colloidal fluxes of organic carbon, major and trace elements in the Severnaya Dvina River and its tributary. *Chemical Geology*, *273*(1), 136-149.

Pokrovsky, O. S., Shirokova, L. S., Kirpotin, S. N., Audry, S., Viers, J., & Dupré, B. (2011). Effect of permafrost thawing on organic carbon and trace element colloidal speciation in the thermokarst lakes of western Siberia.*Biogeosciences*, *8*(3), 565-583.

Poulton, S. W., & Raiswell, R. (2002). The low-temperature geochemical cycle of iron: from continental fluxes to marine sediment deposition.*American Journal of Science*, *302*(9), 774-805.

Lara, R. J., Rachold, V., Kattner, G., Hubberten, H. W., Guggenberger, G., Skoog, A., & Thomas, D. N. (1998). Dissolved organic matter and nutrients in the Lena River, Siberian Arctic: Characteristics and distribution. *Marine Chemistry*, *59*(3), 301-309.

Raiswell, R., Tranter, M., Benning, L. G., Siegert, M., De'ath, R., Huybrechts, P., & Payne, T. (2006). Contributions from glacially derived sediment to the global iron (oxyhydr) oxide cycle: implications for iron delivery to the oceans. *Geochimica et Cosmochimica Acta*, *70*(11), 2765-2780.

Raiswell, R., Benning, L. G., Davidson, L., & Tranter, M. (2008). Nanoparticulate bioavailable iron minerals in icebergs and glaciers.*Mineralogical Magazine*, *72*(1), 345-348.

Raiswell, R., & Canfield, D. E. (2012). The iron biogeochemical cycle past and present. *Geochemical Perspectives*, *1*(1), 1-2.

Romanovsky, N.N., (1993), Principles of cryogenesis in the lithosphere [Osnovy Kriogeneza Litosfery]: Moscow, Moscow State University Press, 335 p. [In Russian.]

Romanovsky, V. E., Sazonova, T. S., Balobaev, V. T., Shender, N. I., & Sergueev, D. O. (2007). Past and recent changes in air and permafrost temperatures in eastern Siberia. *Global and Planetary Change*, *56*(3), 399-413.

Rouxel, O. J., Bekker, A., & Edwards, K. J. (2005). Iron isotope constraints on the Archean and Paleoproterozoic ocean redox state. *Science*, *307*(5712), 1088-1091.

Rouxel, O., & Sholkovitz, E. (2006). Large scale iron isotope fractionation in subterranean estuaries. In *Geophysical Research Abstracts* (Vol. 8, p. 05141).

Schoenberg, R., & von Blanckenburg, F. (2005). An assessment of the accuracy of stable Fe isotope ratio measurements on samples with organic and inorganic matrices by high-resolution multicollector ICP-MS.*International Journal of Mass Spectrometry*, *242*(2), 257-272.

Schroth, A. W., Crusius, J., Sholkovitz, E. R., & Bostick, B. C. (2009). Iron solubility driven by speciation in dust sources to the ocean. *Nature Geoscience*, *2*(5), 337-340.

Severmann, S., Johnson, C. M., Beard, B. L., & McManus, J. (2006). The effect of early diagenesis on the Fe isotope compositions of porewaters and authigenic minerals in continental margin sediments. *Geochimica et Cosmochimica Acta*, *70*(8).

Sholkovitz, E. R. (1976). Flocculation of dissolved organic and inorganic matter during the mixing of river water and seawater. *Geochimica et Cosmochimica Acta*, *40*(7), 831-845.

SLRS-5, Riverine Water Reference Material for Trace Metals, National Research Council, Canada

Stein, R. (2000). Circum-Arctic river discharge and its geological record: an introduction. *International journal of earth sciences*, *89*(3), 447-449.

Strahler, A. N. (1957). Quantitative analysis of watershed geomorphology.*Eos, Transactions American Geophysical Union*, *38*(6), 913-920.

Stolpe, B., Guo, L., Shiller, A. M., & Aiken, G. R. (2013). Abundance, size distributions and trace-element binding of organic and iron-rich nanocolloids in Alaskan rivers, as revealed by field-flow fractionation and ICP-MS.*Geochimica et Cosmochimica Acta*, *105*, 221-239.

Stumm, W., Morgan, J. J., & Drever, J. I. (1996). Aquatic Chemistry. *Journal of Environmental Quality*, *25*(5), 1162.

Tananaev, N. I. (2016). Hydrological and sedimentary controls over fluvial thermal erosion, the Lena River, central Yakutia. *Geomorphology*, *253*, 524-533.

Tarnocai, C., Canadell, J. G., Schuur, E. A. G., Kuhry, P., Mazhitova, G., & Zimov, S. (2009). Soil organic carbon pools in the northern circumpolar permafrost region. *Global biogeochemical cycles*, *23*(2).

Vasyukova, E. V., Pokrovsky, O. S., Viers, J., Oliva, P., Dupré, B., Martin, F., & Candaudap, F. (2010). Trace elements in organic-and iron-rich surficial fluids of the boreal zone: Assessing colloidal forms via dialysis and ultrafiltration. *Geochimica et Cosmochimica Acta*, *74*(2), 449-468.

Vasyukova, Ekaterina, et al. "New operational method of testing colloid complexation with metals in natural waters." *Applied geochemistry* 27.6 (2012): 1226-1237.

Viers, J., Dupré, B., & Gaillardet, J. (2009). Chemical composition of suspended sediments in World Rivers: new insights from a new database.*Science of the total Environment*, *407*(2), 853-868.

Vonk, J. E., & Gustafsson, Ö. (2013). Permafrost-carbon complexities.*Nature Geoscience*, *6*(9), 675-676.

Vonk, J. E., Tank, S. E., Mann, P. J., Spencer, R. G., Treat, C. C., Striegl, R. G., ... & Wickland, K. P. (2015). Biodegradability of dissolved organic carbon in permafrost soils and aquatic systems: a meta-analysis.*Biogeosciences*, *12*(23), 6915-6930.

Wells, M. L. (1999). Manipulating iron availability in nearshore waters.*Limnology and Oceanography*, *44*(4), 1002-1008.

Woo, M. K. (2012). *Permafrost hydrology*. Springer Science & Business Media.

Ye, B., Yang, D., & Kane, D. L. (2003). Changes in Lena River streamflow hydrology: Human impacts versus natural variations. *Water resources research*, *39*(7).

Yang, D., Kane, D. L., Hinzman, L. D., Zhang, X., Zhang, T., & Ye, H. (2002). Siberian Lena River hydrologic regime and recent change. *Journal of Geophysical Research: Atmospheres*, *107*(D23).

Yesavage, T., Fantle, M. S., Vervoort, J., Mathur, R., Jin, L., Liermann, L. J., & Brantley, S. L. (2012). Fe cycling in the Shale Hills Critical Zone Observatory, Pennsylvania: An analysis of biogeochemical weathering and Fe isotope fractionation. *Geochimica et Cosmochimica Acta*, *99*, 18-38.

Zhang, Y., Carey, S. K., Quinton, W. L., Janowicz, J. R., Pomeroy, J. W., & Flerchinger, G. N. (2010). Comparison of algorithms and parameterisations for infiltration into organic-covered permafrost soils. *Hydrology and earth system sciences, 14*(5), 729-750

10. Appendix

10.1 Study 1: Manuscript

The size distribution and composition of iron in the Lena River catchment, NE Russia

[*]Catherine Hirst[a,b], Liselott Kutscher[a,b], Melissa Murphy[c], Sam Shaw[d]; Ian T. Burke[e]; Burkhard Kaulich[f] , Trofim Maximov[g]; Carl-Magnus Mörth[b]; Per S. Andersson[a]; Don Porcelli[c]

a Department of Geosciences, Swedish Museum of Natural History, 104 05, Stockholm, Sweden

b Department of Geological Sciences, Stockholm University, SE106-91, Stockholm, Sweden

c Department of Earth Sciences, Oxford University, OX1 3AN, Oxford, UK

d Atmospheric and Environmental Sciences, University of Manchester, M13 9PL, Manchester, UK

e School of Earth and Environment, University of Leeds, LS2 9JT, Leeds, UK

f Diamond Light Source, Hardwell Science Park,

g Institute of Biological Problems of the Cryolithozone, Yakutsk, 677891, Russia

*Corresponding author: Catherine Hirst, catherine.hirst@nrm.se

Abstract

The size and composition of iron particles in the Lena River catchment were investigated during July 2012 and June 2013. Samples were taken from 77 tributaries and the main channel, and so representing watersheds that span a wide range in topography, lithology and permafrost extent. Water samples were processed in the field via conventional filtration and dialysis and for all samples, 70% of iron (Fe) was found in the particulate (> 0.22 µm) fraction. In the dissolved (< 0. 22 µm) fraction, 90% of the Fe was observed in the 0.22 µm – 10 kDa fraction. In contrast to the size distribution of Fe, > 50% of the total organic carbon (OC) was observed in the <1 kDa fraction for all analysed samples. Larger particles (>0.22 µm) and colloidal particles (< 0.22 µm) were analysed using Transmission Electron Microscopy (TEM). Various Fe rich particles were identified: (i) clay minerals with Fe within the framework (ii) 10 nm wide aggregates of nanocrystalline ferrihydrite (in the < 0.22 µm fraction), (ii) 100 - 500 nm aggregates of nanocrystalline ferrihydrite, (iii) 100nm wide haematite particles. Scanning transmission X-ray (STXM) spectroscopy was used to confirm the observations

made with STEM and that particulate ferrihydrite was associated with the surface of organic, and clay particles. Selective dissolution indicated that Fe in nanocrystalline ferrihydrite contributes ≥55% of the >0.22 μm Fe particles in all analysed subcatchments. The greatest proportion of nanocrystalline ferrihydrite was observed in tributaries draining the low-lying plateau. Ferrihydrite is the dominant form of secondary mineral iron in the major tributaries and main channel of the Lena River catchment area maybe due to the near neutral pH of the river and the absence of labile organic carbon (OC). This combined evidence suggests that the Lena River main channel and its high order tributaries have reached a point of chemostasis whereby OC is mainly in the < 1 kDa fraction and Fe is mainly in particulate form, hence Fe is only associated with a minor portion of the total organic carbon (TOC) in the river. Ferrihydrite is a highly reactive form of iron and its ubiquitous presence during this post-spring flood period will help to constrain the transport of Fe and trace element (TE) to the shelf of the Arctic Ocean.

1. Introduction

Iron enters the ocean via rivers, aeolian dust, ice-rafted sediments and by hydrothermal vents at the sea floor (see review by Raiswell and Canfield, 2012). Iron is a key requirement for metabolic processes and is therefore a limiting nutrient for primary productivity in the oceans (Wells., 1999) and an important element for atmospheric carbon dioxide sequestration (Field et al., 1998). Rivers transport a large amount of Fe but the river to ocean flux is limited by the removal of Fe in estuaries (Mayer et al., 1982). The supply of particulate (larger particles and smaller colloids) Fe from river to ocean is three orders of magnitude greater (Martin and Maybeck, 1979; Poulton and Raiswell, 2002) than that supplied in dissolved form. Particulate Fe will sediment onto the continental shelf and can contribute to the flux of bioavailable Fe released from shelf sediments (Moffett., 2001). The transport and bioavailability of Fe particles is determined by their composition, particle size and associated phases (Warren and Haack, 2001). It is therefore important to characterise the Fe particles in rivers in order to understand their eventual role on the continental shelf.

Extensive work has been done to characterise the Fe particle mineralogy in aeolian dust (Schroth et al., 2009), ice rafted sediments (Raiswell. 2011), glaciers (Hawkings et al., 2014) and tropical rivers (Allard et al., 2004). Fe-bearing particles are a combination of detrital phases (with Fe within the framework of sheet silicates and crystalline Fe oxides) and secondary mineral Fe (mainly in the form of amorphous to poorly crystalline Fe oxides). Fe-bearing secondary mineral particles play a greater role in ocean “fertilization” due to their greater solubility (Schroth et al., 2009; Lam et al., 2012). Further, the reactivity of Fe-bearing particles is also controlled by their association with organic carbon (OC) (Boyle et al., 2010). Studies of organic-rich tropical rivers (Benedetti et al., 2003; Allard et al., 2004) have observed particles of Fe-OC complexes, where Fe is coprecipitating with the OC in the river. The surface properties of a particle of coprecipitated Fe-OC differ from an inorganic Fe-bearing particle that is absorbed to the surface of OC (Esterhues et al., 2011). Subsequently, OC will also affect the transport and reactivity of Fe particles. However, the mineralogy of Fe-bearing particles and their association with OC remains understudied in boreal rivers.

Previous studies of Fe in boreal rivers have used a variety of size separation techniques, including membrane filtration, ultrafiltration and dialysis techniques (Ingri et al., 2000; Pokrovsky and Schott 2002; Pokrovsky et al., 2005; Ingri et al., 2006; Bagaard et al., 2010; Vasyukova et al., 2011; Illina et al., 2013; Stolpe et al., 2013) to analyse the composition of Fe-rich particles and their association with trace elements (TE) and organic carbon (OC). These studies focussed on the dissolved (< 0.22 μm or < 0.45 μm) fraction and suggest that Fe is either in the form of Fe (oxyhydr) oxides or Fe-OC complexes (Ingri et al., 2000). Iron isotope analysis has been used to identify different Fe-bearing particle compositions (Ingri et al., 2006) and also suggests that Fe and OC are coprecipitating in smaller (<1 kilo Dalton (kDa)) size fractions (Illina et al., 2013). Nonetheless, observations of Fe-OC associations are confined to low to medium order boreal rivers with high OC concentrations. Therefore, the aim of this study is to characterise the mineralogy of Fe particles in a major boreal river system, the Lena River in NE Russia. This drains into the Arctic Ocean and thus of significant interest in response to climate change predictions (IPCC 2013).

Enhanced surface temperatures across the Arctic (Fedorov and Konstantinov, 2003) have resulted in (i) increased seasonal active layer thickness in regions of permafrost that store substantial OC (Zhang et al., 2005; Romanovsky et al., 2007), (ii) increased river water temperature (Liu et al., 2005), (iii) increased river discharge (Peterson et al., 2002; Yang et al., 2002) and (iv) enhanced thermal erosion from the river banks (Costard et al., 2007). Future predicted temperature and precipitation increases are predicted to alter the flux of river constituents into the Arctic Ocean (Stein et al., 2000). It is therefore important to determine the present day formation and transport of Fe particles, in order to predict future changes in the flux of Fe to the Arctic Ocean.

Samples were taken from the main channel and in high order tributaries from a wide latitudinal range that have varying topography, lithology and permafrost extent. The objectives of this study were to (i) determine the size distribution of Fe particles in the Lena River catchment area, (ii) identify the dominant composition of Fe particles in the main channel and its sub-catchments and (iii) quantify the identified particles in different catchment areas. The Fe bearing particles were identified using scanning transmission electron microscopy (STEM) and analysed using X-ray absorption near edge structure (XANES) spectroscopy and scanning transmission X-ray (STXM) spectroscopy, in order to identify the relationships between Fe and OC in the particles. The identified Fe phases were then quantified by preferential dissolution.

2. Sample Area

Samples were collected from the Lena River catchment area in July 2012 and June 2013.The Lena River is 4260 km long (Fig. 1 a) and has a catchment area of 2.5 million km^2 (Rachold et al., 1996) The river (Fig 1) has an annual freshwater discharge to the Arctic Ocean of 581 km^3 (Amon et al., 2012). The Lena River catchment is subject to long cold winters (with an average winter temperature of -45 to -50°C from November to March) and short hot summers (with an average temperature of +30°C to +35°C from June to August) (Rachold et al., 1996). The average annual precipitation in the Lena River catchment is 330 mm, with 70 – 80% occurring during the summer (Gordeev and Siderov, 1993). The hydrological year can be divided into four major periods: (i) winter base flow of low discharge, (ii) spring snow melt, (iii) spring flood, of highest discharge, (iv) summer - autumn base The exact timing of spring flood in the Lena sub-basins depends on its latitude and altitude (Rachold et al., 1996).

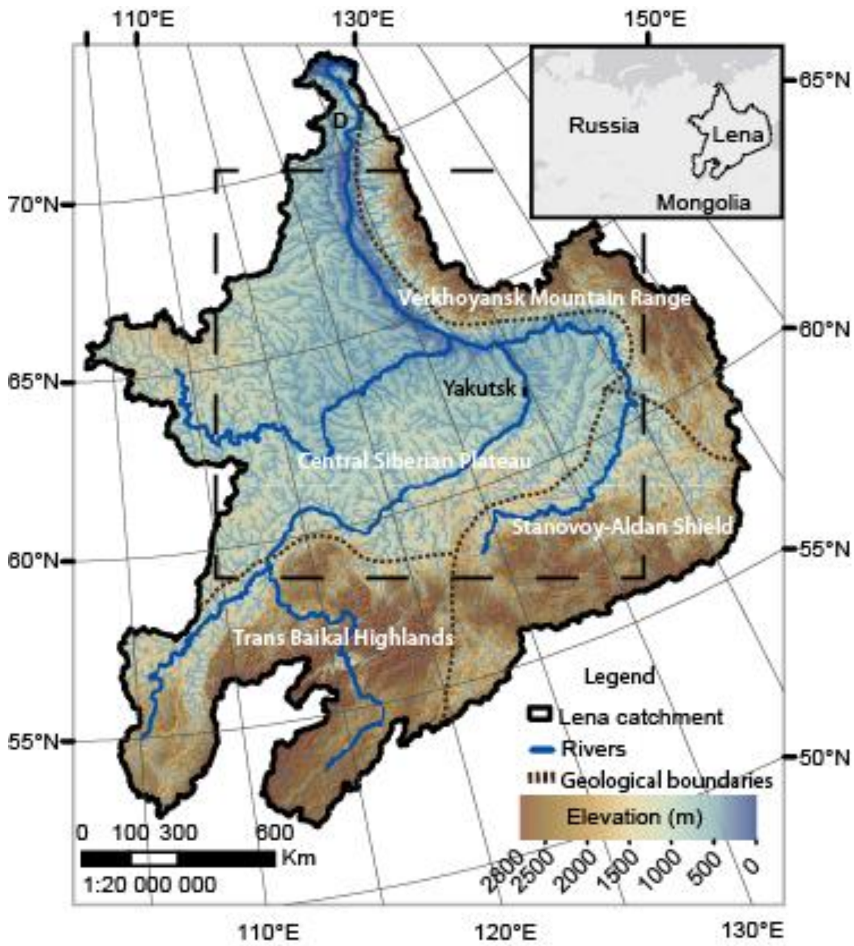

Fig.1 a Overview of the Lena River catchment area. Sampling routes from July 2012 and June 2013 are outlined. The catchment area spans a wide range in elevation: mountains in the south and east and lowlying plateau in the north and west of the catchment area. The Lena River and two major tributaries (the Aldan River and Viliuj River) are outlined. Sampled tributaries are categorized according to their geological units: the Central Siberian Plateau, Verkhoyansk Mountain Range and Stanovoy-Aldan Shield and grouped according to Table , as outlined in Fig 1 b. Adapted from Kutscher et al., in press.

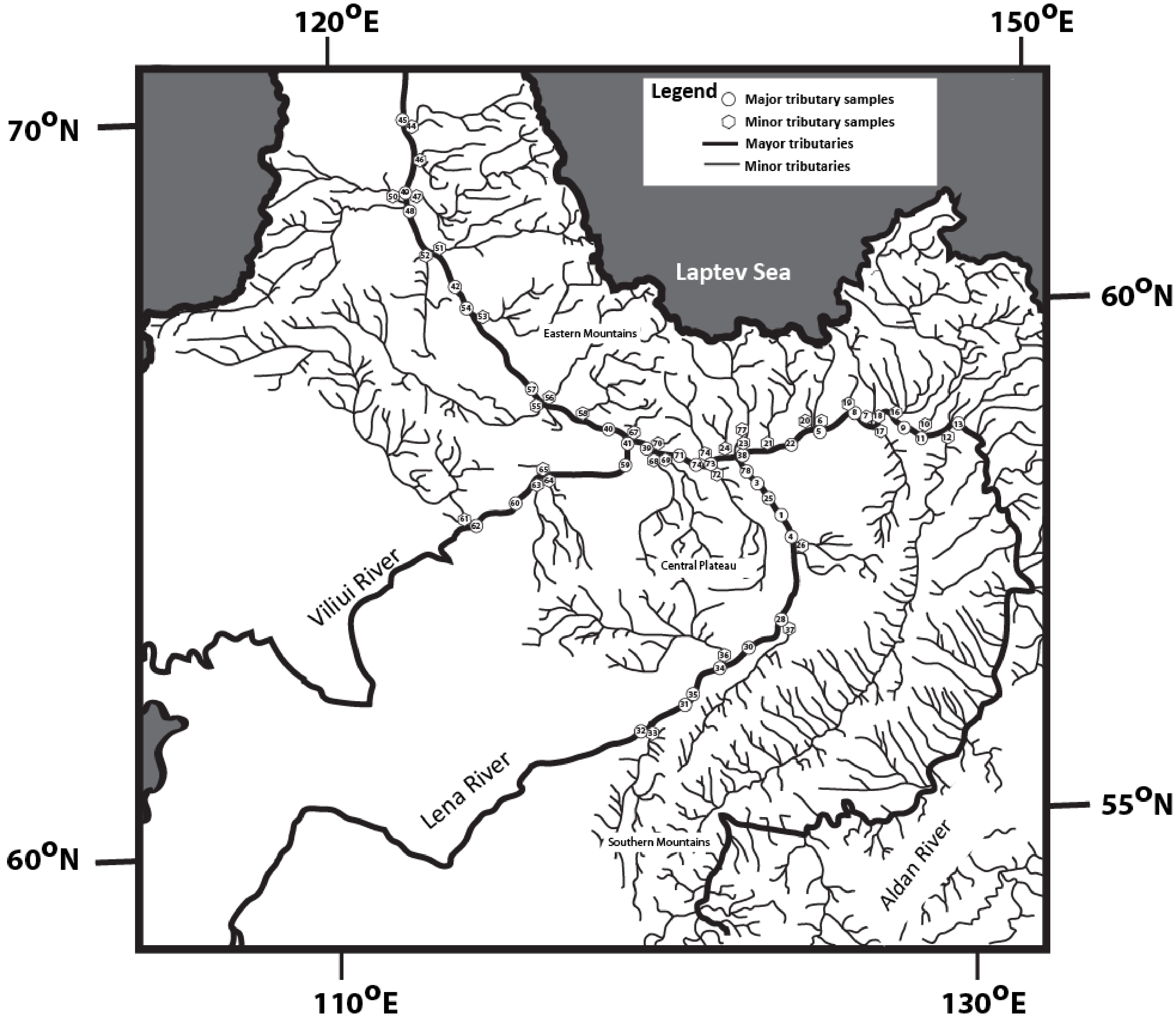

Fig. 1 b Samples were collected from the Lena River, Aldan River and Viliui River. Samples were also collected from smaller tributaries which drain varying topography and permafrost extent. On this map, the sample stations are outlined and correspond with the numbers in Table 4 of the Supplementary Information. The summary names for each region (e.g. Southern Mountains) are outlined and correspond with Table 1. Adapted from Kutscher et al., in press

The whole Lena River basin is underlain by permafrost, which is discontinuous in the south (thickness 25-100m) and continuous in the north (thickness 100-200m) (Gordeev and Siderov, 1993). The permafrost thickness reaches 400-600m in the Vilyuy lowlands. The active layer varies between1.4 – 2.5m for sandy/clayey soils and 0.6 – 0.8m for peat bog soils (Huh et al., 1998). Thermokarst lakes and bogs are prevalent in the northern lowlands (Gordeev and Siderov, 1993). The permafrost is mainly composed of cryogenic mineral soils (Tarnocai et al., 2009). However, there is extensive Yedoma along the banks of the Vilyuy River and in central low lying regions adjacent to the main channel (Romanovskii, 1993). The catchment area is dominated by larch and salix forest in the south with exposed rock outcrop in alpine areas; whereas in the tundra, the vegetation is mainly small shrubs, mosses and lichen (Gordeev and Sidorov, 1993). This study subdivides the data according to the regional geology. These subdivisions are outlined in Table 1 and the geology of the Lena River catchment area is outlined in detail by Resources of surface waters of the USSR (1972).

3. Sampling and Processing

3.1. Field sampling

River water samples were collected at 77 locations in July 2012 and June 2013. Fig. 1 a shows the sampling route and the sampling sites are outlined in Fig. 1 b and Table 1. Waters were stored in 10 L HDPE containers. All sampling and analytical equipment were acid washed using 0.5M HNO_3 and deionised water. All acid washing and sample analysis was conducted in Class 100 laminar flow hoods. Mineral acids from Seastar® and 18MΩ grade deionised water from a MilliQ® system was used throughout preparations and analysis.

3.2. Field Measurements

The pH of the water was measured in *situ* using an YSI 556 multi probe system (MPS) calibrated against NIST buffer solutions (pH 4, 6.5 and 9 at 25^{o}C) with an accuracy of ± 0.03 pH units, along with temperature (accuracy: 0.1^{o}C) and conductivity (accuracy: 1 uS/cmC). Sample positions were taken using a GPS receiver.

Geographical Region	Summary name	Number of Samples	Geology	Permafrost
Lena River	**Lena River**	22	Trans Baikal Mountain Range is the source of the Lena River.	Talik (unfrozen ground) along the base of the river. Areas of thermal erosion along the banks of the river (Costard et al.,) Islands formed from Quarternary sand deposits are evident in central section of the main channel (in the region between Yakutsk and the Viliui tributary)
Aldan River	**Aldan River**	7	Draining the Verkhoyansk Mountain Range and Stanovoy Mountain Range	Talik (unfrozen ground) along the base of the river. Areas of thermal erosion along the banks of the river (Costard et al.,2007)
Vilyuy River	**Vilyuy River**	5	Draining the Central Plateau	Talik (unfrozen ground) along the base of the river. Areas of thermal erosion along the banks of the river (Costard et al.,2007). River bank with unconsolidated Quarternary sands.
Central Siberian Plateau **Lena-Amgansk Inter River Area**	**Central plateau**	19	Mesozoic sediments (carbonate, evaporites), Quarternary sands in the south and east of the plateau. Cambrian Lena Pillars?!??!	Continous. Intra and supra permafost groundwater influx in areas of carbonate karst and quarternary sands. Yedoma permafrost in the center and east of the plateau.
Verkhoyansk Mountain Range	**Eastern mountains**	22	Carboniferous and Permian sediments.	Continuous. Bed rock exposure at high elevations.
Stanovoy Mountain Range	**Southern mountains**	1	Proterozoic schist, gneiss, quartzite and marble.	Continuous. Bed rock exposure at high elevations.
Trans Baikal Mountain Range	**Source Region**		Proterozoic schist, gneiss, quartzite and marble.	Discontinous. Bed rock exposure at high elevations.

Table 1 The geographical and geological regions in the Lena River catchment area. The collected samples are grouped according to the geological region. These regions are allocated a summary name in this study (e.g. Central Siberian Plateau is referred to as Central Plateau). A description of the underlying permafrost is also outlined.

3.3 Filtration and Dialysis

Table 2 provides an outline of the Fe fractions analysed in this study. The collected waters were filtered within 3 h through 142 mm diameter, 0.22 µm nitrocellulose filters (Millipore®) with diameter of 142 mm. The filters were prewashed in 5% acetic acid for 72 hours following Odman et al., 2006 and subsequently rinsed in ultrapure (MilliQ®) water for a week. Filtrations were carried out using silicon tubing, a peristaltic pump and a polycarbonate filter holder. The first 200ml was systematically discarded and the filtration unit was rinsed with MilliQ® water between each sample. The filters were frozen (-18 °C) immediately after filtration. Water samples were refrigerated (+8 °C) and acidified to pH 2 with 8M HNO_3 Seastar® three weeks after sampling.

For 29 samples, the $[Fe]_{colloiodal}$ and $[Fe]_{dialysis}$ fractions were separated from the < 0.22 µm filtered water using dialysis membranes (Fig. 2) following Pokrovsky et al., (2011), and Vasyukova et al., (2012). Tubular dialysis membranes with a molecular weight cut-off of 1 kDa and 10 kDa from Spectrapore® were used. The membranes were first rinsed in 2% HNO_3 and then MilliQ® in a clean laboratory, then filled with 50 ml of MilliQ® water and sealed and stored refrigerated in MilliQ® water. During sample processing, dialysis membrane was transferred to a 1 L bottle containing the sample (< 0.22 µm filtered water) and left for 72 hours (Pokrovsky et al., 2011). The contents of the membrane were then transferred to a 50 ml bottle and refrigerated. All processing was carried out in a portable glove box. The reliability of the dialysis method was tested by comparing the concentrations of major anions (e.g. SO_4^{2-} and F^-) in the dialysis water and in the external solution. In this study, the concentrations of SO_4^{2-} and F^- in the external and dialysis solutions agree to within 10 %, suggesting that membrane charging effects do not affect the distribution of Fe in the dialysis size separation. The combined filtration and dialysis blank for Fe was 2.8 ppb (n =5), 2% of the average 0.22 µm filtered Lena River [Fe]. Samples for DOC were collected using 25 mm pre-combusted glass fibre filters (GF/F) (Whatman GF/F) with pore size 0.7 µm. Samples were also taken at < 10 kDa and < 1 kDa size fractions using dialysis membranes. Particulate Organic Carbon (POC) was determined by combustion of the 0.7 µm GF/F filters. Filtered water were refrigerated in dark HDPE bottles.

3.4 Particulate analysis

Particulate material from 36 sample stations was analysed. Fig. 3 outlines the chemical and size separation subdivisions referred to in this study and details of this analysis. Two filters generally were analyzed from each station, unless otherwise outlined. One filter underwent total dissolution to determine the $[Fe]_{particulate}$. The second filter was leached using 0.5M HCl at room temperature for 24 hours (Leventhal and Taylor 1990; Lam et al., 2006; Lam and Bishop, 2008) to separate the secondary amorphous Fe and crystalline Fe oxides, as $[Fe]_{leach}$, leaving behind $[Fe]_{residual}$. This is equivalent to a

24 hour extraction using Na-dithionite (Leventhal and Taylor, 1990) and has been used in more recent iron isotope studies (Rouxel et al., 2005; Severmann et al., 2006; Fehr et al., 2008). The combined acid blank for filter dissolution was 0.3 µg Fe / filter (n =10), and the washed (5% acetic acid) filter blank was 1.8 µg Fe /filter (n =7). Blank corrections ranged from only 0.6% of the $[Fe]_{particulate}$ on filter LR52, analysed in the same run. The filter dissolution method (Fig. 2) was tested with three standards and the complete analysis is outlined in Table 1 and Table 2 in the Supplementary Information. Analysis of SLRS-5 (The International Geostandard - Riverine Water Reference Material for Trace Metals) showed a recovery of 108% (n =3). Recoveries for the dissolution of BCR-1 (Columbian River Basalt) and W2 (Diabase) were 97% (n = 8) and 90 % (n = 7) respectively.

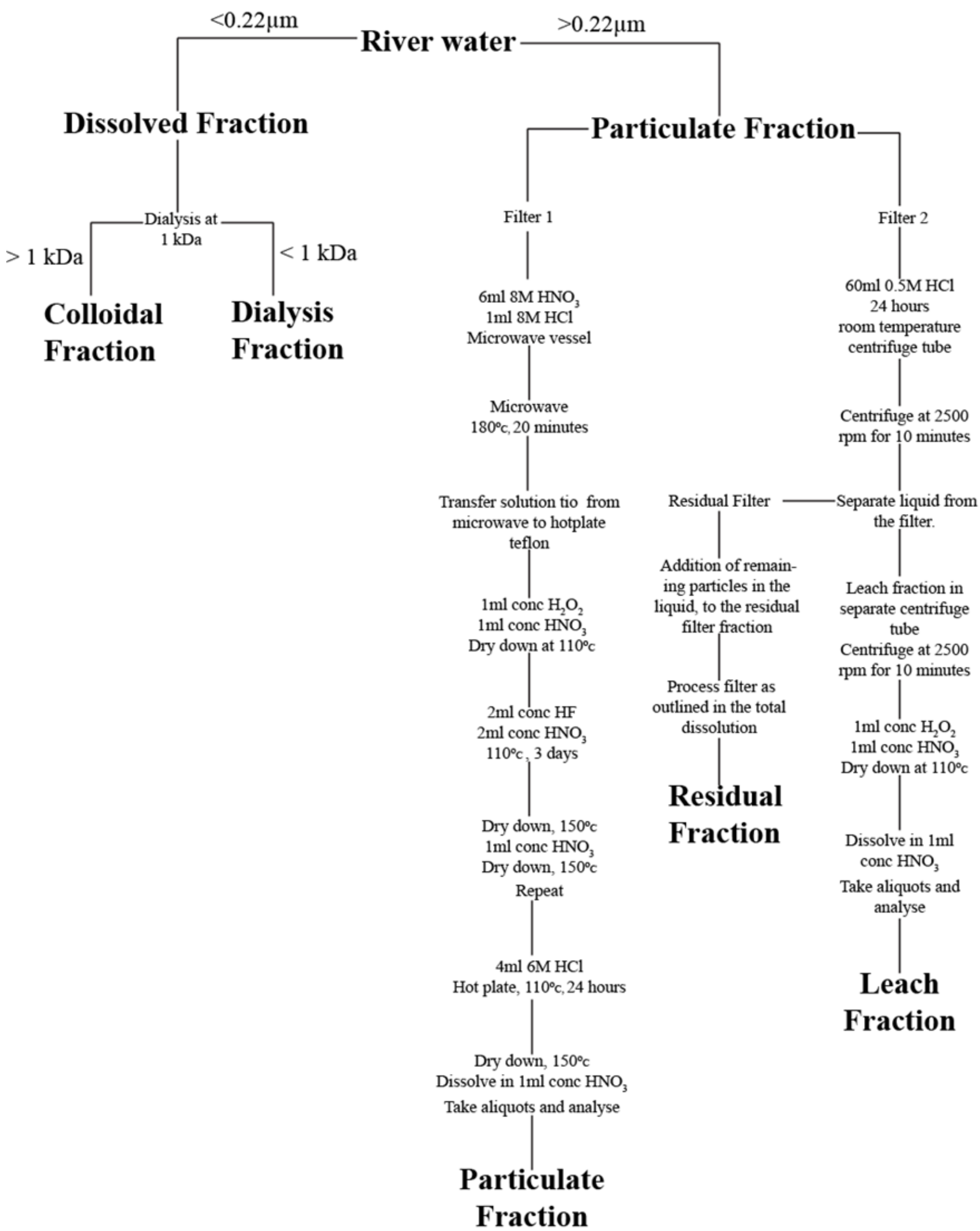

Fig. 2 Schematic of the size and chemical separation methods applied to Lena River water.

3.5 Major and Trace Element analysis

Major and trace element (TE) concentrations were measured within 6 months of sample collection. The major element analysis was done on an ICP-OES (Thermo ICAP 6500 Duo) with detection limits of 1 ppb and precision of ±5%, estimated from measurements of NIST 1640a. Trace element analysis was done using a single collector Element ICP-MS (Nu Instruments). The detection limit was 0.1 ppb for Fe. The analyses were done by standard addition where samples were calibrated against three Lena River water samples spiked with 1 ppb, 10 ppb and 100 ppb standard stock solution The international geostandard SLRS-5 was used as an external standard. A good agreement was obtained between replicated measurements of SLRS-5 and certified values for ICP-OES and ICP-MS analysis (relative difference < 5%, n = 3). DOC were determined by high-temperature catalytic oxidation (Shimadzu TOC-VCPH) at the Department of Applied Environmental Science, Stockholm University (0.7 µm) and Abisko Research Station (10 kDa and 1 kDa), with a detection limit of 0.1 mg/L and uncertainty in measurement of 0.1 to 2.0 mg/L.

3.3.3. TEM imaging and analyses

Scanning Transmission Electron Microscopy (STEM) was used to analyse the particles collected on the 0.22 µm nitrocellulose filters (7 samples) and particles in the < 0.22 µm water (3 samples). Little aging of Fe oxides was expected after collection since the half-life of transformation to crystalline forms is > 500 days when refrigerated or frozen (see Hawkings et al., 2014). A 100 mm^2 area of filter was suspended in 1 ml of MilliQ® water. One drop of the suspension was pipetted onto a holey carbon film-Cu grid (Agar scientific™) supported on filter paper, and allowed to dry.

The Fe bearing phases in < 0.22 µm filtered water were observed on three functionalised grids: (i) positively charged (attracts negatively charged particles), (ii) negatively charged and (iii) PEG (Polyethyleneglycol) silicon nitride film Cu grids. The PEG coated grid was effective in attracting OC particles but not effective at trapping Fe-bearing particles. The grids were stirred in the filtered water sample for ~3 minutes, washed in MilliQ® and air-dried prior to investigation in the STEM. All samples were imaged and analysed using an FEI Tecnai F20 200 kV FEGTEM fitted with a Gatan Orius SC600 CCD camera and an Oxford Instruments X-Max 80 mm2 EDX SDD running INCA software. Scanning Electron Diffraction patterns (SAED) were acquired for the particulate material but no usable patterns were collected for the < 0.22 µm filtered water due to the very small particle size and interferences with the silicon nitride film.

3.3.4. Spectroscopy imaging and analysis

The SXM operates similarly to a scanning electron microscope. An X-ray microprobe is formed by means of diffractive focusing lenses and the sample is raster-scanned across the microprobe. The SXM is well adapted to elemental and chemical analysis as it allows multi-detector geometries and simultaneous acquisition of transmission and secondary photon emission signals (Kirz 1996, Howells 2008, Kaulich 2011, Hitchcock 2014). TEM offers superior optical resolution, however the X-ray specific interaction with matter is superior for chemical analysis making these techniques complimentary for analysis of naturally heterogeneous particles. The SXM technique achieves strong chemical sensitivity through XANES (Stoehr, 1991) with analysis of the strong chemically specific contrast based on the intrinsic properties of the components of the sample. Such analysis can be complemented by elemental mapping and detecting element specific X-ray microfluorescence (XRF) (Jenkins, 1991). For this work, the I08-SXM facility at the Diamond Light Source (http://www.diamond.ac.uk) has been used. I08-SXM is optimised for spectromicropy in the 280-4400 eV photon energy range, can offer better than 30nm optical resolution depending on the imaging mode and photon energy, and a spectral resolution of better than 4000 over the entire photon energy range. For the NEXAFS study on Fe oxidation states, a stack of up to 100 SXM energies have been acquired at different photon energies, and the NEXAFS spectra were depicted from the image stack for each pixel of the raster scan using computational programs as Mantis (Lerotic, 2014)). XRF elemental mapping has been used to associate the Carbon to the Iron distribution.

4. Results

4.1. The distribution of Fe in different size fractions

Data for Fe concentrations in the particles for 36 samples are outlined in Table 3. On average, 70% of Fe is in the particulate fraction ($[Fe]_{particulate}$) in all sub-catchments and Lena River main channel. The central plateau region contains the highest average $[Fe]_{particulate}$ at 443 µg/L (n = 12, standard deviation (SD) = 463 µg/L). There are anomalously high values for the $[Fe]_{particulate}$ in the central plateau (LR61 = 1230 µg/L and LR37 = 1550 µg/L). When these $[Fe]_{particulate}$ are excluded the average $[Fe]_{particulate}$ in the central plateau is 254 µg/L (n = 10, SD = 130 µg/L). This value is similar to the Lena River main channel, which has an average $[Fe]_{particulate}$ at 294 µg/L (n= 9, SD = 175 µg/L). The Aldan River and eastern mountains have similar averages of $[Fe]_{particulate}$ of 230 µg/L (n = 3, SD = 123 µg/L) and 263 µg/L (n = 8, SD = 121 µg/L), respectively, while the southern mountains and Vilyuy River contains the lowest average $[Fe]_{particulate}$ at 43 µg/L (n = 3, SD = 23) and 118 µg/L (n = 2, SD = 58 µg/L), respectively.

The $[Fe]_{dissolved}$ for all 77 samples collected are reported in Table 3 in the Supplementary Information. In all samples, the $[Fe]_{colloidal}$ contributes 92% of the $[Fe]_{dissolved}$ in the system (Fig. 3 a), as such $[Fe]_{dissolved}$ is referred to as $[Fe]_{colloidal}$. The central plateau contains the highest average $[Fe]_{colloidal}$ of 115 µg/L (n = 22, SD= 75 µg/L) whereas tributaries draining the eastern mountains contain the lowest average [Fe] $_{colloidal}$ of 44 μg/l (n=22 SD =28 μg/L). The Vilyuy River which drains the central plateau, contains an average [Fe] $_{colloidal}$ of 64 μg/L (n = 5, SD 29 μg/L) and the highest proportion of Fe in the < 1 kDa fraction, 11% of the total [Fe] $_{dissolved}$. In contrast, the remaining tributaries of the central plateau have 3% of the Fe in < 1 kDa fraction.

Particulate Analysis (μg / L)							
Lena River	**$[Fe]_{particulate}$**	**$[Fe]_{residual}$**	**$[Fe]_{leach}$**	**$[Fe]_{dissolved}$**	**$[Fe]_{total}$**	**% Particulate**	**% Dissolved**
LR78	155	70	84	34	189	82	18
LR31	336	170	162	88	424	79	21
LR42	32	15	10	130	162	20	80
LR57	328	188	138	65	393	83	17
LR45	269	126	140	84	353	76	24
LR4	524	387	195	161	685	77	23
LR2	469	458	186	103	572	82	18
LR1	448	271	177	112	560	80	20
LR71	80	***	***	67	147	54	46
Average	**294**	**210**	**136**	**94**	**387**	**70**	**30**
SD	**175**	**153**	**62**	**38**	**195**	**21**	**21**
Aldan River							
LR38	***	***	496	104	***	***	***
LR5	215	105	57	108	323	67	33
LR8	360	118	65	105	465	77	23
LR13	115	***	40	77	192	60	40
Average	**230**	**112**	**164**	**99**	**326**	**68**	**32**
SD	**123**	**9**	**221**	**14**	**137**	**9**	**9**
Viliui River							
LR59	159	81	78	28	187	85	15
LR60	77	***	***	78	155	50	50
Average	**118**	**82**	**79**	**53**	**171**	**67**	**33**
SD	**58**	*****	*****	**35**	**23**	**25**	**25**
Central Plateau							
LR55	388	78	350	198	586	66	34
LR63	216	27	228	189	405	53	47
LR50	185	81	101	128	313	59	41
LR52	266	62	197	169	435	61	39
LR69	68	22	49	46	114	59	41
LR65	478	89	488	283	761	63	37
LR72	146	***	***	76	222	66	34
LR61*	1230	***	***	80	1310	94	6
LR37*	1550	907	483	106	1656	94	6
LR17	409	113	292	469	878	47	53
LR26	177	***	***	106	283	63	37
LR43	206	***	***	165	371	56	44
Average	**443**	**172**	**273**	**168**	**611**	**65**	**35**
SD	**463**	**298**	**162**	**115**	**194**	**14**	**14**
Eastern mountains							
LR58	217	117	98	72	289	75	25
LR56	205	79	123	20	225	91	9
LR67	169	57	112	35	204	83	17
LR16	463	119	160	87	550	84	16
LR53	356	157	196	20	376	95	5
LR46	166	83	154	84	250	66	34
Average	**263**	**102**	**140**	**53**	**316**	**82**	**18**
SD	**121**	**36**	**36**	**32**	**130**	**10**	**10**
Southern mountains							
LR33	32	15	10	21	53	61	39
LR12	27	11	12	21	48	57	43
LR27	70	27	22	61	131	53	47
Average	**43**	**18**	**15**	**34**	**78**	**57**	**43**
SD	**23**	**8**	**6**	**23**	**46**	**4**	**4**

Table 3. Fe concentration in the particulate, leach, residual and dissolved fraction for the 36 samples, for which particulate analysis was done. The proportion of particulate and dissolved iron is given as a percentage (%) of the total iron.

4.2. Relationship between Fe, OC and pH

Fig. 3 b shows that > 50 % of OC is found in the < 10 kDa fraction in all samples that underwent dialysis. In contrast, the particulate organic carbon (POC) constitutes the lowest proportion of the OC, < 8 % of the OC in all samples. The central plateau contains the highest average DOC at 120 µg/L (n = 14, SD = 33 µg/L). In contrast, the eastern mountains contain the lowest average DOC at 36 µg/L (n = 22 SD =27 µg/L).

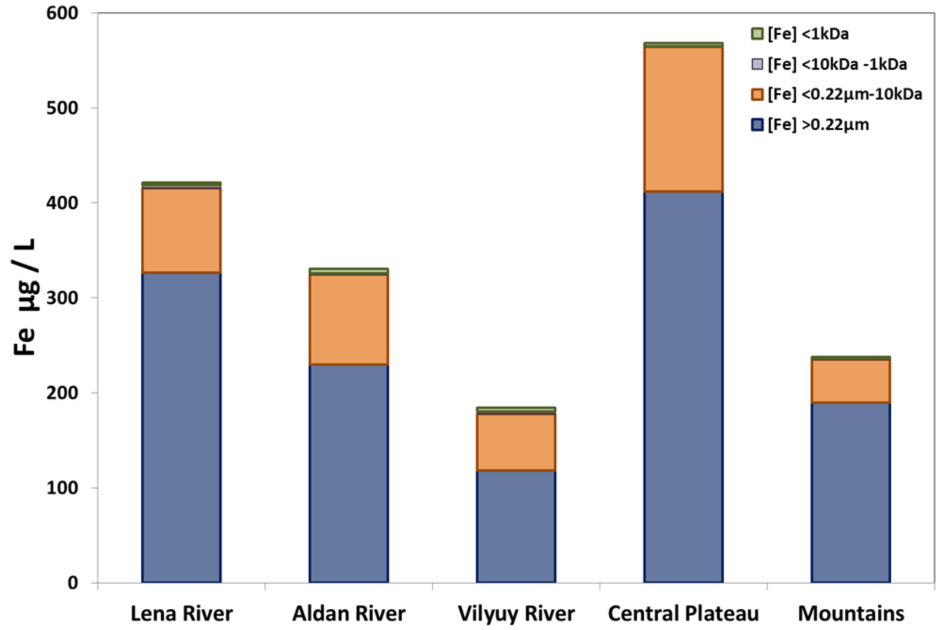

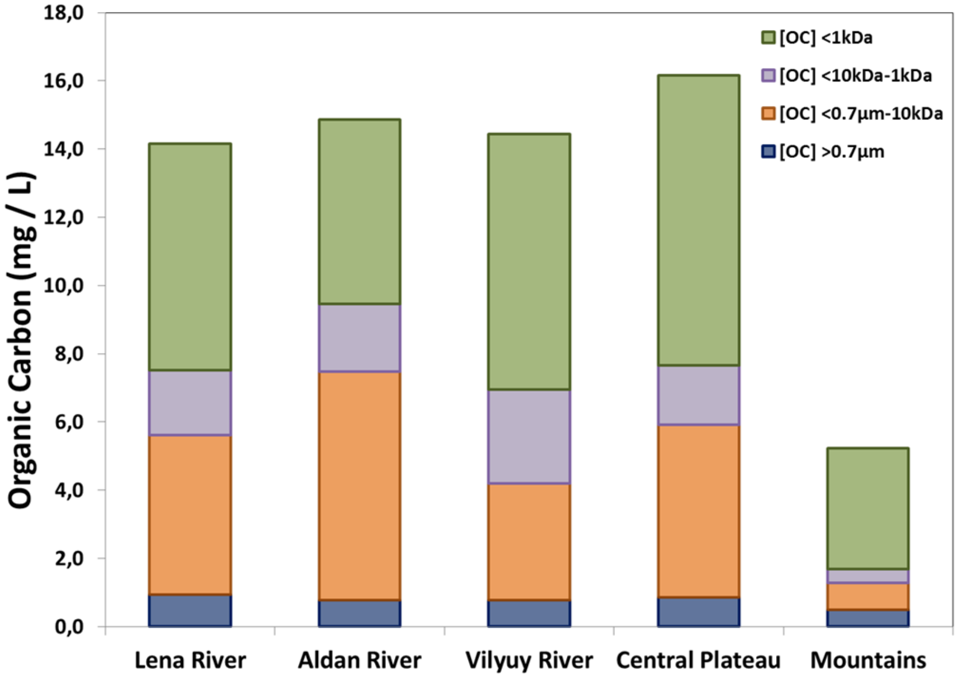

Fig. 3 a The proportion of iron in different size fractions: > 0.22 µm to < 1 kDa.

Fig. 3 b The proportion of organic carbon (OC) in different size fractions: > 0.7 µm to < 1 kDa

All water samples lie within a pH range of 6.5 to 9.0. Values greater that pH 8, only occur in the southern mountains. The relationship between $[Fe]_{particulate}$ and pH is outlined in Fig. 4. The southern mountain has the highest pH and lowest $[Fe]_{particulate}$. Between pH 7.0 and 7.5, there is a broad range in $[Fe]_{particulate}$.

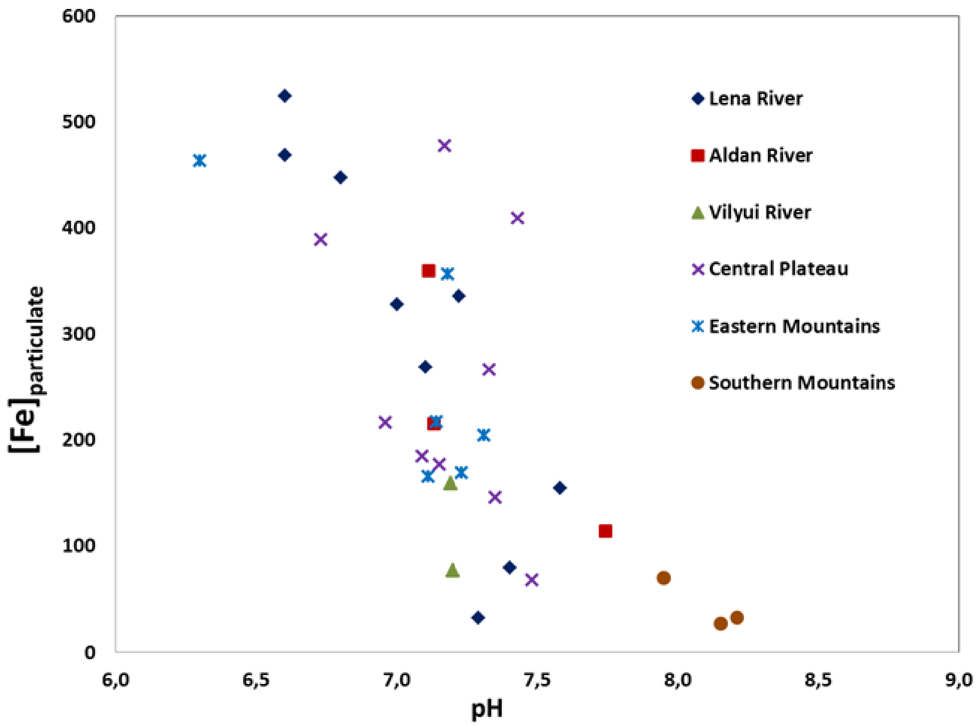

Fig. 4 The relationship between particulate Fe and pH for all measured samples.

4.3. Scanning Transmission Electron Microscopy (STEM)

4.3.1 TEM analysis of the >0.22 µm fraction

STEM has been used previously to characterize colloidal particles in river systems (Benedetti et al., 2003; Allard et al., 2004), especially in the identification of poorly crystalline Fe oxides, such as ferrihydrite (e.g. Banfield et al., 2000) and clay minerals (Raiswell et al., 2006). Overall, 8 filters (> 0.22 µm) were analysed: eastern mountains (LR51, LR44, LR70), Vilyuy River (LR62), central plateau (LR52, LR43), southern mountains (LR17) and main channel (LR70, LR45).

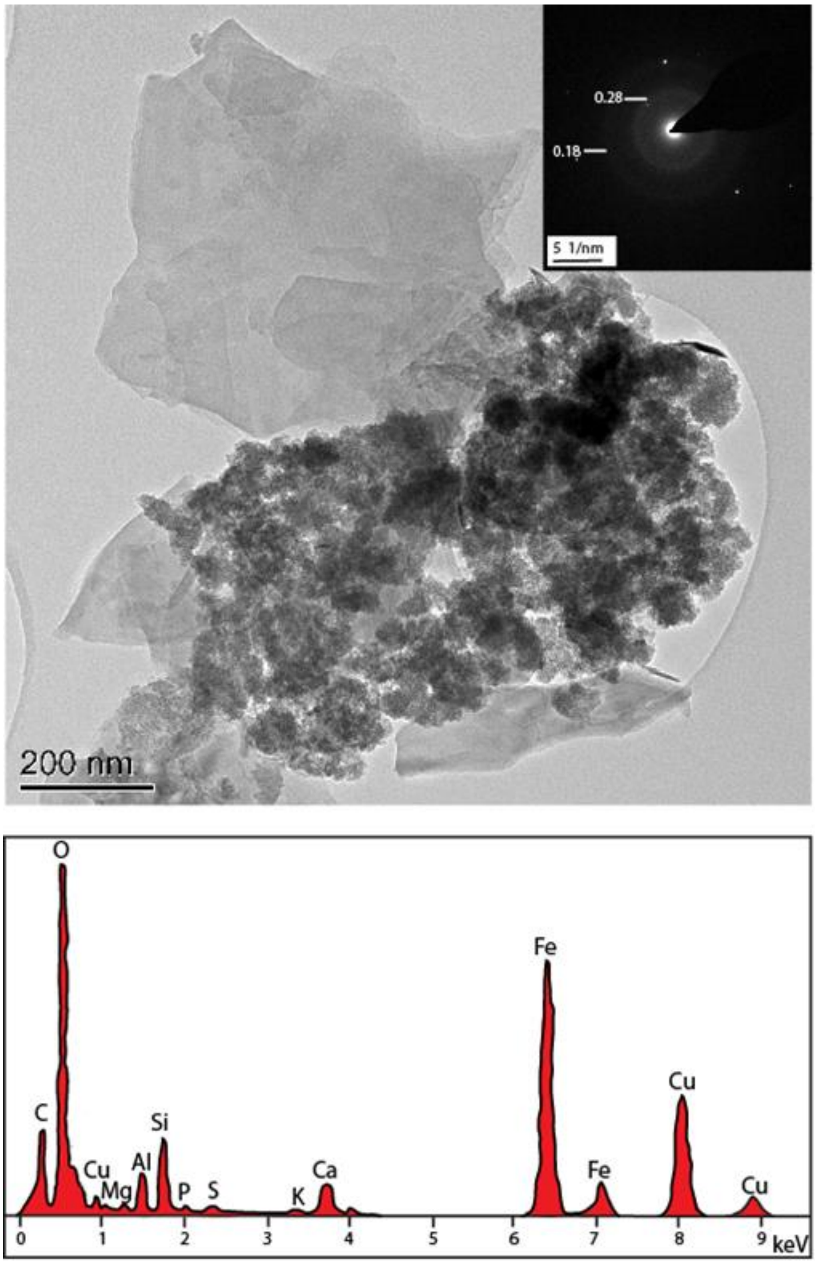

Fig. 5 a and b. TEM image, SAED pattern and EDX spectra from >0.22µm particulate material on LR17 (Tatta River, Central Plateau). The SAED pattern was indexed to 2-Line ferrihydrite, with major diffraction rings at 0.18 and 0.28 nm. The STEM image shows an aggregation of rounded aggregates of ferrihydrite nanoparticles. This is representative of the Fe particles observed in all samples analysed (see Fig. 6) The EDX spectra shows that Mg, Al, Si, P, S, K and Ca are associating with the ferrihydrite. The copper detected by the EDX originates from the copper disc and there is a background signal of carbon from the underlying grid.

Fig. 5 a shows a STEM image of a representative Fe-bearing secondary mineral particle. The particles are sub rounded and in turn composed of an aggregation of nanoparticles. The EDX spectra (Fig. 5 c) show peaks at Fe and O, indicating that this is an iron oxide. The SAED pattern (Fig. 4 b) shows two major rings at 0.18 nm and 0.28 nm, which is indicative of poorly crystalline iron – two line ferrihydrite (Janney, Cowley and Bouseck 2000; Hawkings et al., 2014). These particles, contain Mn, P, S, Ca, Al, Si, K and are most commonly attached to clay particles. The following trace elements (TE) are associating with the ferrihydrite, Mn, P, S, Ca, Al, Si, K. More rarely, (Fig. 6 c), the aggregates of ferrihydrite have aged and there is needle shaped alignment of crystals, indicative of goethite. Detrital iron was observed mainly in the clay minerals (Fig. 7 a) and haematite (Fig. 7 c). The SAED of the crystalline aggregate has major diffraction rings at 0.75 nm, 0.45 nm, 0.40 nm, 0.35 nm, 0.31 nm. These haematite nanoparticles were abundant in particulate material from the eastern mountains but were not observed in particulate material from the central plateau, Vilyuy River, Aldan River or Lena River. Further, Fe is also observed in iron – manganese (Fe - Mn) oxides in particulate material from the eastern mountain tributaries (Fig. 7 b). In summary, the main Fe-bearing particles in the Lena River catchment area were identified as (i) nanocrystalline ferrihydrite, (ii) Fe in clay minerals and (iii) Fe as hematite (only in tributaries draining the eastern mountains).

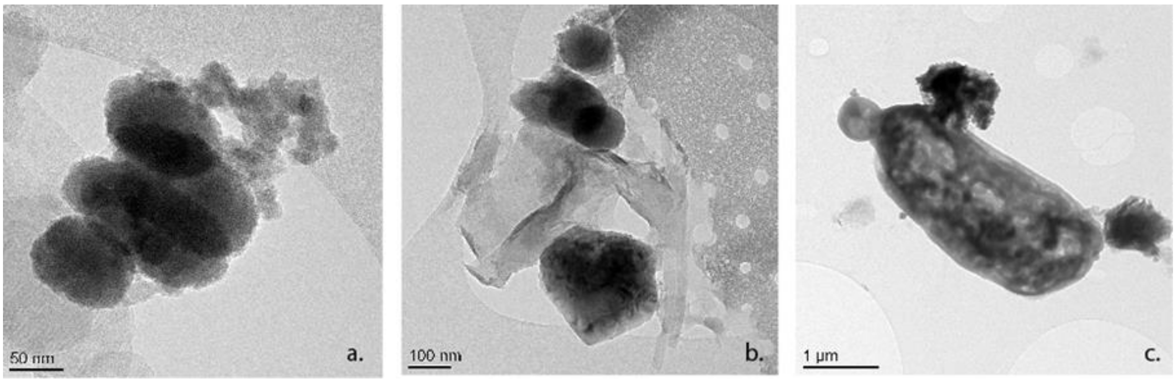

Fig. 6 TEM images of aggregated nanoparticles of ferrihydrite. The aggregates are 500 to 70 nanometer wide and sub-rounded (a) to rounded (b). The aggregates are more crystalline in places, and in image c, there is needle like alignment of nanocrystals which suggest that the ferrihydrite has aged to form goethite.

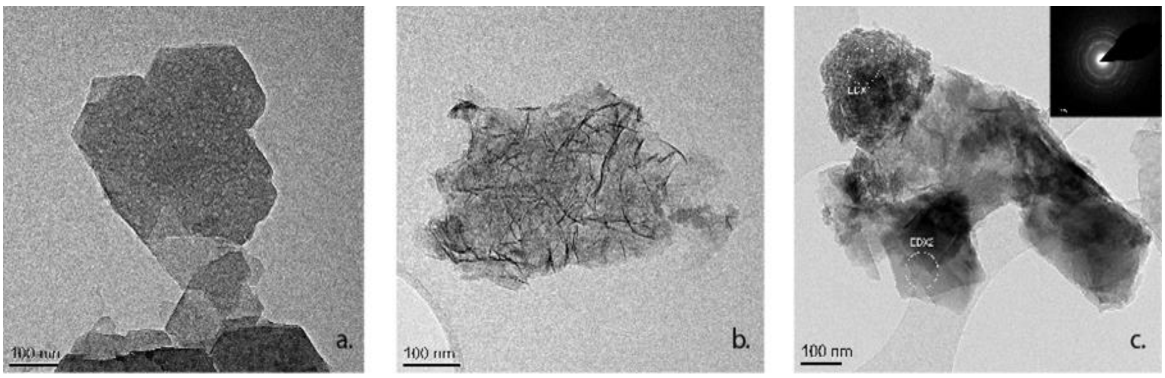

Fig. 7 STEM images of detrital particles from the Lena River (a) and eastern mountains (b and c). Image a shows a clay mineral, approximately 300 nm wide. Image (b) shows an Fe-Mn oxide, commonly found in the analysed samples from the eastern mountains. The particle has a crystalline mineralogy and high Mn content. Image (c) shows a haematite particle in the top left, which is attached to clay minerals. The SAED pattern is indicative of haematite with major rings at 0.75nm, 0.45nm, 0.40nm, 0.35nm, 0.31nm. Haematite was only observed in the eastern mountains.

4.3.2 TEM analysis of the <0.22 µm fraction

Three unacidified filtered water samples were analysed with TEM. Fig. 8 shows a representative Fe particle identified in the < 0.22 µm filtered water from the eastern mountains (LR51). Fe particles were attracted to both positive and negatively charged grids. The dominant Fe particles in < 0.22 µm fractions were 20-30 nm aggregates of 2-5 nm ferrihydrite particles. In the Vilyuy River and central plateau these particles had only minor association with OC. In the eastern mountains the Fe aggregates displayed a minor carbon peak but retained the amorphous ferrihydrite structure as seen in the particulate phase. More rarely, Al-Si-O rich 200 nm wide particles were observed on the eastern mountain positively charged grid and 100 nm long calcium rich particles were observed on the eastern mountain tributary PEG coated grid.

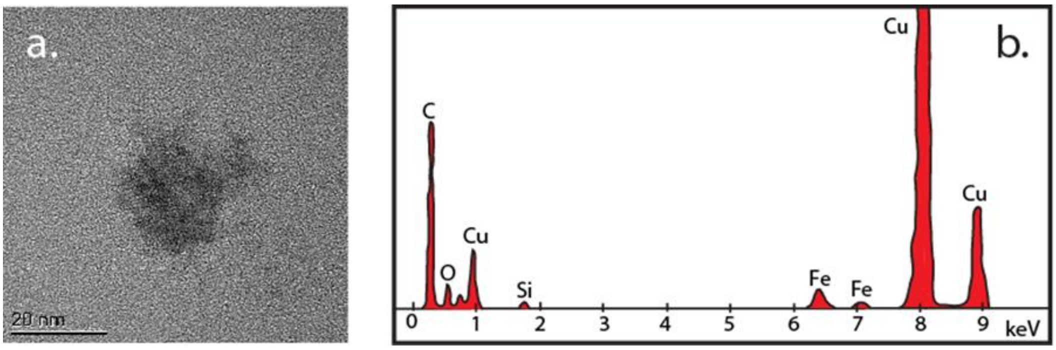

Fig. 8 TEM image of a particle in the < 0.22µm filtered water from LR55 (Central Plateau). No EDX spectra was determined on particles in filtered water, but this is a representative image of the Fe – rich nanoparticles observed in the three water samples that were imaged. The copper and part of the silica detected by the EDX originates from the copper disc and there is a background signal of carbon from the underlying grid.

4.3.3 Scanning Transmission X-ray spectroscopy (STXM)

STXM was used to characterise the association between > 0.22 µm Fe and OC particles. Fig. 9 a shows an STEM image of a particle in the Lena River main channel (LR75) associated with a clay mineral. The XRD map in Fig. 8 b indicates that this is a Fe rich particle and the XANES spectra taken on the Fe-L edge, (Fig. 9 c) is indicative of ferrihydrite (Von der Heyden et al., 2014). This analysis confirms the presence of ferrihydrite in the Lena River catchment area.

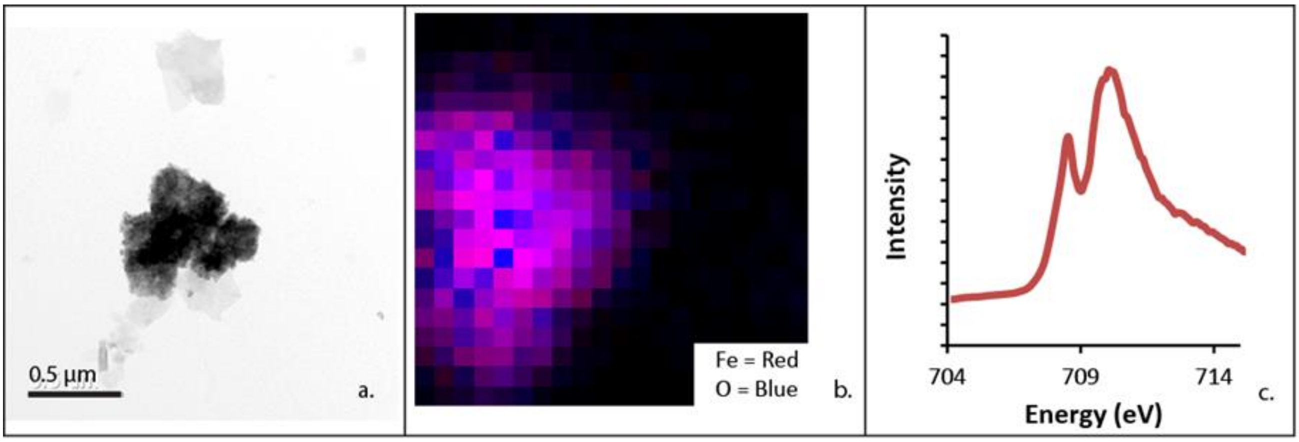

Fig. 9 STEM image of a particle from the Lena River main channel (LR75). The STEM image was taken and then XRF mapping was performed on the particle, as outlined in b. The particle is iron rich, as was previously identified with STEM in other samples. The XANES spectra was determined on the same particle (a) identified with STEM and this intensity ratio of the two peaks in this spectra, is indicative of ferrihydrite.

TEM analysis identified that smaller, darker aggregates are within a network of OC (Fig. 10 a). This was a common observation in tributaries that drain the eastern mountains. XRF mapping identified that these aggregates are Fe rich and STEM imaging at higher magnification (Fig.10 d) indicated that these iron particles are nanocrystalline and similar to the ferrihydrite aggregates observed in the < 0.22 µm fraction and the XANES spectrum correspond to ferrihydrite (Fig. 10 c). This association could be an artifact of filtration, however it was observed multiple times and only on filters draining the eastern mountain range.

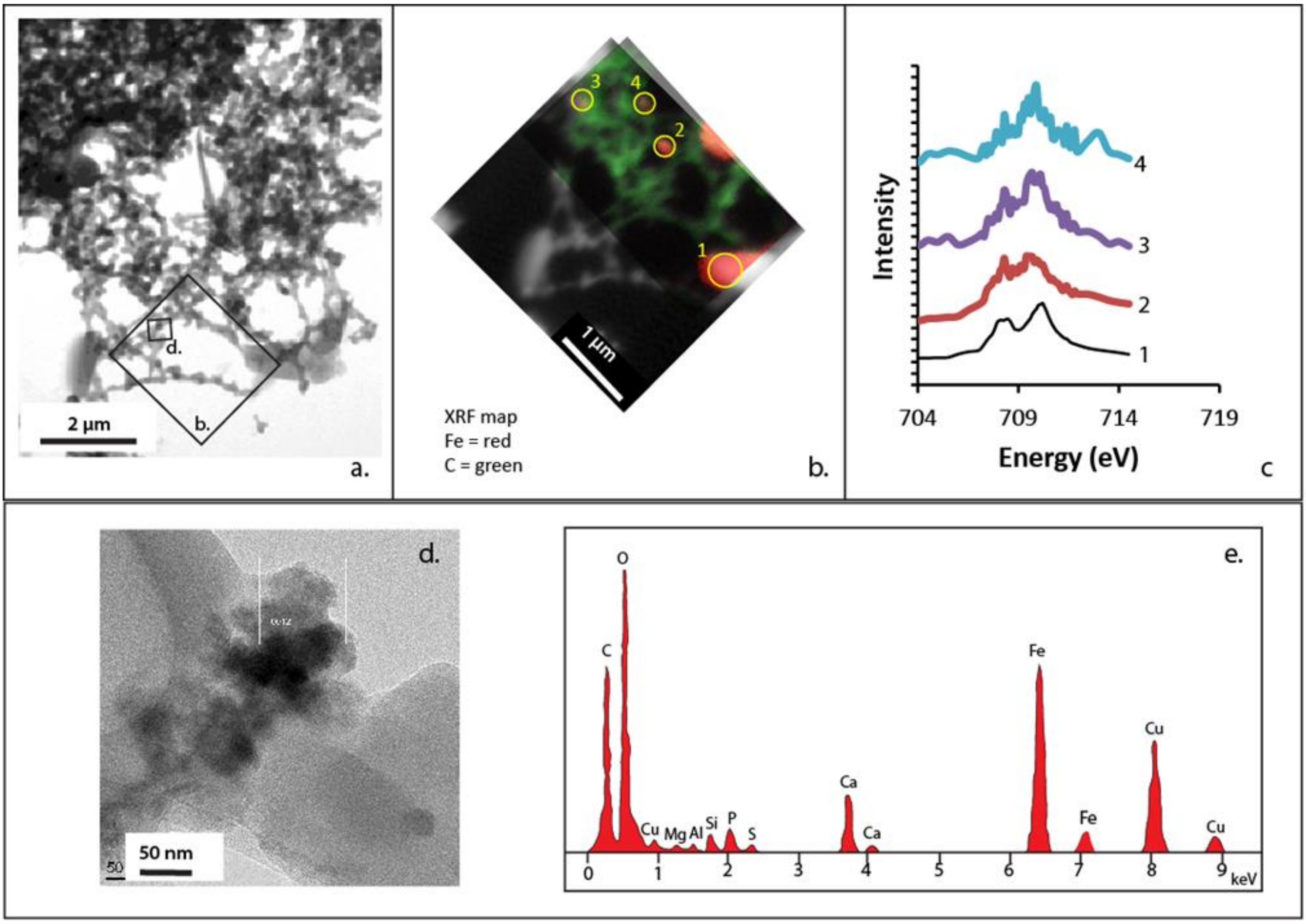

Fig. 10 a shows a representative TEM image of an organic particle from the eastern mountain tributary (LR75). Darker "inclusions" were initially observed within the particle and investigated further here. Fig. 9 b shows a soft X-ray, Scanning Transmission Electron Microscopy (STXM) XRF map. The organic rich region is highlighted in green. Iron rich regions are dispersed amongst the organics, in red. Fig. 10 c shows the X-Ray Absorption Near Edge Spectroscopy (XANES) spectra that corresponds with the map in b. This spectrum was taken on the Fe L-edge and the L_3 peak splitting is determined according to its eV value (difference in energy between high energy and low energy peaks) and its intensity ratio value (peak intensity quotient i_1 / i_2). The peak intensity quotient is indicative of ferrihydrite. Fig. 10 d shows a TEM image of poorly crystalline ferrihydrite particles, as observed in Fig.5 and Fig. 6 with an EDX spectra as in Fig. 4b.

4.4 Quantifying the observed Fe phases

The proportion of $[Fe]_{leach}$, $[Fe]_{residual}$ and $[Fe]_{colloidal}$ in the major sub catchments and the main channel are outlined in Fig. 11. The central plateau contains the highest proportion of secondary iron, identified as nanocrystalline ferrihydrite, $[Fe]_{leach}$ = 273 µg/L (n = 8, SD = 162 µg/L), 76 % (n = 8, SD = 27%) of the $[Fe]_{particulate.}$ In contrast, the Aldan River contains $[Fe]_{leach}$ of 54 µg/L (n = 5, SD = 13 µg/L), which is 23% of the $[Fe]_{particulate}$. In contrast, $[Fe]_{particulate}$ in the eastern and southern mountains, contains approximately 50 % $[Fe]_{leach}$.

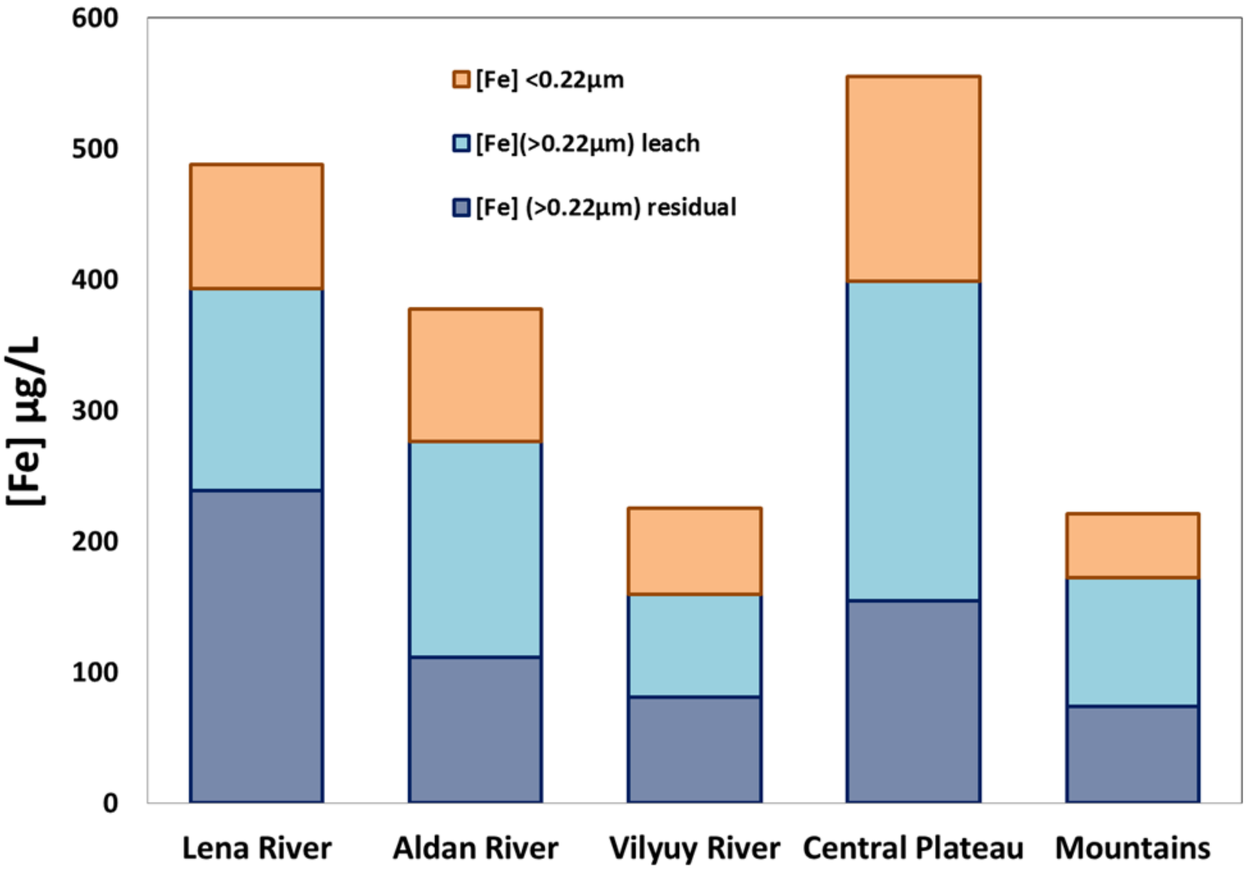

Fig.10 The proportion of [Fe] in (i) the colloidal (< 0.22µm) fraction (ii) leached (0.5M HCl,. 24 hours) and (iii) residual particulate fraction.

5. Discussion

5.1 Size distribution of Fe in the Lena River catchment area

The results show that in July 2012 and June 2013 the particulate fraction contains the highest proportion of Fe in the Lena River and sub catchments. This is consistent with other major global rivers (see summary by Viers et al., 2009) where Fe is mainly found in the suspended fraction. Further, the concentration of colloidal Fe is consistent with other Arctic rivers sampled during same season (Pokrovsky et al., 2006, 2010; Ingri et al., 2000) but greater than in tropical rivers (Allard et al., 2004), where 95 % of the Fe is transported as particulate Fe. However, in both the Amazon River and Lena River, > 50 % of the particulate material is transported as secondary mineral Fe particles (Allard et al., 2004). Therefore, the particle size distribution varies between major boreal and tropical rivers, but both boreal rivers and tropical rivers contribute a substantial proportion of secondary reactive Fe.

In smaller systems underlain by permafrost, a substantial fraction of the $[Fe]_{dissolved}$ and OC is found in the < 1 kDa (Vasyukova et al., 2012; Illina et al., 2013). In contrast, in this study there is a large difference in the size distribution of the OC and Fe in major tributaries and the Lena River (Fig. 3 a and b), which is consistent with major tributaries of other Arctic Rivers. For example, Stolpe et al., 2013 analysed the size of Fe-bearing particles in major tributaries of the Yukon River, during summer base-flow. With the use of field flow fractionation techniques the size of inorganic Fe-bearing particles was constrained to 4 – 40nm wide and not observed to complex with OC. Therefore, this study supports observations from larger boreal rivers, which show the size distribution of Fe-bearing particles and their relationship with OC, to differ from small boreal river catchments. However, microscopic and spectroscopic evidence in this study shows that inorganic Fe-bearing particles span a range of sizes which encompass the operationally defined in the colloidal (<0.22 μm) and particulate (>0.22 μm) fraction.

The secondary mineral Fe-bearing particles are identified as aggregated particles of nanocrystalline ferrihydrite and variation in the size of these aggregates, demonstrated in Fig. 5, Fig. 6, Fig. 8 and Fig. 9, shows that the size of Fe-bearing particles in the colloidal and particulate fraction of major boreal rivers is not easily constrained. The degree of aggregation and phase transformation of ferrihydrite is governed by its associated phases. Ferrihydrite is metastable and more crystalline and less bioavailable iron-bearing particles can form under the specific conditions (see review by Raiswell and Canfield, 2012). In this study, there is a minor contribution of goethite particles, characterized by their needle shaped crystal structure (Fig. 6c and Supplementary Information Fig. 2). This is suggestive of ferrihydrite particle dissolution at very low or high pH (Schwertmann & Murad., 1983) which may have occurred in soil pore fluids or the water column. However, the haematite observed in this study is unlikely to have formed in the river as it requires a rearrangement of the ferrihydrite poorly ordered crystal lattice at medium pH values (Schwertmann & Murad., 1983) and is commonly a product of weathering of Fe-rich sedimentary rocks and is not an example of ferrihydrite transformation to a more crystalline form during transport. Selective particle dissolution shows that secondary Fe-bearing particles encompass ≥ 70 % of the particulate fraction (Fig. 10) and subsequently, a substantial fraction of the particles transported in the Lena River is in the reactive form of ferrihydrite.

The phase transformation of ferrihydrite is retarded by the absorption of sorbed species such as silica (Zhao et al., 1994), phosphate and sulphate (Cornell, 1987). These ions bind to the tetrahedral sites on the surface of ferrihydrite (Zhao et al., 1994) and form inner sphere complexes. This process inhibits the rearrangement of atoms within the poorly crystalline ferrihydrite structure and formation of more crystalline goethite and haematite (Jambor & Dutrizac., 1998). Laboratory experiments (Carlson and Schwertmann, 1987) suggest that a Si concentration between 7 to12 mg/L inhibits the crystallization of ferrihydrite, by increasing the temperature required to convert ferrihydrite to haematite (Jambor and Dutrizac, 1998). Silica is present mainly in the dissolved fraction in all sub catchments with concentrations varying from 2 mg/l to 0.5 mg/l in the dissolved fraction. However, clay mineral and diatom dissolution (e.g. Fig. 6 b) will increase the local concentration of soluble cations (Jambor and Dutrizac 1998) and reduced the degree of crystallisation. Evidence from the EDX measurements of ferrihydrite in the Lena River sub catchments show Si, P and S (Fig. 4 c) to associate with the surface of ferrihydrite aggregates. The presence of clay and organic particles (Fig. 6) also reduces the size of ferrihydrite aggregates and thus the likelihood of reorganization of the crystal lattice (Jambor and Dutrizac, 1998). Further, in this study, aggregates of ferrihydrite occur in a spherical shape (Fig. 6 b) which indicates that the charges in the inner-sphere complex are neutralized which is inhibiting repulsive forces and favoring aggregation (Carlson and Schwertmann, 1981). Therefore, the particles of aggregated ferrihydrite in the Lena River catchment area persist as a result of access to dissolved anions, cations and organic carbon (OC), all of which prevent rapid transformation to more crystalline phases. There is therefore an enhanced likelihood that the ferrihydrite will be sustained within the main channel.

5.2 Relationship between Fe- bearing particles and organic carbon

The relationship between Fe and OC in a river is dependent on the pH (Karlsson and Persson., 2012) concentration of dissolved Fe and OC (Illina et al., 2013), reactivity of dissolved OC (Amon and Benner, 1996) and competitive carrier phases, such as clay minerals (Raiswell et al., 2010). Previous work in smaller boreal river systems has outlined the key role of OC as a carrier phase for Fe. However, in this study Fe is mainly observed in the particulate and colloidal fraction (Fig. 3) whereas the OC is mainly observed in the < 1 kDa fraction. We now explore possible reasons for this size discrepancy in the Lena River and major tributaries.

Compiled data of Fe-OC complexation and pH measurements from tropical, temperate and boreal rivers show that Fe-OC complexation decreases with increasing pH for all rivers (Neubauer et al, 2013). Further, modelling results show a decrease in Fe-OC complexation from almost 100% at pH 4 to about 10% or less at pH 7 (Lofts and Tipping, 2008). However, the pH values in the Lena River catchment area span a range from 6.3 – 9.0 (Fig. 4). This is in contrast to pH values in thermokarst lakes and low order tributaries in boreal rivers which have lower pH values (Vasyukova et al., 2012; Pokrovsky et al., 2011). The pH range of samples in this study is within the low solubility range for ferrihydrite, which is at minimum between pH 7 and pH 8.5 (Stumm and Morgan, 1996). In this study the proportion of Fe in the < 1kDa fraction is low (Fig. 3 b) and so the total contribution of any Fe-OC complexes to the total Fe budget is also low. In summary, the pH range and scarcity of Fe in the < 1 kDa fraction is consistent with the formation of ferrihydrite, in preference to Fe-OC particles.

The speciation and complexation of the resulting Fe phase is highly dependent on its relationship with the organic carbon (OC) (Perret et al., 2000). Amon & Benner 1996 propose a size reactivity model for organic carbon which suggested that OC in the < 1kDa is more refractory than larger particles of OC. The highest concentrations of OC and Fe are observed in tributaries draining the central plateau. However, STEM did not identify any Fe-OC complexes in central plateau tributaries and we suggest, based on this relationship between organic carbon size and reactivity (Amon et al., 1996), that the larger particles of OC are more labile and degraded in the smaller sub catchments, which shifts the OC size range towards smaller, less reactive fractions. The secondary mineral ferrihdyrite is observed to either be attached to the surface of primary produced OC (for example in Fig. 6 c) as larger aggregates or is entrapped as smaller ferrihydrite aggregates, in a network of OC. Both of these associations were commonly observed on the particulate material in the central plateau and eastern mountains, but not observed on particulate material in the Lena River. This association could be an artifact of filtration, however it was observed multiple times and only on filters draining the eastern mountain range. This suggests that although POC contributes a small percentage of the total OC (Fig. 3 b), it may provide an attachment surface for colloidal ferrihydrite in sub catchment Fe transport. However, in this study ferrihydrite is mainly associated with clay mineral phases (Fig. 7), which are the dominant particle observed by STEM of the >0.22 μm fraction in the Lena River main channel (Fig. 5). This association is consistent with studies in the Amazon River (Allard et al., 2004) and in glacially fed rivers (Raiswell et al., 2006) where ferrihydrite is commonly found attached to the surface of clay minerals. In summary, microscopy and spectroscopy analysis suggests that POC and clay minerals in major tributaries provide a surface on which ferrihydrite can aggregate and be transported. Nonetheless, ferrihydrite is only observed with clay mineral surfaces in the main channel.

5.3 Formation of secondary mineral Fe-bearing particles

Previous studies in smaller boreal river catchments (Ingri et al., 2000; Dahlqvist et al., 2007) show that Fe (oxy) hydroxides are the most abundant Fe particle in boreal rivers during the winter months and form upon oxidation of Fe(II) from groundwater. In contrast, Pokrovsky et al., (2005) suggest that Fe-OC complexes are the dominant colloidal particle during the post spring flood period. It is argued that following the spring flood, Fe-Al-OC colloids form in the leaf litter layer where the pH remains low, relative to surface waters and the Fe-OC relationship is sustained. It is then inferred that these Fe-Al-OC rich fluids migrate from the litter layer into the boreal streams and dominate the riverine colloidal fraction in the summer. However, unlike previous studies of iron-bearing particles in boreal catchments (Ingri et al., 2006; Pokrovsky et al., 2005; Dahlvqvist et al., 2007; Vasyukova et al., 2012; Illina et al., 2013), the Lena River main channel and tributaries are often greater than 100 m wide and can be as wide as 10 km. They are, by definition, high order streams (Strahler, 1957). Previous work has shown that OC reaches a point of "chemostasis" when transported from low to high order streams

(Creed et al., 2015) as the sources of OC are non-longer spatially connected (Freeman et al., 2007) and there is therefore no direct replenishment of reactive OC. Subsequently, in this study, Fe-bearing particles may be derived from sources that are distal from these low order tributaries. For example, ferrihydrite may form due to the influx of reduced supra permafrost and talik derived groundwaters (Dia et al., 2000), which enter the main channel and major tribuaries during summer baseflow (Gordeev et al., 2004). Ferrihydrite may also derive from abiotic oxidation of Fe(II) upon the weathering of clay and haematite in mineral soils (Bagard et al., 2011), during summer base flow. Conversely, Fe bearing particles may from alteration of Fe-OC complexes, via microbial or photo degradation, during transport from low order tributaries. These Fe-OC complexes were formed in low order tributaries and lakes, in conditions of lower pH, labile OC and dissolved Fe (Vasyukova et al., 2012).

Regardless of origin, the ferrihydrite is sustained because the processes of disaggregation and Fe-OC complexation appear to be minimal in the Lena River main channel as suggested by the low concentration of Fe in the < 1kDa fraction, scarcity of primary produced OC particles on the filters of the Lena River main channel, which were observed in the central plateau tributaries (Fig 1 Supplementary Information) and dominance of OC in the < 1 kDa fraction. Moreover, there is a sufficient supply of soluble cations derived from clay, diatom and POC surfaces to prevent the aggregates of ferrihydrite from forming more crystalline, less reactive phases. In summary, particles of ferrihydrite are being transported in a system with conditions that are favorable to sustain it. Nonetheless, this system may be unbalanced by the predicted warming and resulting enhanced thermal and mechanical erosion of connected sources of OC (Costard et al., 2007) that may contribute a pool of larger and more labile OC, which would alter the Fe-OC relationship in high order rivers.

6. Conclusions

Our data show that > 70 % of iron in water from the Lena River occurs in the particulate fraction. In contrast > 50 % of DOC occurs in the truly dissolved (< 1 kDa) fraction. Results from leaching experiments show that tributaries draining the central plateau contain the highest proportion of ferrihydrite.

We propose that the formation of ferrihydrite is mainly due to the abiotic oxidation of Fe(II) at a close to neutral pH and under conditions devoid of larger reactive OC particles. Ferrihydrite is sustained in these high order rivers is the result of favourable conditions of high Si, dissolved cations and anions, which results from the association of ferrihydrite with the surface of particulate organic carbon and clay minerals.

This study shows that ferrihdyrite is the dominant form of iron particle phase forming in the Lena River catchment area, during this post-spring flood period. Consequently, ferrihydrite is the dominant iron particle transported to the Lena River delta, estuary and to the Laptev Sea.

7. Acknowledgements

This study was funded by the European Union Seventh Framework Programme for research, technological development and demonstration under grant agreement no. 290336 and the Swedish Research Council. Support of both funding bodies is highly acknowledged. Special thanks to the crew of R/V Merelotoved, Karin Wallner, Hans Schöberg, Phil Holdship and Mike Ward, for their technical support.

8. References

Allard, T., Menguy, N., Salomon, J., Calligaro, T., Weber, T., Calas, G., & Benedetti, M. F. (2004). Revealing forms of iron in river-borne material from major tropical rivers of the Amazon Basin (Brazil). *Geochimica et Cosmochimica Acta*, *68*(14), 3079-3094.

Amon, R. M., & Benner, R. (1996). Bacterial utilization of different size classes of dissolved organic matter. *Limnology and Oceanography*, *41*(1), 41-51.

Amon, R. M. W., Rinehart, A. J., Duan, S., Louchouarn, P., Prokushkin, A., Guggenberger, G., ... & McClelland, J. W. (2012). Dissolved organic matter sources in large Arctic rivers. *Geochimica et Cosmochimica Acta*, *94*, 217-237.

Bagard, M. L., Chabaux, F., Pokrovsky, O. S., Viers, J., Prokushkin, A. S., Stille, P., ... & Dupré, B. (2011). Seasonal variability of element fluxes in two Central Siberian rivers draining high latitude permafrost dominated areas.*Geochimica et Cosmochimica Acta*, *75*(12), 3335-3357.

Banfield, J. F., Welch, S. A., Zhang, H., Ebert, T. T., & Penn, R. L. (2000). Aggregation-based crystal growth and microstructure development in natural iron oxyhydroxide biomineralization products. *Science*, *289*(5480), 751-754.

Benedetti, M. F., Ranville, J. F., Allard, T., Bednar, A. J., & Menguy, N. (2003). The iron status in colloidal matter from the Rio Negro, Brasil. *Colloids and Surfaces A: Physicochemical and Engineering Aspects*, *217*(1), 1-9.

Boyd, P. W., and M. J. Ellwood (2010). "The biogeochemical cycle of iron in the ocean." *Nature Geoscience* 3.10, 675-682.

Costard, F., Gautier, E., Brunstein, D., Hammadi, J., Fedorov, A., Yang, D., & Dupeyrat, L. (2007). Impact of the global warming on the fluvial thermal erosion over the Lena River in Central Siberia. *Geophysical Research Letters*, *34*(14).

Creed, I. F., McKnight, D. M., Pellerin, B. A., Green, M. B., Bergamaschi, B. A., Aiken, G. R., ... & Aulenbach, B. T. (2015). The river as a chemostat: fresh perspectives on dissolved organic matter flowing down the river continuum. *Canadian Journal of Fisheries and Aquatic Sciences*, *72*(8), 1272-1285.

Dahlqvist, R., Andersson, K., Ingri, J., Larsson, T., Stolpe, B., & Turner, D. (2007). Temporal variations of colloidal carrier phases and associated trace elements in a boreal river. *Geochimica et Cosmochimica Acta*, *71*(22), 5339-5354.

Fehr, M. A., Andersson, P. S., Hålenius, U., & Mörth, C. M. (2008). Iron isotope variations in Holocene sediments of the Gotland Deep, Baltic Sea.*Geochimica et Cosmochimica Acta*, *72*(3), 807-826.

Fedorov, A., & Konstantinov, P. (2003, July). Observations of surface dynamics with thermokarst initiation, Yukechi site, Central Yakutia. In*Proceedings of the VII International Permafrost Conference* (pp. 239-243).

Field, C. B., Behrenfeld, M. J., Randerson, J. T., & Falkowski, P. (1998). Primary production of the biosphere: integrating terrestrial and oceanic components. *Science*, *281*(5374), 237-24

Freeman, M. C., Pringle, C. M., & Jackson, C. R. (2007). Hydrologic connectivity and the contribution of stream headwaters to ecological integrity at regional scales.

Gordeev, V. V., & Sidorov, I. (1993). Concentrations of major elements and their outflow into the Laptev Sea by the Lena River. *Marine Chemistry*, *43*(1-4), 33-45.

Grosse, G., Robinson, J. E., Bryant, R., Taylor, M. D., Harper, W., DeMasi, A.& Harden, J. (2013). Distribution of late Pleistocene ice-rich syngenetic permafrost of the Yedoma Suite in east and central Siberia, Russia. *US Geological Survey Open File Report*, *2013*(1078), 1-37.

Hawkings, J. R., Wadham, J. L., Tranter, M., Raiswell, R., Benning, L. G., Statham, P. J.& Telling, J. (2014). Ice sheets as a significant source of highly reactive nanoparticulate iron to the oceans. *Nature communications*

Howells, M., Jacobsen, C., Warwick, T., Principles and Applications of Zone Plate X-ray Microscopes (2008), *in: Science of Microscopy (Springer Verlag, eds.: Hawkes, P.W., & Spence, J.C.H.), Volume 2, 835-926, ISBN 978-0-387-49762-4*

Hiemstra, T., & Van Riemsdijk, W. H. (2009). A surface structural model for ferrihydrite I: Sites related to primary charge, molar mass, and mass density.*Geochimica et Cosmochimica Acta*, *73*(15), 4423-4436.

Hitchcock, A.P., Soft X-ray Imaging and Spectromicroscopy (2012), *in: Handbook of Nanoscopy (Wyley, eds.: Van Tendeloo, G., Van Dyck, D., & Pennycook, S.J.), Volume 2, 745-792, ISBN: 978-3-527-31706-6*

Ilina, S. M., Poitrasson, F., Lapitskiy, S. A., Alekhin, Y. V., Viers, J., & Pokrovsky, O. S. (2013). Extreme iron isotope fractionation between colloids and particles of boreal and temperate organic-rich waters. *Geochimica et Cosmochimica Acta*, *101*, 96-111.

Ingri, J., Widerlund, A., Land, M., Gustafsson, Ö., Andersson, P., & Öhlander, B. (2000). Temporal variations in the fractionation of the rare earth elements in a boreal river; the role of colloidal particles. *Chemical Geology*,*166*(1), 23-45.

Ingri, J., Malinovsky, D., Rodushkin, I., Baxter, D. C., Widerlund, A., Andersson, P., ... & Öhlander, B. (2006). Iron isotope fractionation in river colloidal matter. *Earth and Planetary Science Letters*, *245*(3), 792-798.

Jambor, J. L., & Dutrizac, J. E. (1998). Occurrence and constitution of natural and synthetic ferrihydrite, a widespread iron oxyhydroxide. *Chemical Reviews*, *98*(7), 2549-2586.

Janney, D. E., Cowley, J. M., & Buseck, P. R. (2000). Structure of synthetic 2-line ferrihydrite by electron nanodiffraction. *American Mineralogist*, *85*(9), 1180-1187.

Jenkins, R., (1999), X-ray Fluorescence Spectrometry. *Wiley*, ISBN: 978-0-471-29942-4

Kaulich, B., Thibault, P., Gianoncelli, A., & Kiskinova.M (2011). Transmission and emission x-ray microscopy: operation modes, contrast mechanisms and applications. *J. Phys: Condens. Matter, 23(8), 083002. http://dx.doi.org/10.1088/0953-8984/23/8/083002*

Kirz, J., Jacobsen, C., & Howells, M. (1996). Soft X-ray microscopes and their biological applications. *Quarterly Reviews in Biophysics*, 28(1), 33-130.

Lam, P. J., Ohnemus, D. C., & Marcus, M. A. (2012). The speciation of marine particulate iron adjacent to active and passive continental margins.*Geochimica et Cosmochimica Acta*, *80*, 108-124.

Lam, P. J., & Bishop, J. K. (2008). The continental margin is a key source of iron to the HNLC North Pacific Ocean. *Geophysical Research Letters*, *35*(7).

Lerotic M, Mak R, Wirick S, Meirer F, Jacobsen C (2014). MANTiS: a program for the analysis of X-ray spectromicroscopy data. *J. Synchrotron Rad. 21(5); 1206–121. doi:10.1107/S1600577514013964*

Leventhal, J., & Taylor, C. (1990). Comparison of methods to determine degree of pyritization. *Geochimica et Cosmochimica Acta*, *54*(9), 2621-2625.

Liu, B., Yang, D., Ye, B., & Berezovskaya, S. (2005). Long-term open-water season stream temperature variations and changes over Lena River Basin in Siberia. *Global and Planetary Change*, *48*(1-3 SPEC. ISS.), 96–111.

Lofts, S., Tipping, E., & Hamilton-Taylor, J. (2008). The chemical speciation of Fe (III) in freshwaters. *Aquatic Geochemistry*, *14*(4), 337-358.

Martin, J. M., & Meybeck, M. (1979). Elemental mass-balance of material carried by major world rivers. *Marine chemistry*, *7*(3), 173-206.

McClelland, J. W., Holmes, R. M., Dunton, K. H., & Macdonald, R. W. (2012). The Arctic ocean estuary. *Estuaries and Coasts*, *35*(2), 353-368.

Moffett, J. W. (2001). Transformations among different forms of iron in the ocean. *IUPAC Series on Analytical and Physical Chemistry of Environmental Systems*, *7*, 343-372.

Neubauer, E., Schenkeveld, W. D., Plathe, K. L., Rentenberger, C., Von Der Kammer, F., Kraemer, S. M., & Hofmann, T. (2013). The influence of pH on iron speciation in podzol extracts: Iron complexes with natural organic matter, and iron mineral nanoparticles. *Science of the Total Environment*,*461*, 108-116.

Ödman, F., Ruth, T., Rodushkin, I., & Pontér, C. (2006). Validation of a field filtration technique for characterization of suspended particulate matter from freshwater. Part II. Minor, trace and ultra trace elements. *Applied geochemistry*, *21*(12), 2112-2134.

Perret, Didier, et al. "The diversity of natural hydrous iron oxides."*Environmental science & technology* 34.17 (2000): 3540-3546.

Peterson, B. J., Holmes, R. M., McClelland, J. W., Vörösmarty, C. J., Lammers, R. B., Shiklomanov, A. I & Rahmstorf, S. (2002). Increasing river discharge to the Arctic Ocean. *science*, *298*(5601), 2171-2173.

Pokrovsky, O. S., & Schott, J. (2002). Iron colloids/organic matter associated transport of major and trace elements in small boreal rivers and their estuaries (NW Russia). *Chemical Geology*, *190*(1), 141-179.

Pokrovsky, Oleg S., B. Dupré, and J. Schott. "Fe–Al–organic colloids control of trace elements in peat soil solutions: results of ultrafiltration and dialysis."*Aquatic Geochemistry* 11.3 (2005): 241-278.

Pokrovsky, O. S., Schott, J., & Dupré, B. (2006). Trace element fractionation and transport in boreal rivers and soil porewaters of permafrost-dominated basaltic terrain in Central Siberia. *Geochimica et Cosmochimica Acta*, *70*(13), 3239-3260.

Pokrovsky, O. S., Viers, J., Shirokova, L. S., Shevchenko, V. P., Filipov, A. S., & Dupré, B. (2010). Dissolved, suspended, and colloidal fluxes of organic carbon, major and trace elements in the Severnaya Dvina River and its tributary. *Chemical Geology*, *273*(1), 136-149.

Pokrovsky, O. S., Shirokova, L. S., Kirpotin, S. N., Audry, S., Viers, J., & Dupré, B. (2011). Effect of permafrost thawing on organic carbon and trace element colloidal speciation in the thermokarst lakes of western Siberia.*Biogeosciences*, *8*(3), 565-583.

Poulton, S. W., & Raiswell, R. (2002). The low-temperature geochemical cycle of iron: from continental fluxes to marine sediment deposition.*American Journal of Science*, *302*(9), 774-805.

Lara, R. J., Rachold, V., Kattner, G., Hubberten, H. W., Guggenberger, G., Skoog, A., & Thomas, D. N. (1998). Dissolved organic matter and nutrients in the Lena River, Siberian Arctic: Characteristics and distribution. *Marine Chemistry*, *59*(3), 301-309.

Raiswell, R., Tranter, M., Benning, L. G., Siegert, M., De'ath, R., Huybrechts, P., & Payne, T. (2006). Contributions from glacially derived sediment to the global iron (oxyhydr) oxide cycle: implications for iron delivery to the oceans. *Geochimica et Cosmochimica Acta*, *70*(11), 2765-2780.

Raiswell, R., Benning, L. G., Davidson, L., & Tranter, M. (2008). Nanoparticulate bioavailable iron minerals in icebergs and glaciers.*Mineralogical Magazine*, *72*(1), 345-348.

Raiswell, R., & Canfield, D. E. (2012). The iron biogeochemical cycle past and present. *Geochemical Perspectives*, *1*(1), 1-2.

Resources of surface waters of the USSR (1972). In Zhilq I.M., and Alyshinskaya, N.M., editors, Northern Region, 1972. V. Liningrad, Gidrometeoizdat, 663 p. (in Russian)

Romanovsky, N.N., (1993), Principles of cryogenesis in the lithosphere [Osnovy Kriogeneza Litosfery]: Moscow, Moscow State University Press, 335 p. [In Russian.]

Romanovsky, V. E., Sazonova, T. S., Balobaev, V. T., Shender, N. I., & Sergueev, D. O. (2007). Past and recent changes in air and permafrost temperatures in eastern Siberia. *Global and Planetary Change*, *56*(3), 399-413.

Rouxel, O. J., Bekker, A., & Edwards, K. J. (2005). Iron isotope constraints on the Archean and Paleoproterozoic ocean redox state. *Science*, *307*(5712), 1088-1091.

Schroth, A. W., Crusius, J., Sholkovitz, E. R., & Bostick, B. C. (2009). Iron solubility driven by speciation in dust sources to the ocean. *Nature Geoscience*, *2*(5), 337-340.

Schwertmann, U. (1987). Properties of Iron Oxides in Two Finnish Lakes in Relation to the Environment of Their Formation. *Clays and Clay Minerals*, *35*(4), 297–304.

Schwertmann, U., and E. Murad. "Effect of pH on the formation of goethite and hematite from ferrihydrite." *Clays and Clay Minerals* 31.4 (1983): 277-284.

Severmann, S., Johnson, C. M., Beard, B. L., & McManus, J. (2006). The effect of early diagenesis on the Fe isotope compositions of porewaters and authigenic minerals in continental margin sediments. *Geochimica et Cosmochimica Acta*, *70*(8).

Sholkovitz, E. R. (1976). Flocculation of dissolved organic and inorganic matter during the mixing of river water and seawater. *Geochimica et Cosmochimica Acta*, *40*(7), 831-845.

Stein, R. (2000). Circum-Arctic river discharge and its geological record: an introduction. *International journal of earth sciences*, *89*(3), 447-449.

Stoehr, J. (1992), NEXAFS Spectroscopy, *Springer Series in Surface Sciences,* ISBN 978-3-662-02853-7

Strahler, A. N. (1957). Quantitative analysis of watershed geomorphology.*Eos, Transactions American Geophysical Union*, *38*(6), 913-920.

Stolpe, B., Guo, L., Shiller, A. M., & Aiken, G. R. (2013). Abundance, size distributions and trace-element binding of organic and iron-rich nanocolloids in Alaskan rivers, as revealed by field-flow fractionation and ICP-MS.*Geochimica et Cosmochimica Acta*, *105*, 221-239.

Stumm, W., Morgan, J. J., & Drever, J. I. (1996). Aquatic Chemistry. *Journal of Environmental Quality*, *25*(5), 1162.

Tarnocai, C., Canadell, J. G., Schuur, E. A. G., Kuhry, P., Mazhitova, G., & Zimov, S. (2009). Soil organic carbon pools in the northern circumpolar permafrost region. *Global biogeochemical cycles*, *23*(2).

Vasyukova, E. V., Pokrovsky, O. S., Viers, J., Oliva, P., Dupré, B., Martin, F., & Candaudap, F. (2010). Trace elements in organic- and iron-rich surficial fluids of the boreal zone: Assessing colloidal forms via dialysis and ultrafiltration. *Geochimica et Cosmochimica Acta*, *74*(2), 449–468.

Vasyukova, E., Pokrovsky, O. S., Viers, J., & Dupré, B. (2012). New operational method of testing colloid complexation with metals in natural waters. *Applied Geochemistry*, *27*(6), 1226–1237.

Viers, J., Dupré, B., & Gaillardet, J. (2009). Chemical composition of suspended sediments in World Rivers: New insights from a new database. *Science of the Total Environment*, *407*(2), 853–868.

Vonk, J. E., & Gustafsson, Ö. (2013). Permafrost-carbon complexities.*Nature Geoscience*, *6*(9), 675-676.

Warren, L.A, & Haack, E. a. (2001). Biogeochemical controls on metal behaviour in freshwater environments. *Earth-Science Reviews*, *54*(4), 261–320.

Wells, M. L. (1999). Manipulating iron availability in nearshore waters. *Limnology and Oceanography*, *44*(4), 1002–1008. http://doi.org/10.4319/lo.1999.44.4.1002

Yang, D., Kane, D. L., Hinzman, L. D., Zhang, X., Zhang, T., & Ye, H. (2002). Siberian Lena River hydrologic regime and recent change. *Journal of Geophysical Research: Atmospheres*, *107*(23), 1–10.

Zakharova, E. a., Pokrovsky, O. S., Dupré, B., & Zaslavskaya, M. B. (2005). Chemical weathering of silicate rocks in Aldan Shield and Baikal Uplift: Insights from long-term seasonal measurements of solute fluxes in rivers. *Chemical Geology*, *214*(3-4), 223–248.

10.2 Study 1: Supplementary Information

Acid Blank (µg/teflon container)	Calculation: Conc (ppb) * Volume (5ml)/1000										
Sample Number	**Mn (µg)**	**Fe (µg)**	**Li (µg)**	**Zn (µg)**	**Sr (µg)**	**Ba (µg)**	**Ti (µg)**	**V (µg)**	**Ce (µg)**	**Cr (µg)**	**Rb (µg)**
5A	0,0	0,2	<DL	0,1	<DL	0,1	0,0	0,0	0,0	0,0	<DL
5B	0,0	0,1	<DL	0,1	<DL	0,1	0,0	<DL	<DL	0,0	<DL
5C	0,0	0,0	<DL	0,1	<DL	0,0	0,1	<DL	<DL	0,0	<DL
5D	0,0	0,3	<DL	0,2	0,0	0,0	0,0	0,0	0,0	0,0	0,0
5F	0,0	0,2	<DL	0,0	<DL	<DL	0,0	<DL	<DL	0,0	<DL
5G	0,0	1,4	<DL	0,0	<DL	<DL	0,1	0,0	0,0	0,0	<DL

Washed Filter (µg/filter)	Calculation: Washed Filter and Acid (µg/teflon container)										
Sample Number	**Mn (µg)**	**Fe (µg)**	**Li (µg)**	**Zn (µg)**	**Sr (µg)**	**Ba (µg)**	**Ti (µg)**	**V (µg)**	**Ce (µg)**	**Cr (µg)**	**Rb (µg)**
1A	0,1	1,5	<DL	0,9	0,1	0,1	0,2	0,0	0,0	0,6	0,0
1B	0,1	2,0	<DL	0,7	0,1	0,1	0,2	0,0	0,0	0,6	0,0
1C	0,1	1,1	<DL	0,6	0,1	0,1	0,1	0,0	0,0	0,7	0,0
1D	0,1	1,7	<DL	4,8	0,2	0,1	0,2	0,0	0,0	0,6	0,0
1F	0,1	1,1	<DL	1,5	0,0	0,0	0,0	0,0	0,0	1,1	<DL

Unwashed Filter (µg/filter)	Calculation: Unwashed Filter and Acid (µg/teflon container)										
Sample Number	**Mn (µg)**	**Fe (µg)**	**Li (µg)**	**Zn (µg)**	**Sr (µg)**	**Ba (µg)**	**Ti (µg)**	**V (µg)**	**Ce (µg)**	**Cr (µg)**	**Rb (µg)**
2A	0,1	1,3	<DL	0,5	0,1	0,1	0,1	0,0	0,0	1,0	0,0
2B	0,1	1,3	<DL	0,3	0,1	0,1	0,1	0,0	<DL	1,1	0,0
2C	0,1	1,5	<DL	0,2	0,1	0,2	0,1	0,0	0,0	1,1	0,0
2D	0,1	1,4	<DL	0,4	0,1	0,1	0,1	0,0	0,0	1,0	0,0
2F	0,1	2,0	<DL	2,5	0,1	0,1	0,0	0,0	0,0	1,9	0,0
2G	0,1	2,0	<DL	2,6	0,1	0,1	0,0	0,0	0,0	2,0	0,0

Lena River Filter (µg/filter)	Calculation: Lena Filter and Acid (µg/teflon container)										
Sample Number	**Mn (µg)**	**Fe (µg)**	**Li (µg)**	**Zn (µg)**	**Sr (µg)**	**Ba (µg)**	**Ti (µg)**	**V (µg)**	**Ce (µg)**	**Cr (µg)**	**Rb (µg)**
3A	37,5	1246,8	1,2	4,3	7,0	21,1	93,2	2,9	3,2	3,6	2,7
3C	77,9	241,4	0,1	1,2	2,0	4,4	8,0	0,3	0,3	1,5	0,3

SLRS-5 (µg / teflon container)	Calculation: SLRS-5 and Acid (µg/teflon container)										
Sample Number	**Mn (µg)**	**Fe (µg)**	**Li (µg)**	**Zn (µg)**	**Sr (µg)**	**Ba (µg)**	**Ti (µg)**	**V (µg)**	**Ce (µg)**	**Cr (µg)**	**Rb (µg)**
4A	0,0	0,8	<DL	0,4	0,3	0,1	0,1	0,0	0,0	0,0	0,0
4B	0,0	0,5	<DL	0,1	0,2	0,1	0,0	0,0	<DL	0,0	0,0
4C	0,0	0,5	<DL	0,1	0,3	0,1	0,0	0,0	<DL	0,0	0,0
4D	0,0	0,4	<DL	0,1	0,2	0,1	0,0	0,0	0,0	0,0	0,0
4G	0,0	0,5	<DL	0,1	0,2	0,1	0,0	0,0	0,0	0,0	0,0
Method DL (µg/l)											
	0,0	0,4	0,4	0,0	0,3	0,2	0,3	0,0	0,0	0,0	0,1
Certified SLRS-5 (µg/l)											
	4,3	91,2		0,8	53,6	14,0		0,3		0,2	
SLRS-5 (µg / 5g)											
	0,0	0,5		0,0	0,3	0,1		0,0		0,0	

Table 1. Outline of the standard materials (BCR-2, basalt; W1, diorite) that were used to analyse the recovery of Fe, Al and Mn in the filter dissolution method development.

Sample Number	Standard	Fe Recovery	Fe	Al Recovery	Al	Mg Recovery	Mg	Mn Recovery	Mn
		%	µg/sample	%	µg/sample	%	µg/sample	%	µg/sample
J1	BCR-2 filter	82	3987	124	4453	98	1067	90	69
L1	BCR-2 filter	96	7135	120	6622	105	1752	101	118
J2	BCR-2 no filter	94	5723	123	5520	104	1409	99	95
L2	BCR-2 no filter	155	6726	204	6557	169	1643	162	111
K1	W1 filter	88	8546	37	7166	52	4199	71	151
M1	W1 filter	96	5747	60	7192	63	3169	77	102
K2	W1 no filter	95	9104	43	8346	52	4191	72	152
M2	Wi no filter	97	6242	61	7949	64	3456	77	110
N3	Lena Filter		422		290		41		16
H3	BCR-2 and filter	87	8368	67	4812	26	557	80	121
I1	BCR-2 and filter	89	8630	70	4996	27	582	73	112
H4	BCR-2 no filter	92	8902	67	4810	31	663	81	123
I2	BCR-2 no filter	84	8136	65	4664	32	691	76	115
H1	W1 and filter	87	6576	27	4126	18	1156	64	107
I3	W1 and filter	88	6686	32	4890	20	1259	62	103
H2	W1 no filter			26	3882	17	1055		
I4	W1 no filter	80	6088	28	4180	19	1235	59	99

Table 2. Outline of the standard materials (BCR-2, basalt; W1, diorite) that were used to analyse the recovery of Fe, Al and Mn in the filter dissolution method development.

Central Plateau	Fe	% Difference
	µg / L	$(([Fe]_{leach} + [Fe]_{residual}) - [Fe]_{particulate})*100$
65B	478	
65R	89	21
65L	488	
69B	68	
69R	22	4
69L	49	
55B	388	
55R	78	10
55L	350	
37B	1550	
37R	907	10
37L	483	
Aldan River		
5B	215	
5R	105	24
5L	57	
8B	360	
8R	118	49
8L	65	
Lena River		
2B	469	
2R	458	39
2L	186	
4B	524	
4R	387	33
4L	195	
2B	469	
2R	458	37
2L	186	
Eastern Mountains		
16B	463	
16R	119	40
16L	160	
Southern Mountains		
12 B	27	
12 R	11	12
12 L	12	
33B	32	
33R	15	23
33L	10	
27B	70	
27R	27	30
27L	22	

Table 3. Outline of sequential extraction mass balance.

Lena River	Location	Date	Latitude	Longitude	T Air °C	T H_2O °C	pH	Cond (uS/cm^C)	Alkalinity (meqv/l)	DOC mg/L	POC mg/L	Fe µg/L	Al µg/L
LR2012-32	Lena upstream outflow of Tuolba/Туолба	2012-07-27	60,609200	124,188467	13	15,7	7,9	174	1,1	12,3	7,7	97	64
LR2012-31	Lena upstream Kytyl-Diura/Кытыл-Дюра	2012-07-26	60,872233	125,633500	21	16,9	7,2	146	0,6	11,1	0,0	88	69
LR2012-34	Lena upstream Kytyl-Diura/Кытыл-Дюра	2012-07-27	60,873600	125,643750	22	15,8	7,4	159	1,0	11,9	6,8	257	186
LR2012-30	Lena at Sinsk/Синск, outflow of Siniaia/Синяя	2012-07-25	61,107917	126,890483	25	16,9	7,7	125	0,6	12,1	1,4	84	75
LR2012-28	Lena at Bulgunniakhtakh/Булгунняхтах, upstream outflow of Buotama/Буотама	2012-07-24	61,263717	128,739717	23	16,2	7,5	80	0,5	12,1	1,5	133	123
LR2012-04	Lena downstream Yakutsk/Якутск	2012-07-14	62,157700	129,908017	31	18,7	6,6	81	0,5	11,8	0,6	161	102
LR2012-01	Lena downstream Tupagino/Тупагино	2012-07-12	62,262633	130,017183	23	16,7	6,8	90	0,4	11,1	0,7	112	102
LR2012-25	Lena upstream Khatas/Хатас	2012-07-22	62,649150	129,907433	25	19,6	6,9	90	0,5	10,1	0,0	95	66
LR2012-03	Lena at Stolby/Столбы	2012-07-13	63,019350	129,684650	27	17,2	6,5	84	0,4	11,4	1,0	133	100
LR2013-78	Lena at Kharyialakh/Харыялах	2013-06-28	63,132667	129,623200	26	19,8	7,6	139	0,7	7,1	0,2	34	39
LR2012-02	Lena upstream outflow of Aldan/Алдан	2012-07-12	63,387917	129,539267	25	16,7	6,6	69	0,4	11,7	0,8	103	88
LR2013-75	Lena upstream outflow of Belianka/Белянка	2013-06-27	63,528167	128,859967	24	16,3	7,6	92	0,7	8,0	0,1	55	37
LR2013-73	Lena between outflow of Belianka/Белянка and Kengkeme/Кенгкеме	2013-06-27	63,490417	128,803050	23	18,1	7,3	142	0,7	8,1	0,2	38	20
LR2013-71	Lena upstream Sangar/Сангар	2013-06-27	63,885917	127,542100	***	16,1	7,4	85	0,7	8,6	0,4	67	72
LR2013-39	Lena upstream outflow of Viliui/Вилюи	2013-06-12	64,218250	126,864350	25	12,0	7,6	101	1,0	11,6	0,5	94	47
LR2013-41	Lena downstream outflow of Viliui/Вилюи	2013-06-13	64,394467	126,365850	28	18,9	7,0	140	0,9	15,1	0,8	84	7
LR2013-57	Lena downstream outflow of Linde/Линде and Dianyshka/Дянышка	2013-06-21	65,051117	124,805500	22	14,9	7,0	83	0,7	10,8	0,2	65	53
LR2013-54	Lena channel west side - No name (close to North Polar circle)	2013-06-19	65,948567	123,914000	18	19,5	7,1	128	0,7	14,1	0,6	101	17
LR2013-42	Lena channel west side - Demon stream	2013-06-14	66,343933	123,675933	18	15,1	7,3	139	0,7	13,9	0,4	130	22
LR2013-48	Lena upstream outflow of Muna/Муна	2013-06-16	67,873733	123,092267	24	16,1	7,1	121	0,7	13,3	0,1	121	22
LR2013-49	Lena channel downstream outflow of Muna/Муна	2013-06-16	67,929067	123,002050	28	16,1	7,0	130	0,3	13,6	0,3	119	19
LR2013-45	Lena downstream Dzhardzhan/Джарджан	2013-06-15	68,743317	123,996567	21	14,2	7,1	91	0,7	10,1	0,4	84	24
Aldan River													
LR2012-13	Aldan upstream of outflow Amga/Амга	2012-07-19	62,638267	134,921883	18	19,1	7,7	86	0,7	8,4	0,4	77	73
LR2012-11	Aldan upstream Megino-Aldan/Мегино-Алдан,	2012-07-18	62,710583	134,695200	22	18,5	7,3	99	0,7	8,0	0,0	103	67
LR2012-09	Aldan upstream research site Mammals Task	2012-07-18	62,922883	134,172767	***	18,4	7,5	94	0,7	8,7	0,0	111	76
LR2012-08	Aldan downstream outflow of Baraiy/Барайы	2012-07-17	63,223117	133,246183	25	17,9	7,1	92	0,7	8,8	0,3	105	84
LR2012-05	Aldan downstream outflow of Baibakan/Байбакан	2012-07-16	63,349517	131,677083	20	18,3	7,1	91	0,6	8,8	0,4	108	90
LR2012-22	Aldan at outflow	2012-07-21	63,438167	129,666683	***	19,2	6,8	105	0,6	9,5	0,2	145	71
LR2013-38	Aldan upstream outflow of Aldan	2013-06-12	63,433850	129,639833	19	10,9	7,4	86	0,8	13,1	1,1	104	57
Vilyuy River													
LR2013-62	Viliui at Viliuisk/Вилюйск	2013-06-23	63,758217	121,598283	25	20,0	7,4	111	0,7	12,5	0,4	69	8
LR2013-60	Viliui downstream Kysyl-Syr/Кысыл-Сыр	2013-06-23	63,908933	123,145650	24	19,4	7,2	110	0,7	12,5	0,4	78	7
LR2013-59	Viliui downstream Khatyryk-Khomo/Хатырык-Хомо	2013-06-22	63,870033	125,166733	24	20,0	7,2	110	0,7	12,6	0,5	28	7
LR2013-66	Viliui 42 km from outflow	2013-06-24	64,053000	126,069133	24	19,4	7,4	112	0,7	12,5	0,8	53	5
LR2013-40	Viliui by outflow	2013-06-13	64,327967	126,372017	21	17,9	7,2	140	0,9	14,7	1,0	91	6
Central Plateau													
LR2012-29	Siniaia/Синяя	2012-07-25	61,146133	126,862033	25	23,4	8,6	163	1,6	24,9	1,8	92	6
LR2012-36	Siniaia/Синяя	2012-07-28	61,167983	126,867683	23	23,8	9,4	171	1,6	25,4	1,7	55	7
LR2012-35	Siniaia/Синяя	2012-07-28	61,165083	126,910950	17	22,3	9,0	170	1,6	25,0	1,7	60	11
LR2013-72	Kengkeme/Кенгкеме	2013-06-27	63,467750	128,789867	23	19,1	7,4	201	0,9	9,4	0,5	76	12
LR2013-69	Berge-Tiugene/Берге-Тюгене	2013-06-26	63,974233	127,029033	22	18,8	7,5	346	1,3	10,5	0,6	46	1
LR2013-68	Lungkha/Лунгха	2013-06-26	64,108617	126,740583	22	19,6	7,5	288	1,2	11,4	0,9	68	2
LR2013-61	Tiung/Тюнг	2013-06-23	63,780367	121,522933	25	22,9	7,6	118	1,2	11,5	0,6	80	2
LR2013-63	Tangnary/Тангнары	2013-06-24	64,024900	123,885183	24	19,2	7,0	50	0,4	14,2	0,8	189	7
LR2013-64	Bappagai/Баппагай	2013-06-24	64,027633	124,092333	21	17,7	8,4	159	1,1	15,4	0,6	14	4
LR2013-65	Uoranga/Уоранга	2013-06-24	64,026833	124,398883	25	18,4	7,2	70	0,6	20,9	2,6	283	6
LR2013-55	Linde/Линде	2013-06-21	64,952017	124,596250	22	20,6	6,7	58	0,5	15,6	0,8	198	7
LR2013-43	Outflow at Zhigansk/Жиганск	2013-06-14	66,771133	123,360117	26	16,2	6,9	52	0,3	9,4	0,5	165	21
LR2013-52	Khoruogka/Хоруонгка	2013-06-17	67,214133	123,135417	20	21,2	7,3	42	0,3	11,6	0,6	169	11
LR2013-50	Muna/Муна	2013-06-16	67,876283	123,036433	30	16,9	7,1	134	0,7	13,3	0,5	128	25
LR2012-37	Oddokun/Оддокун	2012-07-29	61,194633	128,284017	21	12,5	7,3	336	3,5	41,2	0,9	106	9
LR2012-26	Tamma/Тамма	2012-07-24	61,903883	129,847183	***	19,0	7,2	106	0,7	11,0	0,5	187	51
LR2012-15	Mammals task	2012-07-19	62,946450	134,008383	19	8,6	6,5	145	1,5	21,1	0,0	162	29
Eastern Mountains (Verkhoyansk Moutain Range)													
LR2012-10	Tompo/Томпо	2012-07-18	62,708483	134,721167	22	16,4	7,0	148	1,0	2,6	0,0	12	6
LR2012-16	De pinne/Де пинне, Uiana/Уяна, Paygy/Пайгы	2012-07-20	63,103250	134,038350	23	14,6	6,3	103	0,4	3,9	0,5	87	6
LR2012-07	Baraiy/Барайы/Baraiy	2012-07-17	63,204400	133,234033	25	15,6	7,0	168	0,7	1,6	0,1	22	2
LR2012-18	No name - upstream Urasa iuriage/Ураса Юряге	2012-07-20	63,367733	133,273617	24	19,9	6,6	118	1,1	23,3	0,3	79	15
LR2012-19	Urasa/iuriage/Ураса Юряге	2012-07-20	63,385867	133,136867	26	14,8	6,6	50	0,2	3,3	0,1	105	7
LR2012-06	Tukulan/Тукулан	2012-07-16	63,320900	131,930900	20	16,4	7,4	206	0,8	1,3	0,1	7	2
LR2012-20	Baibakan/Байбакан	2012-07-20	63,355833	131,753183	***	18,0	6,8	60	0,5	2,7	0,0	32	4
LR2012-21	Kele/Келе	2012-07-21	63,343983	130,379050	22	18,1	7,0	244	0,7	2,0	0,1	80	4
LR2012-23	Tumara/Тумара	2012-07-21	63,461483	129,569300	23	22,3	7,1	170	0,7	4,9	0,0	48	26
LR2013-77	Tumara/Тумара	2013-06-28	63,468067	129,594183	23	15,3	7,6	206	0,8	2,0	0,2	34	2
LR2012-24	Batamai/Батамай	2012-07-21	63,520217	129,399783	***	18,7	6,8	50	0,3	2,8	0,3	45	7
LR2013-76	Batamai/Батамай	2013-06-28	63,522083	129,396250	18	14,8	7,5	49	0,3	2,9	0,1	32	4
LR2013-74	Belianka/Белянка	2013-06-27	63,520267	128,831833	24	17,0	7,8	93	0,6	1,9	0,1	3	2
LR2013-70	Chochuma/Чочума	2013-06-26	64,019100	127,350150	***	19,3	7,4	88	0,6	6,0	0,2	40	9
LR2013-67	Liunkiubei/Люнкюбей	2013-06-26	64,163517	126,966633	25	16,2	7,2	73	0,6	7,1	0,2	35	14
LR2013-58	Liapiske/Ляписке	2013-06-22	64,600150	125,717933	16	15,5	7,1	89	0,7	10,2	0,1	72	48
LR2013-56	Dianyshka/Дянышка	2013-06-21	65,005533	124,944167	23	14,1	7,3	178	0,7	4,9	0,3	20	15
LR2013-53	Undiuliung/Ундюлюнг	2013-06-18	66,232850	124,161383	27	18,1	7,2	159	0,6	2,8	0,3	20	5
LR2013-51	Sobolokh Maian/Соболох Маян	2013-06-17	67,252100	123,408417	20	15,8	7,4	140	0,7	4,3	0,3	38	10
LR2013-47	Menkere/Менкере	2013-06-16	68,021550	123,415083	28	11,2	7,1	104	0,6	5,3	1,4	39	17
LR2013-46	Natara/Натара	2013-06-15	68,388550	123,973767	19	15,7	7,1	64	0,3	5,7	0,4	84	19
LR2013-44	Dzhardzhan/Джарджан	2013-06-15	68,732517	124,059683	20	18,8	7,2	182	0,9	1,1	0,4	28	4
Southern Mountains (Stanovoy Mountain Range)													
LR2012-33	Tuolba/Туолба	2012-07-27	60,593650	124,272600	19	17,7	8,2	305	***	***	0,0	21	***
LR2012-12	Amga/Амга	2012-07-19	62,614683	134,922883	18	20,3	8,2	299	2,8	7,0	0,0	21	3
LR2012-27	Buotama/Буотама	2012-07-24	61,251017	128,769533	24	20,6	8,0	310	3,4	6,9	0,5	61	2
LR2012-17	Tatta/Татта	2012-07-20	63,020317	133,408150	23	20,7	7,4	133	1,3	12,8	1,3	469	56

Table 4. Overview of the samples collected in July 2012 and June 2013, Outlined is a description of the sample location and grid reference. Also outlined are the measured field parameters, the particulate organic carbon (POC), dissolved organic carbon (DOC) and dissolved (<0.22 µm) Fe and Al concentrations.

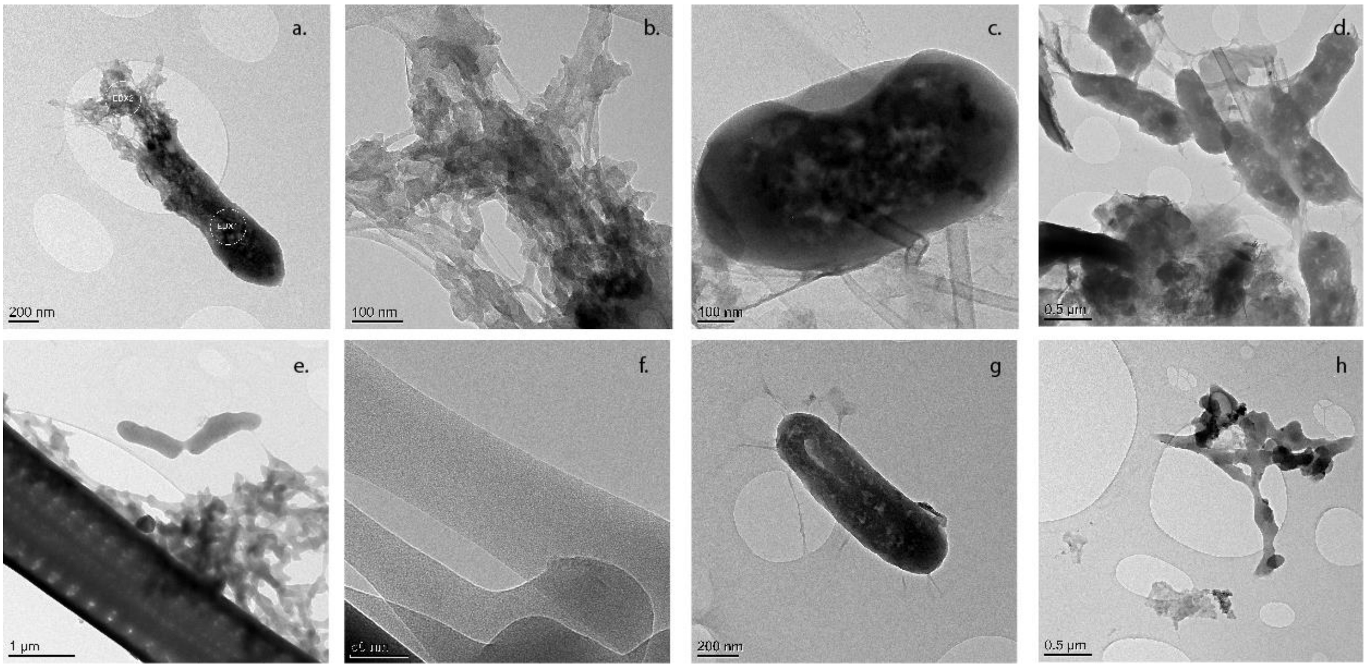

Fig. 1 Examples of the Particulate Organic Carbon that were observed in the Lena River catchment area using Scanning Transmission Electron Microscopy. Ferrihydrite was observed to attach to the surface of POC in a, c, d, e, from the central plateau However, ferrihydrite was trapped within the network of OC outlined in b, f and h, from the eastern mountain range.

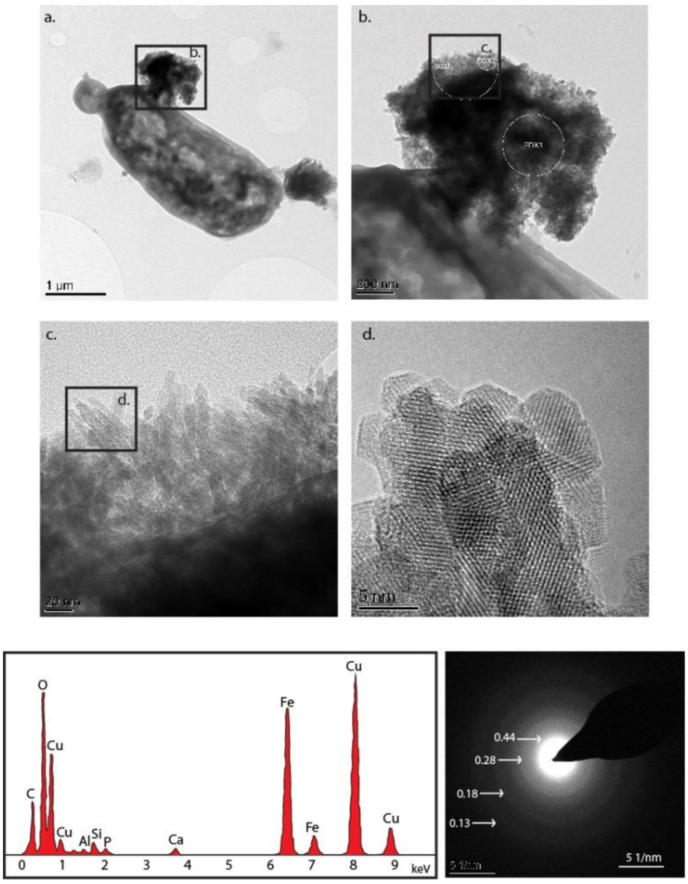

Fig. 2 Examples of nano-goethite that were observed in the Lena River catchment area using Scanning Transmission Electron Microscopy. In this example, c) and d) show the needle like aggregates of nanocrystalline goethite. Further, the EDX diffraction spectra shows more rings, than is observed for ferrihydrite which suggests that this is a more crystalline iron – bearing particle. The goethite is associating with the surface of an organic particle (a) and (b). The association between Fe and POC surfaces was common on particulate material from the central plateau.

10.3 Study 2: Data Tables

		56Fe	2*RSD	57Fe	2*RSD	$[Fe]_{particulate}$	$[Fe]_{residual}$	$[Fe]_{leach}$	$[Fe]_{dissolved}$	$[Fe]_{total}$	% Particulate	% Dissolved
Total Particulate	**Sample**	**‰**	**‰**	**‰**	**‰**	**µg/L**	**µg/L**	**µg/L**	**µg/L**	**µg/L**	**%**	**%**
Lena River	LR42	-0,27	0,23	-0,16	0,17	32	15	10	130	162	20	80
Lena River	LR71	0,09	0,08	0,16	0,11	80	***	***	67	147	54	46
Lena River	LR2	-0,1	0,12	-0,15	0,15	469	458	186	103	572	82	18
Aldan River	LR5	-0,11	0,09	-0,08	0,05	215	105	57	108	323	67	33
Aldan River	LR13	-0,06	0,13	-0,13	0,17	115	***	40	77	192	60	40
Aldan River	LR8	-0,03	0,06	-0,02	0,11	360	118	65	105	465	77	23
Vilyuy River	LR60	-0,01	0,08	0,08	0,16	77	***	***	78	155	50	50
Central Plateau	LR55	-0,58	0,14	-0,87	0,06	388	78	350	198	586	66	34
Central Plateau	LR63	-0,11	0,02	-0,17	0,11	216	27	228	189	405	53	47
Central Plateau	LR50	0,28	0,08	0,39	0,11	185	81	101	128	313	59	41
Central Plateau	LR43	-0,04	0,07	-0,1	0,18	206	***	***	165	371	56	44
Southern Mountains	LR17	-0,12	0,08	0,13	0,13	409	113	292	469	878	47	53
Eastern Mountains	LR46	-0,06	0,09	-0,07	0,11	166	83	154	84	250	66	34
Eastern Mountains	LR58	0,1	0,02	0,08	0,14	217	117	98	72	289	75	25
Southern Mountains	LR33	0,07	0,03	0,10	0,10	32	15	10	21	53	61	39
Southern Mountains	LR12	0,01	0,04	0,03	0,08	27	11	12	21	48	57	43
Southern Mountains	LR27	-0,33	0,08	-0,51	0,2	70	27	22	61,00	131	53	47
Residual	**Sample**											
Lena River	LR45	0,09	0,16	0,28	0,17	269	126	140	84	353	76	24
Lena River	LR42	0,22	0,08	0,35	0,17	32	15	10	130	162	20	80
Lena River	LR31	0,16	0,08	0,07	0,36	336	170	162	88	424	79	21
Lena River	LR2	0,05	0,11	0,08	0,13	469	458	186	103	572	82	18
Aldan River	LR5	0,03	0,05	0,09	0,15	215	105	57	108	323	67	33
Aldan River	LR8	0,24	0,04	0,44	0,07	360	118	65	105	465	77	23
Vilyuy River	LR59	0,26	0,08	0,34	0,16	159	81	78	28	187	85	15
Central Plateau	LR63	-0,04	0,10	0,06	0,04	216	27	228	189	405	53	47
Central Plateau	LR65	0,00	0,11	0,01	0,15	478	89	488	283	761	63	37
Southern Mountains	LR17	0,14	0,06	0,18	0,2	409	113	292	469	878	47	53
Eastern Mountains	LR56	0,17	0,02	0,25	0,07	205	79	123	20	225	91	9
Leach	**Sample**											
Lena River	LR45	-2,1	0,16	-2,1	0,14	269	126	140	84	353	76	24
Central Plateau	LR31	-0,16	0,22	-0,22	0,24	336	170	162	88	424	79	21
Aldan River	LR5	-0,19	0,03	-0,33	0,2	215	105	57	108	323	67	33
Aldan River	LR8	-0,21	0,1	-0,29	0,2	360	118	65	105	465	77	23
Vilyuy River	LR59	-0,39	0,03	-0,56	0,11	159	81	78	28	187	85	15
Central Plateau	LR55	-0,92	0,07	-1,28	0,17	388	78	350	198	586	66	34
Central Plateau	LR63	-0,84	0,05	-1,16	0,2	216	27	228	189	405	53	47
Central Plateau	LR50	-0,65	0,07	-0,84	0,12	185	81	101	128	313	59	41
Central Plateau	LR65	-0,74	0,08	-1,07	0,12	478	89	488	283	761	63	37
Southern Mountains	LR17	-0,20	0,04	-0,29	0,12	409	113	292	469	878	47	53
Eastern Mountains	LR46	-0,71	0,04	-1,00	0,15	166	83	154	84	250	66	34
Eastern Mountains	LR56	-0,12	0,06	-0,14	0,1	205	79	123	20	225	91	9
Eastern Mountains	LR58	-0,26	0,03	-0,37	0,09	217	117	98	72	289	75	25
Southern Mountains	LR27	-0,40	-0,08	-0,56	0,11	70	27	22	61	131	53	47
Colloidal	**Sample**											
Lena River	LR45	0,41	0,28	0,63	0,14	269	126	140	84	353	76	24
Lena River	LR31	0,49	0,15	0,66	0,13	336	170	162	88	424	79	21
Lena River	LR2	0,93	0,08	1,35	0,11	469	458	186	103	572	82	18
Aldan River	LR5	1,83	0,15	2,76	0,18	215	105	57	108	323	67	33
Aldan River	LR13	0,72	0,11	1,08	0,07	115	***	40	77	192	60	40
Aldan River	LR8	0,73	0,09	1,03	0,09	360	118	65	105	465	77	23
Vilyuy River	LR59	0,15	0,12	0,21	0,12	159	81	78	28	187	85	15
Vilyuy River	LR60	0,73	0,04	1,03	0,14	77	***	***	78	155	50	50
Central Plateau	LR55	-0,06	0,13	-0,11	0,18	388	78	350	198	586	66	34
Central Plateau	LR63	-0,22	0,09	-0,33	0,18	216	27	228	189	405	53	47
Central Plateau	LR43	-0,21	0,14	-0,15	0,18	206	***	***	165	371	56	44
Southern Mountains	LR17	0,00	0,03	-0,01	0,08	409	113	292	469	878	47	53
Eastern Mountains	LR46	0,15	0,20	0,33	0,22	166	83	154	84	250	66	34
Eastern Mountains	LR51	0,21	0,09	0,23	0,15	***	***	***	***	***	***	***
Eastern Mountains	LR58	0,61	0,11	0,90	0,28	217	117	98	72	289	75	25
Eastern Mountains	LR16	0,62	0,04	0,95	0,11	463	119	160	87	550	84	16
Southern Mountains	LR12	0,01	0,06	-0,22	0,16	27	11	12	21	48	57	43

					$[Fe]_{particulate}$	$[Fe]_{residual}$	$[Fe]_{leach}$	$[Fe]_{dissolved}$	$[Fe]_{total}$	Particulate	Dissolved
Particulate Fe Average	**56Fe**	**2*RSD**	**57Fe**	**2*RSD**	**µg/L**	**µg/L**	**µg/L**	**µg/L**	**µg/L**	**%**	**%**
Lena River (n= 3)	-0,09	0,14	-0,05	0,14	194	236	98	100	294	52	48
Aldan River (n=3)	-0,07	0,09	-0,08	0,11	230	112	54	97	326	68	32
Eastern Mountains (n=2)	0,02	0,05	0,01	0,13	191	100	126	78	269	71	29
Southern Mountains (n=4)	-0,09	0,05	-0,13	0,13	43	18	15	34	78	57	43
Vilyuy River (n=1)	-0,01	0,08	0,08	0,16	77	***	***	78	155	50	50
Central Plateau (n=4)	-0,11	0,08	-0,12	0,12	281	75	243	230	511	56	44
Lena River	-0,09	0,14	-0,05	0,14	194	236	98	100	294	52	48
Mountains	-0,05	0,07	-0,07	0,12	150	68	57	69	219	64	36
Central Plateau	-0,09	0,08	-0,09	0,13	247	75	243	204	451	55	45
Colloidal Fe Average											
Lena River (n=3)	0,61	0,17	0,88	0,13	358	251	163	92	450	79	21
Aldan River (n=3)	1,10	0,12	1,63	0,11	230	112	54	97	326	68	32
Eastern Mountains (n=4)	0,40	0,11	0,60	0,19	282	106	137	81	363	75	25
Southern Mountains (n=2)	0,01	0,06	-0,22	0,16	27	11	12	21	48	57	43
Vilyuy River (n=2)	0,44	0,08	0,62	0,13	118	81	78	53	171	67	33
Central Plateau (3)	-0,16	0,10	-0,15	0,15	305	73	290	255	560	55	45
Lena River	0,61	0,17	0,88	0,13	358	251	163	92	450	79	21
Mountains	0,61	0,11	0,88	0,16	223	92	84	79	302	69	31
Central Plateau	0,08	0,09	0,11	0,15	243	75	237	188	431	59	41
Residual Fe Average											
Lena River (n=4)	0,13	0,11	0,20	0,21	277	192	125	101	378	64	36
Aldan River (n=2)	0,14	0,05	0,27	0,11	287	112	61	107	394	72	28
Eastern Mountains (n=1)	0,17	0,02	0,25	0,07	205	79	123	20	225	91	9
Southern Mountains (n=1)	0,14	0,06	0,18	0,20	409	113	292	469	878	47	53
Vilyuy River (n=1)	0,26	0,08	0,34	0,16	159	81	78	28	187	85	15
Central Plateau (n=2)	-0,02	0,11	0,04	0,10	347	58	358	236	583	58	42
Lena River	0,13	0,11	0,20	0,21	277	192	125	101	378	64	36
Mountains	0,15	0,04	0,24	0,12	297	104	134	176	473	70	30
Central Plateau	0,07	0,10	0,14	0,12	284	66	265	167	451	67	33
Leach Fe Average											
Lena River (n=1)	-2,10	0,16	-2,10	0,14	269	126	140	84	353	76	24
Aldan River (n=2)	-0,20	0,07	-0,31	0,20	287	112	61	107	394	72	28
Eastern Mountains (n=3)	-0,36	0,04	-0,50	0,11	196	93	125	59	254	78	22
Southern Mountains (n=2)	-0,30	-0,02	-0,43	0,12	239	70	157	265	504	50	50
Vilyuy River (n=1)	-0,39	0,03	-0,56	0,11	159	81	78	28	187	85	15
Central Plateau (n=6)	-0,66	0,10	-0,91	0,17	321	89	266	177	498	64	36
Lena River		0,16	-2,10	0,14	269	126	140	84	353	76	24
Mountains	-0,30	0,03	-0,43	0,14	234	92	116	131	366	68	32
Central Plateau	-0,71	0,06	-0,98	0,14	285	71	249	165	450	65	35

Table 2. Average of 2012 and 2013 iron isotope composition on total particle, residual, leach and colloidal iron fractions. The data is subdivided according to Table 1 in Manuscript 1 (11.1)

10.4 Study 3: Data Tables

	Particulate (> 0.22 µm)					Dissolved (<0.22 µm)				
	Fe	56Fe	2*RSD	57Fe	2*RSD	Fe	56Fe	2*RSD	57Fe	2*RSD
Date	µg/L	‰	‰	‰	‰	µg/L	‰	‰	‰	‰
Sept	446	0,09	0,02	0,13	0,08	48	0,17	0,03	0,19	0,11
Oct	309	-0,07	0,09	0,02	0,20	103	0,04	0,05	0,01	0,03
Nov	584	0,05	0,12	-0,02	0,08	37	0,04	0,06	0,05	0,07
Dec	208	-0,13	0,10	-0,26	0,16	47	0,16	0,05	0,26	0,15
Feb	830	-0,37	0,16	-0,56	0,21	46	-0,08	0,05	-0,10	0,11
March	150	-0,20	0,06	-0,44	0,14	4	0,21	0,09	0,41	0,18

Table. 1 Outline of 2012-13 winter samples stations, measured field parameters, iron (Fe), aluminium (Al) and organic carbon (OC) concentrations and iron isotope composition.

Sample	Location	Longitude	Latitude	Date	pH	Cond	TDS	Water Temp	Alkalinity	POC	DOC (<0.7µm)	DOC (<10kDa)	DOC (<1kDa)	Fe (>0.22µm)	Fe (<0.22µm)	Fe (<10kDa)	Fe (<1kDa)
						uS/cm	ppm	°C	meqv/l	mg/L	mg/L	mg/L	mg/L	µg/L	µg/L	µg/L	µg/L
LR86	Tabaga	61°47'12"N	129°39'55"E	2015-05-06	7,57	321	300	0,44	1,7	0,7	6			288	115		
LR93	Tabaga	61°47'17.0"N	129°39'59.6"E	2015-05-08	7,56	362	181	0,98	1,5	1,6	17	7,5	3,7	970	711	26	<DL
LR95	Tabaga	61°48'04.0"N	129°40'02.5"E	2015-05-11	7,48	192	96	0,75	0,7	1,3	18	4,0	3,2	767	282	<DL	<DL
LR96	Tabaga	61°47'47.6"N	129°40'00.2"E	2015-05-14	7,40	195	99	1,63	0,7	1,1	18	5,1	4,7	502	243	30	<DL
LR99	Tabaga	61°48'04.4"N	129°39'58"E	2015-05-17	7,70	180	90	1,13	0,6	0,9	18	20,9	5,3	641	255	23	<DL
LR106	Tabaga	61°48'04.1"N	129°40'02"E	2015-05-20	7,47	126	63	3,83	0,6	1,0	20	6,0	3,7	3701	279	19	<DL
LR107	Tabaga	61°48'03.9"N	129°40'01.8"E	2015-05-23	7,48	109	55	4,81	0,6	1,4	20	7,8	6,5	2124	221	<DL	<DL
LR115	Tabaga	61°48'04.3"N	129°40'02.1"E	2015-05-26	7,9	109	54	6,48	0,6	1,2	19	6,6	4,9	2208	204	<DL	<DL
LR122	Tabaga	61°48'04.4"N	129°40'02.2"E	2015-05-28	7,70	111	55	6,84	0,6	0,6	19			4999	169		

Table. 5 Outline of 2015 sampling. Included in the table are field measurements and the organics carbon (OC) and iron (Fe) in the particulate (>0.22 µm), colloidal (<0.22 µm, <10 kDa) and dissolved (<1 kDa) fractions.

	Particles (‰)				Residual (‰)				Leach (‰)				Water (‰)			
Sample	$\delta^{56}Fe$	2SD	$\delta^{57}Fe$	2SD	$\delta^{56}Fe$	2SD	$\delta^{57}Fe$	2SD	$\delta^{56}Fe$	2SD	$\delta^{57}Fe$	2SD	$\delta^{56}Fe$	2SD	$\delta^{57}Fe$	2SD
LR86	-0,3	0,09	-0,42	0,06	0,07	0,14	0,09	0,19	-0,43	0,1	-0,7	0,18	-0,66	0,08	-0,97	0,16
LR93	0,06	0,14	0,06	0,13	0,21	0,06	0,34	0,1	-0,23	0,09	-0,31	0,13	-0,50	0,11	-0,76	0,14
LR95	0,07	0,08	0,1	0,11	0,24	0,08	0,4	0,11	-0,18	0,2	-0,26	0,19	0,12	0,10	0,20	0,09
LR96	-0,04	0,09	-0,08	0,07	0,17	0,02	0,21	0,04	-0,21	0,08	0,13	0,13	-0,29	0,06	-0,39	0,11
LR99	-0,04	0,08	-0,02	0,08	0,13	0,04	0,22	0,05	-0,46	0,04	-0,7	0,06	0,05	0,10	0,03	0,18
LR106	-0,05	0,16	-0,09	0,16	0,11	0,03	0,19	0,03	-0,33	0,11	-0,43	0,13	0,00	0,09	0,03	0,18
LR107	-0,01	0,07	-0,04	0,12	0,19	0,07	0,23	0,08	-0,17	0,12	-0,25	0,09	0,23	0,11	0,29	0,12
LR115	-0,02	0,12	0,02	0,18	0,12	0,06	0,2	0,16	-0,21	0,08	-0,32	0,06	0,24	0,11	0,35	0,12
LR122	0,08	0,06	0,13	0,06	0,19	0,06	0,33	0,17	-0,21	0,04	-0,31	0,01	0,10	0,06	0,13	0,05

Table. 6 Iron isotope ($\delta^{56}Fe$) composition of the particulate, residual, leach and colloidal fraction in the 2015 spring flood samples.